UNIVERSITY OF CALIFORNIA,
IRVINE

Opportunities and Challenges for Net-Zero Emissions Energy and Food Systems

DISSERTATION

submitted in partial satisfaction of the requirements
for the degree of

DOCTOR OF PHILOSOPHY

in Earth System Science

by

Julianne T. DeAngelo

Dissertation Committee:
Professor Steven J. Davis, Chair
Associate Professor Kristen A. Davis
Assistant Professor Angela J. Rigden

2023

DEDICATION

I've grown impatient with the kind of debate we used to have about whether optimists or the pessimists are right. Neither are right. There is too much bad news to justify complacency. There is too much good news to justify despair.

Donella Meadows

TABLE OF CONTENTS

	Page
LIST OF FIGURES	iv
LIST OF TABLES	v
ACKNOWLEDGEMENTS	vi
VITA	vii
ABSTRACT OF THE DISSERTATION	ix
INTRODUCTION	1
CHAPTER 1: Energy systems in scenarios at net-zero CO_2 emissions	**5**
1.1 Introduction	5
1.2 Results	7
1.3 Discussion	18
1.4 Methods	22
1.5 Figures and Tables	29
CHAPTER 2: Seaweed farming for climate change mitigation	**34**
2.1 Introduction	34
2.2 Results	37
2.3 Discussion	44
2.4 Methods	48
2.5 Figures and Tables	69
CHAPTER 3: Net-zero emissions food systems	**76**
3.1 Introduction	76
3.2 Food system outputs	78
3.3 Levers for mitigating food system emissions	82
3.4 Summary and Conclusions	101
3.5 Methods	102
3.6 Figures	107
SUMMARY AND CONCLUSIONS	111
REFERENCES	115
APPENDIX A: Supplementary Information for Chapter 1	1 37
APPENDIX B: Supplementary Information for Chapter 2	1 57
APPENDIX B: Supplementary Information for Chapter 3	1 80

LIST OF MAIN CHAPTER FIGURES

		Page
Figure 1.1	Global net-zero emissions energy systems	29
Figure 1.2	Characteristics of regional energy systems and emissions when global emissions reach net-zero	30
Figure 1.3	Residual and negative emissions when global emissions reach net-zero	31
Figure 1.4	Relative characteristics of scenarios in the year in which global emissions reach net-zero	32
Figure 2.1	Seaweed production costs	69
Figure 2.2	Net cost of potential seaweed climate benefits	70
Figure 2.3	Key cost sensitivities of seaweed production and climate benefits	71
Figure 2.4	Cumulative potential climate benefits of large-scale seaweed farming	72
Figure 3.1	Food system emissions in 2017	107
Figure 3.2	Potential for dietary shifts to reduce food system emissions	108
Figure 3.3	Historical and projected cereal yields through 2050	109
Figure 3.4	Emissions mitigation levers for 2050 from the Pale identity	110

LIST OF MAIN CHAPTER TABLES

		Page
Table 1.1	Summary statistics of net-zero scenarios	33
Table 2.1	Selected parameter ranges for technoeconomic model	73

ACKNOWLEDGEMENTS

First and foremost, thank you to my advisor, Steven J. Davis. When we first met at AGU in 2018, I remember admiring your solutions-oriented perspective and clarity of thought. I still admire those qualities, and I am deeply grateful that I got the opportunity to learn from you over these past four years.

Thank you to my committee for providing thoughtful support as I progressed through my PhD. Your feedback and discussions have significantly improved my scholarship, and I am a much better researcher as a result of your guidance.

Thank you to my lab group for being my research family at UCI. You continually inspire me to keep working toward my goals, ask tough questions, and have fun while doing it.

Last but certainly not least, thank you to my family, my friends, and my partner for their unwavering support throughout my PhD journey. I truly could not have done this without each of you.

The text of Chapter 1 of this dissertation is adapted from the material as it appears in Nature Communications, used with permission from Springer Nature. The co-authors listed in this publication are Inês Azevedo, John Bistline, Leon Clarke, Gunnar Luderer, Edward Byers & Steven J. Davis. Steven J. Davis directed and supervised research which forms the basis for the dissertation.

The text of Chapter 2 of this dissertation is adapted from the material as it appears in Nature Plants, used with permission from Springer Nature. The co-authors listed in this publication are Benjamin T. Saenz, Isabella B. Arzeno-Soltero, Christina A. Frieder, Matthew C. Long, Joseph Hamman, Kristen A. Davis & Steven J. Davis. Kristen A. Davis & Steven J. Davis directed and supervised research which forms the basis for the dissertation.

VITA

JULIANNE T. DEANGELO

EDUCATION

University of California, Irvine, Irvine, CA **2023**
Ph.D., Earth System Science

University of California, Irvine, Irvine, CA **2021**
M.S., Earth System Science

Dartmouth College, Hanover, NH **2019**
B.A., Earth Sciences with Honors

- Academic Honors: Cum Laude, Warren F. Upham 1871 Geology Prize for outstanding senior thesis (2019), National Merit Scholar (2015)

GRADUATE RESEARCH EXPERIENCE

Sustainable Systems Analysis Lab, University of California, Irvine – Irvine, CA **2019 - Present**
Graduate Student Researcher, advised by Dr. Steven J. Davis

- Developed techno-economic modeling tools to assess the biophysical and economic potential of seaweed farming as a carbon dioxide removal (CDR) method.
- Analyzed emissions mitigation scenario data from integrated assessment models to distill policy- and market-relevant insights about energy system decarbonization and carbon dioxide removal.
- Conducted a comprehensive review of scientific literature on achieving net-zero greenhouse gas (GHG) emissions from food systems; aggregated data and insights from multiple research fields to create a system-wide roadmap of opportunities for both near- and long-term food system GHG emissions reductions.

COMMUNITY ENGAGEMENT AND SERVICE

Contributing Author, IPCC 6th Assessment Report (AR6) **2021 - 2023**
Intergovernmental Panel on Climate Change

- Chapter 6: Energy Systems

Technical Contributor, Fifth National Climate Assessment (NCA5) **2022 - 2023**
United States Global Change Research Program

- Chapter 32: Mitigation

Chapter Co-Author, 2023 Billion-Ton Report **2022 - 2023**
United States Department of Energy's Bioenergy Technologies Office

- Macroalgae Chapter

Organizing Committee Member, Aspen Global Change Institute (AGCI) **2022 - present**
Workshop on Reaching Net-Zero Emissions Food Systems

- Conference scheduled for August 20-25, 2023

PEER-REVIEWED PUBLICATIONS

In Preparation

DeAngelo, J., Burney, J., Naylor, R., and S.J. Davis. Net-zero emissions food systems.

Huppmann, D., J. Bistline, **J. DeAngelo**, R. Jones, J. McFarland, J. Weyant and S. J. Davis (2023). NCA5 Scenario Explorer and Data hosted by IIASA. Vienna, Austria, Mitigation Chapter of the Fifth National Climate Assessment & the International Institute for Applied Systems Analysis.

2023

Arzeno-Soltero, I.B., B.T. Saenz, C. Frieder, M.C. Long, **J. DeAngelo**, S.J. Davis, and K.A. Davis. Large global variations in the carbon dioxide removal potential of seaweed farming due to biophysical constraints. *Communications Earth & Environment* **4**, 185 (2023). https://doi.org/10.1038/s43247-023-00833-2

DeAngelo, J., B.T. Saenz, I.B. Arzeno-Soltero, C. Frieder, M.C. Long, J. Hamman, K.A. Davis, and S.J. Davis. Economic and biophysical limits to seaweed farming for climate change mitigation. Nature Plants **9**, 45–57 (2023). https://doi.org/10.1038/s41477-022-01305-9

2021

DeAngelo, J., I. Azevedo, J. Bistline, L. Clarke, G. Luderer, E Byers, and S.J. Davis. Energy systems in scenarios at net-zero CO2 emissions. Nature Communications **12**, 6096 (2021). https://doi.org/10.1038/s41467-021-26356-y

OTHER PUBLICATIONS

2022

J DeAngelo, S Davis, B Saenz, I Arzeno-Soltero, M Long, C Frieder, K Davis, K Martin, F Chay, J Freeman, J Hamman (2022). "Mapping seaweed farming potential for CDR and biomass products" CarbonPlan **https://carbonplan.org/research/seaweed-farming-explainer**

CONFERENCE PARTICIPATION

Ocean Carbon and Biogeochemistry (OCB) Summer Workshop **2023**
Invited speaker for Carbon Dioxide Removal (CDR) plenary session

- Oral presentation: "Economic and biophysical limits to seaweed farming for climate change mitigation"

American Geophysical Union (AGU) Fall Meeting **2018, 2021, 2022**
Presenting Author, Poster Sessions

- **DeAngelo, J.**, Saenz, B.T., Arzeno-Soltero, I.B., Frieder, C., Long, M.C., Hamman, J., Davis, K.A., Davis, S.J., 2022. *Economic and Biophysical Limits to Seaweed Farming for Climate Mitigation*. Abstract B25F-1619 presented at the 2022 AGU Fall Meeting in San Francisco, CA.
- **DeAngelo, J.**, Arzeno-Soltero, I.B., Saenz, B.T., Frieder, C., Long, M.C., Davis, K.A., Davis, S.J., 2021. *Techno-Economic Analysis of Seaweed-Based Climate Solutions*. Abstract GC35E-0752 presented virtually at the 2021 AGU Fall Meeting.
- **DeAngelo, J.**, Osterberg, E.C., Lewis, G., Ferris, D.G., Hawley, R.L., Marshall, H.-P., Birkel, S., Graeter, K., 2018. *Surface melt changes and climate forcing in the Western Greenland percolation zone*. Abstract C43E-1842 presented at the 2018 AGU Fall Meeting in Washington, D.C.

GRANTS AND AWARDS

UCI Solutions that Scale Graduate Research Fellowship **2021 - 2022**
Full tuition and stipend ($37,000)

ABSTRACT OF THE DISSERTATION

Opportunities and Challenges for Net-Zero Emissions Energy and Food Systems

by

Julianne T. DeAngelo

Doctor of Philosophy in Earth System Science

University of California, Irvine, 2023

Professor Steven J. Davis, Chair

Stabilizing global climate will require major transformations to energy and food systems, including drastic reductions in the use of fossil fuels, improvements in energy and material efficiencies, extensive electrification of energy end uses, sustainable intensification of agriculture, and carbon management. Although progress has been made in researching these topics in recent years, several research questions central to framing global energy and agriculture policies deserve further study. In this dissertation, I explore several relevant research topics with the goal of contributing to our understanding of the opportunities and challenges for achieving net-zero emissions energy and food systems, including (1) the characteristics of modeled net-zero CO_2 emissions energy systems; (2) the potential for seaweed farming to deliver globally-scaled carbon removal and emissions mitigation; and (3) potential solutions for hard-to-abate greenhouse gas emissions from the global food system.

In scenarios that successfully reach net-zero CO_2 emissions by the end of this century, renewable energy sources account for 60% of primary energy at net-zero on average

(compared to ~14% today), with slightly less than half of that renewable energy derived from biomass. Meanwhile, electricity makes up approximately half of final energy consumed (compared to ~20% today), highlighting the extent to which solid, liquid, and gaseous fuels remain prevalent in the scenarios even when emissions reach net-zero. Residual emissions and offsetting negative emissions are not evenly distributed across world regions, which may have important implications for negotiations on burden-sharing, human development, and equity.

Sinking farmed seaweed to the deep sea is a potential method to remove carbon from the atmosphere (i.e., negative emissions), and sequestering a gigaton of CO_2 per year with this method may cost as little as \$480/tCO_2 on average. Instead, using farmed seaweed for products that *avoid* a gigaton of CO_2-equivalent greenhouse gas emissions annually – by substituting for more emissions-intensive food or feed sources – could return a profit of \$50/tCO_2-eq. However, these costs depend on low farming costs, high seaweed yields, and assumptions that almost all carbon in seaweed is removed from the atmosphere (i.e., competition between phytoplankton and seaweed is negligible) and that seaweed products can displace products with substantial embodied non-CO_2 GHG emissions, such as agricultural goods.

Modern agriculture is extremely emissions-intensive, and sweeping systemic changes will be needed to reach net-zero. Shifting diets away from beef would have an outsized impact on decreasing the average emissions intensity of caloric production, and closing yield gaps is a top priority to increase production without increasing agricultural land area. Promising methods are being developed to suppress GHG emissions from enteric

fermentation, soils, and rice paddies, although further research is needed to determine the long-term efficacy and scalability of solutions globally. Stopping deforestation is also a top priority, which will require aggressive policy action to enact strict land-use regulations. Ultimately, achieving net-zero emissions energy and food systems will entail an accelerated and coordinated global effort across multiple economic sectors.

INTRODUCTION

Mitigating anthropogenic climate change is the defining global challenge of this century. Limiting global mean temperature increase to 2˚C or even 1.5˚C relative to the preindustrial era (UNFCCC, 2015) requires that global annual CO_2 emissions are net-zero or net-negative by the end of this century (Matthews & Caldeira, 2008; Joeri Rogelj et al., 2015; Joeri Rogelj, Shindell, et al., 2018; Sanderson, O'Neill, & Tebaldi, 2016) and that non-CO_2 greenhouse gas emissions (GHGs) are significantly reduced (Byers et al., 2022). Meeting this goal will require major transformations to both energy and food systems, including drastic reductions in the use of fossil fuels, substantial improvements in energy and materials efficiency, extensive electrification of energy end uses, sustainable intensification of agriculture, and management of carbon (Fuss et al., 2014; GEA, 2012; Hoffert et al., 1998; Hong et al., 2021; IPCC, 2014; Marcucci, Kypreos, & Panos, 2017; Sachs, Schmidt-Traub, & Williams, 2016; Tilman, Balzer, Hill, & Befort, 2011). However, several research areas central to framing global energy and agriculture policies remained understudied until recently, including system-wide characteristics of potential net-zero emissions energy systems, the scalability and feasibility of specific carbon removal technologies, and approaches for mitigating emissions from the most difficult-to-decarbonize agricultural sectors in the broader context of reaching net-zero emissions. In this dissertation, I explore these topics with the goal of contributing to our understanding the opportunities and challenges for transitioning to net-zero emissions energy and food systems.

Chapter 1 focuses on the energy-system-wide characteristics of scenarios from Integrated Assessment Models (IAMs) that successfully reach net-zero CO_2 emissions by

2100. IAM scenarios provide an integrated perspective on the transformations of the energy-economy-land system and its implications for climate, and are prominently used for informing about the implications of international climate goals. I analyze global and regional model outputs related to energy use, energy sources, residual emissions, electrification, and climate policy in the scenarios at the point when they reach net-zero CO_2 emissions. I also discuss the relationship between amounts of residual emissions – emissions that are particularly hard-to-abate – and the corresponding amounts of carbon removal that present in the net-zero IAM scenarios. These characteristics at the point of net-zero CO_2 can inform policies that might take varying approaches – including potential approaches that are not represented by current scenario pathways – to reach the same goal of net-zero emissions.

Given the importance of carbon removal to offset residual emissions in IAM scenarios, in Chapter 2 I assess the feasibility and scalability of seaweed farming as a potential carbon removal method. Compared to land-based carbon removal approaches, seaweed farming has the advantages of not requiring inputs of land or freshwater and might also have environmental co-benefits (e.g., (AIEEP, 2021; Bach et al., 2021; Duarte, Wu, Xiao, Bruhn, & Krause-Jensen, 2017; Froehlich, Afflerbach, Frazier, & Halpern, 2019; Gao, L., Jiang, Jian, & He, 2021; Gattuso, Williamson, Duarte, & Magnan, 2021; Krause-Jensen & Duarte, 2016; NASEM, 2021; Wu, Keller, & Oschlies, 2022)). Additionally, seaweed products might help to lower greenhouse gas emissions, for example by reducing methane emissions from ruminants (Roque, Salwen, Kinley, & Kebreab, 2019), and replacing fossil fuels (Freeman & von Keitz, 2017) and emissions-intensive agricultural products (Hong et al., 2021). To evaluate the potential of seaweed farming to help achieve global net-zero GHG emissions, I

use coupled biophysical and technoeconomic models to systematically assess the economic costs and potential climate benefits of seaweed farming, testing their sensitivity across large ranges in individual variables and comparing different product pathways. Based on simulated global seaweed yields from a newly-developed biophysical model (G-MACMODS) (Arzeno-Soltero et al., 2022; Frieder et al., 2022), I calculate spatially-explicit costs per ton of seaweed harvested and either costs per ton of GHG emissions avoided (when used as food, feed, or for biofuels) or costs per ton of carbon removed from the atmosphere as a carbon removal strategy. Given the large uncertainty in technoeconomic parameters, I use a Monte Carlo approach to assess a large scope of potential cost outcomes and discuss the key variables that have the largest impact on cost per ton of CO_2 removed or avoided. The primary goal of the chapter is to inform more targeted research into the potential of seaweed farming for climate benefits by identifying relative differences, sensitivities and trade-offs that are robust across many simulations of potential cost.

Lastly, in Chapter 3 I assess the potential of reaching net-zero GHG emissions from the global food system. Achieving net-zero GHG emissions from agriculture is particularly challenging, because the majority of agriculture emissions are powerful non-CO_2 GHGs from disparate area sources that are fundamentally linked to how we produce food. The challenges to mitigating food system emissions will continue to grow with increasing population and affluence, and the impacts of climate change on agriculture will increasingly undermine progress in agricultural production for many crops and regions (Jägermeyr et al., 2021; Ortiz et al. 2021). Yet despite agriculture's substantial contribution to global GHG emissions and its outsized share of particularly hard-to-abate emissions, it is not yet clear how to reduce the full scope of agricultural emissions to a point compatible with climate

stabilization or even net-zero emissions. In this chapter I review the prospect of transitioning to a net-zero emissions food system and discuss the unique challenges associated with eliminating agricultural emissions. I describe several necessary nutritional outputs of the food system, their current and projected GHG emissions through mid-century, and the key uncertainties of projected demand for food and other agricultural products. Finally, I assess the technical potential of mitigation solutions for different hard-to-abate processes, the role of both demand- and supply-side measures to reduce emissions, and priorities for research and policy action.

CHAPTER 1

Energy systems in scenarios at net-zero CO_2 emissions

The text of this chapter is adapted from:

DeAngelo, J., I. Azevedo, J. Bistline, L. Clarke, G. Luderer, E Byers, and S.J. Davis. Energy systems in scenarios at net-zero CO2 emissions. Nature Communications **12**, 6096 (2021). https://doi.org/10.1038/s41467-021-26356-y

1.1 Introduction

Limiting global mean temperature increase to 2˚C or even 1.5˚C relative to the preindustrial era (UNFCCC, 2015) requires that global annual CO_2 emissions are net-zero or net-negative by the end of this century, and perhaps as soon as 2050 (Matthews & Caldeira, 2008; Joeri Rogelj et al., 2015; Joeri Rogelj, Shindell, et al., 2018; Sanderson et al., 2016). In the broader context of climate stabilization, the magnitude of global temperature increase is directly proportional to cumulative CO_2 emissions, such that adding any amount of CO_2 to the atmosphere will increase future amounts of warming (Matthews & Caldeira, 2008; Matthews, Gillett, Stott, & Zickfeld, 2009). For these reasons, and because it is a clear and absolute target, achieving net-zero emissions is increasingly a goal of energy and emissions policies around the world (IEA, 2020; Peker, 2019; J. Rogelj, Geden, Cowie, & Reisinger, 2021; Joeri Rogelj et al., 2015; Ross & Damassa, 2015). Central to meeting this goal is a rapid and sweeping transformation of energy systems, including drastic reductions in the use of fossil fuels, substantial improvements in energy and materials efficiency, extensive electrification of energy end uses, and management of carbon (Fuss et al., 2014; GEA, 2012; Hoffert et al., 1998; IPCC, 2014; Marcucci et al., 2017; Sachs et al.,

2016). Moreover, this transformation of energy systems must be reconciled with both sustainable development goals (Fay, Hallegatte, Vogt-Schilb, Rozenberg, & Narloch, 2015; McCollum et al., 2018) and the considerable inertia of existing fossil energy infrastructure (Tong et al., 2019).

Given this context, energy analysts are increasingly exploring the challenges and opportunities for net-zero emissions energy systems (Davis et al., 2018), including detailed analyses of specific energy services and/or technologies (Audoly, Vogt-Schilb, Guivarch, & Pfeiffer, 2018; C. Bataille, 2019; Dowling et al., 2020; Jenkins, Luke, & Thernstrom, 2018). But although a number of recent studies have examined the mitigation pathways of energy systems in integrated assessment model (IAM) scenarios that limit warming to below 1.5˚C (Fofrich et al., 2020; Gambhir, Rogelj, Luderer, Few, & Napp, 2019; Grubler et al., 2018; Gunnar Luderer et al., 2018; Joeri Rogelj, Popp, et al., 2018), the common features and tradeoffs of such scenarios at the point when global CO_2 emissions reach net-zero have yet to be systematically assessed. These characteristics at the point of net-zero CO_2 can inform policies that might take varying approaches – including potential approaches that are not represented by current scenario pathways – to reach the same goal of net-zero emissions.

Here, we analyze 177 IAM scenarios from the public 1.5˚C Scenario Database (the SR1.5 database) (Huppmann, Kriegler, et al., 2018; Huppmann, Rogelj, Krey, Kriegler, & Riahi, 2018) in which global sources and sinks (including land use and agriculture) reach net-zero CO_2 emissions by 2100 (see Supplementary Table 1). Details of our processing and analytic approach are described in the Methods section. In summary, we assess global and regional energy use, energy sources, residual emissions, electrification, and climate policy

among the scenarios, finding robust features that span multiple IAMs (Joeri Rogelj, Shindell, et al., 2018). For example, renewable sources represent roughly 60% of primary energy at the point when they reach net-zero CO_2 emissions—and often more than half of such renewable energy is provided by biomass. However, it is important to note that the scenario ensemble is not a representative sample that can be used to infer likelihood; individual scenarios are equally plausible given model constraints.

1.2 Results

Energy Use and Timing of Net-Zero

Figure 1.1 shows the relationships among global energy and socioeconomic variables in the year of global net-zero emissions, broken out by the level of projected global warming. These categories include overshoot scenarios that return to the specified amount of warming by end-of-century (see Methods). Among the 177 net-zero scenarios, those that avoid mean end-of-century warming of 1.5°C (blue points) tend to have lower levels of global energy use (t-statistic = 9.2, $p < 0.001$) and less GDP per capita (t-statistic = 8.6, $p < 0.001$): of the 77 1.5°C scenarios, GDP per capita is <$40,000 per person per year in 91% (median $27,914, range $20,103-$58,506) and total final energy use is <500 EJ in 69% (median 439 EJ, range 227-646; Fig. 1.1a). In contrast, energy use and GDP per capita are substantially higher in scenarios that achieve net-zero emissions but exceed 1.5°C (green and orange points): of the 100 2°C and >2°C scenarios, GDP per capita is <$40,000 per person per year in only 43% (median $43,642, range $20,299-$116,666) and total final energy use is <500 EJ in 24% (median 580 EJ, range 345-857; Fig. 1.1a). Although this may reflect reduced energy use and economic activity in scenarios with the most ambitious

mitigation, it is also related to when net-zero emissions occur in these scenarios. Supplementary Figure A.1 supports this idea by showing that warming level is not strongly related to the levels of energy use and GDP ultimately reached in net-zero scenarios.

Figure 1.1b shows that the warmer scenarios included achieve net-zero emissions in progressively later years (median for all scenarios = 2064, range 2037-2100), because the additional time for the economy and energy system to grow in scenarios that achieve net-zero emissions later leads to higher cumulative CO_2 emissions (and therefore higher levels of subsequent warming). Supplementary Figures A.2 and A.3 support this idea that more ambitious scenarios achieve lower levels of warming via faster energy system transformations. However, in contrast to the timing of net-zero, the timing of peak emissions is consistent across the scenarios (and essentially immediate): emissions peak in 2017 (range 2014-2027) for 1.5°C scenarios, in 2019 (range 2011-2029) for 2°C scenarios, and in 2022 (range 2010-2036) for >2°C scenarios (Fig. 1.1b). Although many scenarios show emissions peaking prior to 2019 (which did not happen), the regional, socio-economic, and technological representations that prevail when these scenarios achieve net-zero emissions may nonetheless provide valuable insights for net-zero emissions policies.

Energy Resources

The use and sources of renewable energy in net-zero scenarios vary considerably, with no obvious relationship to the level of warming (Fig. 1.1c). Although the median share of primary energy derived from renewable sources (including biomass, solar, wind, hydroelectricity, and geothermal, using the direct equivalent method (Macknick, 2014)) is ~60% regardless of warming level, in some cases it is as little as 25% and reaches 80% in a

few others (Fig. 1.1c). Similarly, the median share of these renewables that are not biomass is ~55% regardless of warming level, but ranges from 20% to 89% (Fig. 1.1c). Supplementary Figure A.4 further decomposes the sources of primary energy in net-zero scenarios, showing, for example, that the largest share of primary energy from nuclear is 23%, with nuclear more often contributing a small share of energy (median share across all scenarios is 4.8%, range 0-23.4%). Moreover, the share of primary energy from fossil fuels (coal, oil, and natural gas) in net-zero scenarios with and without carbon capture ranges from 3-64%, with a median share across all scenarios of 33% (Supplementary Figure A.4). Of course, in net-zero scenarios, any residual emissions to the atmosphere from the use of fossil fuels are offset by negative emissions strategies.

Residual Emissions and Electrification

The scale of residual emissions, i.e. emissions that are counter-balanced by equivalent carbon sequestration, is important to consider given many feasibility concerns about negative emissions technologies (Joeri Rogelj, Shindell, et al., 2018; P. Smith et al., 2016). Figure 1.1d shows that the emissions intensity of final energy may remain quite high in net-zero scenarios (e.g., >30 Mt CO_2/EJ compared to the current level of ~81 Mt CO_2/EJ). This "residual" emissions intensity is insensitive to the warming level or the energy intensity of the global economy (although lower warming scenarios do tend to have lower energy intensities based on median values by warming group; Fig. 1.1d). Given that the points depicted in Fig. 1.1d are globally net-zero, the residual emissions are entirely offset by negative emissions.

Complementing the common assertion that everything must be electrified (Jaffe, 2021; Roberts, 2017), the scenario set indicates that reducing final energy use is also an important determinant for achieving 1.5 or 2°C. Electricity accounts for 35-80% of final energy across the range of net-zero scenarios, but is <70% in most >2˚C scenarios (Fig. 1.1e). Even though electrification is a useful mechanism for decarbonization, warmer scenarios tend to exhibit slightly higher levels of electrification at the timing of net-zero: median shares of 1.5°C, 2°C and >2°C scenarios are 46% (range 35-80%), 51% (range 38-77%), and 53% (range 42-67%), respectively, perhaps because they afford greater time for end-uses to transition (Fig. 1.1e). This transition-time effect on the amount of electrification is supported by Supplementary Figure A.3, which shows that scenarios that are later in reaching net-zero tend to compensate with higher amounts of electrification (Supplementary Figure A.3e). Warming amount is also correlated to both net-zero year ($r = 0.73$, $p < 0.001$; Fig. 1.1b) and electrification ($r = 0.27$, $p < 0.001$) in the Fig. 1.1 global scenarios, which further supports the idea that warmer scenarios have slightly higher amounts of electrification because they reach net-zero emissions later, thus allowing more time for end-uses to transition and for costs to decline. However, these are subtle distinctions in comparison to the differences in per capita energy use, where median shares in 1.5°C, 2°C and >2°C scenarios increase from 47, to 63 and 75 GJ per person, respectively. For comparison, in 2019 the average American, EU, and Chinese citizen used 201, 93, and 63 GJ, respectively. Thus, keeping final energy low is clearly important to meet 1.5°C, while there is more flexibility in the level of electrification that is required.

Negative Emissions and Policy

The prevailing carbon prices in net-zero scenarios—a proxy for global climate policies—range from zero to >$1,000/t CO_2, yet with no clear relationship to either warming level or the amount of carbon sequestration through bioenergy with carbon capture and storage (BECCS) (Fig. 1.1f; note that 16 scenarios with prices >$2,000/t CO_2 are not shown). It is important to note that carbon prices in the majority of SR1.5 scenarios are endogenous "shadow" carbon prices that reflect the marginal cost of abatement, and thus do not directly reflect the impact of explicit (exogenous) carbon pricing such as a carbon tax or cap-and-trade system (Guivarch & Rogelj, 2017; Riahi et al., 2017; Joeri Rogelj, Shindell, et al., 2018). Only 23 of the 177 scenarios we analyze here include exogenous carbon pricing. The relationship between BECCS and carbon price should therefore be interpreted as the impact of marginal abatement cost on BECCS deployment. The lack of a clear relationship between the two does not necessarily mean that marginal abatement cost is inconsequential for the magnitude of negative emissions, but rather indicates that other dynamics relating to technology availability and costs may be the main drivers of BECCS deployment. Additionally, the median amount of carbon sequestration from BECCS increases in 1.5°C, 2°C and >2°C scenarios, from 6.4 (range 0-16.7) to 8.0 (range 0-18.8) to 11.3 (range 3.7-16.4) Gt CO_2, respectively (Fig. 1.1f), indicating that warmer scenarios must rely on greater amounts negative emissions technologies to reach net-zero emissions.

Regional Energy Use, Energy Sources, and Electrification

Figure 1.2 shows regional differences in energy and emissions among net-zero scenarios (in the year in which global CO_2 emissions are net-zero). In some cases, these differences are substantial and systematic. For example, Figure 1.2a shows that when global emissions are net-zero, total final energy consumption is typically greatest in Asia (blue points) and the OECD and EU countries (e.g., the U.S., U.K., France, Germany, etc.; pink points)—in some cases more than 3 times the energy use in the Middle East and Africa, Latin America, and Eastern Europe (including Russia; yellow, green and purple points, respectively). Regional differences in GDP per capita in the net-zero year are somewhat less dramatic, but projections in the OECD and EU region are often greatest (median of $67,944 per person, range $47,534-$146,341), and projections in the Middle East and Africa are often lowest (median of $18,960 per person, range $6,263-$97,721; Fig. 1.2a).

As in the case of globally aggregated energy sources (Fig. 1.1c), the share of primary energy derived from renewables and different types of renewables are quite different across scenarios, with relatively little sensitivity to region (Fig. 1.2b). An exception is Latin America (green points), which most scenarios show having both a higher share of primary energy from renewables (median 80%, range 33-98%) and a greater share of those renewables from biomass (median 58%, range 12-83%) than other regions (median shares of renewables 58-67%, and median share of renewables from biomass 35-45%).

Regional variations in electrification are also small (regions' median shares range from 43-52%), though final energy use per capita varies across regions in a pattern similar to GDP per capita (Figs. 1.2a and 1.2c; Supplementary Figure A.5). Despite lower GDP per

capita, energy use per capita in Eastern Europe and Russia are similar to the OECD and EU region (median energy use of 105 and 112 GJ/person, respectively), considerably greater than in the other three regions (where median energy use ranges from 36-61 GJ/person; Fig. 1.2c; note that Eastern Europe and Russia per capita final energy exceeded 200 GJ/person in 2 scenarios that are not shown).

Regional Distribution of Residual and Negative Emissions

Importantly, when global emissions are net-zero, emissions in many scenarios are still net-positive in some regions and (proportionately) net-negative in others. Figure 1.2d shows the regional balance of per capita residual emissions from energy and industry and per capita negative emissions from BECCS—i.e., net energy system emissions in the region (when points are compared to the dashed black line). These differences in residual (F-statistic = 141.6, $p < 0.001$) and negative emissions (F-statistic = 70.7, $p < 0.001$) across regions can be at least partially explained by differences in investment: Supplementary Figure A.6 shows that cumulative investment in non-fossil electricity supply up to the global net-zero year is correlated with regional electrification ($r = 0.55$, $p < 0.001$), negative emissions from BECCS ($r = 0.58$, $p < 0.001$), and residual emissions from energy and industry ($r = 0.86$, $p < 0.001$; Supplementary Figure A.6). The positive correlation between non-fossil electricity investment and both BECCS and residual emissions is likely due to BECCS primarily being used to offset residual emissions, such that scenarios with high amounts of BECCS also have high amounts of residual emissions at net-zero. Of course, investment is not the only cost-related driver of these regional characteristics, but it does

appear to play a significant role in the smaller subset of scenarios that include investment output values.

Residual emissions per capita tend to be greater in regions of Eastern Europe and Russia and the OECD and EU (median values of 1.8 (range 0.2-4.9) and 1.9 (range 0.1-5.2) t CO_2/person, respectively; pink and purple points in Fig. 1.2d). However, these regions also have greater per capita negative emissions from BECCS than Asia and the Middle East and Africa regions, such that they are net-negative in nearly as many scenarios (40.1% and 49.4%, respectively) as they are net-positive (59.9% and 50.6%, respectively). In contrast, Latin America's energy system is net-negative in 78.1% of the scenarios (green points) and the Middle East and Africa and Asia regions are net-negative in just 14.0% and 19.4%, respectively (orange and blue points, respectively). This supports recent research on regional and country-level negative emissions distributions in the context of regional net-zero emissions (Honegger & Reiner, 2018; van Soest, den Elzen, & van Vuuren, 2021) and indicates that burden-sharing between currently less-developed regions may not be well-balanced in IAM outputs when global emissions reach net-zero. While there are many different approaches to defining a well-balanced mitigation effort (Zhou & Wang, 2016), burden-sharing approaches that consider equity as a key component are vital for meeting sustainable development goals (Cantore & Padilla, 2010). Analysis of the SR1.5 scenarios in the context of equitable emissions/negative emissions allocation and sustainable development warrants further research.

Figure 1.3a shows the global distributions of residual and negative emissions in net-zero scenarios, including both those explicitly tied to the energy system (i.e. residual

emissions from energy and industrial processes and negative emissions from BECCS) and those related to agriculture and land use (including afforestation and reforestation), which are major sources of negative emissions in many IAMs (Fuhrman J, 2019). The aggregate patterns are striking: in warmer scenarios, net emissions from agriculture and land use tend to be less negative, residual emissions are higher, and these trends must be compensated for by larger negative emissions from BECCS (Fig. 1.3a). In net-zero scenarios where warming is >2°C, negative emissions from BECCS in the net-zero year are on average 10.5 Gt CO_2, and in no scenario <3.7 Gt (range 3.7-16.4; Fig. 1.3a). In contrast, there are some 1.5°C and <2.0°C scenarios in which there are no negative emissions from BECCS because more modest residual emissions are balanced by larger negative emissions from land uses (excluding BECCS), such as afforestation (Table 1.1). The negative emissions from BECCS also decreases in more ambitious mitigation scenarios, with mean values of 8.7(range 0-18.8) Gt CO_2 and 6.7(range 0-16.7) Gt CO_2 for <2.0°C and 1.5°C scenarios, respectively (Fig. 1.3a; Table 1.1). Although residual emissions outputs by end-use sector were not available for many of the scenarios we assessed, transportation was the dominant source of residual emissions in the 40 scenarios which report these details, followed by either the industry or residential and commercial sectors (see Supplementary Figure A.7).

Global averages conceal considerable regional heterogeneity of emissions in a net-zero world. Figure 1.3b shows that potential negative emissions from land use are largest in Latin America (on average -1.1 Gt CO_2 in the net-zero year, range -4.8-1.7 Gt), while Asia is projected to be by far the largest source of residual emissions (on average 3.8 Gt CO_2 in the net-zero year, range 0.3-10.3 Gt). Asia and the OECD and EU regions are also the largest

sources of negative emissions from BECCS (on average 2.5(range 0-8.7) and 2.4(range 0-6.0) Gt negative CO_2 emissions in the net-zero year, respectively; Fig. 1.3b).

Relationships Between Scenario Characteristics

Figure 1.4 compares all 177 net-zero scenarios according to 6 global characteristics in the net-zero year: the share of final energy that is electricity, the share of primary energy derived from renewables, the share of renewable energy that is derived from non-biomass sources, energy conservation (i.e., the inverse of per capita energy demand), the magnitude of negative emissions from BECCS, and net land use emissions. Each panel in Figure 1.4 sorts all the scenarios according to one of these characteristics, with scenario values shown as z-scores. Pairwise correlation coefficients (r) are also shown at the top of each column to quantitatively compare each set of parameters (Supplementary Figure A.8). Plotted this way, for example in (a), it is evident that those scenarios in which electricity accounts for a greater share of final energy also tend to be associated with greater shares of renewable energy ($r = 0.64$, $p < 0.05$) and non-biomass renewable energy ($r = 0.59$, $p < 0.05$), but less energy conservation (i.e. greater per capita energy use, $r = -0.35$, $p < 0.05$; Fig. 1.4a). Scenarios with greater shares of renewable energy tend to have higher shares of non-biomass renewable energy ($r = 0.50$, $p < 0.05$; Fig. 1.4b), while scenarios with greater amounts of energy conservation tend to have lower shares of non-biomass renewable energy, and vice versa ($r = -0.46$, $p < 0.05$; Fig. 1.4c and 1.4d). The relationship among these characteristics and the magnitude of negative emissions from BECCS and/or net land use emissions is less clear and may be more dependent on the IAM or specific scenario used in each case. Since the process-based IAMs considered here use cost-effectiveness analysis

(CEA) (Joeri Rogelj, Shindell, et al., 2018), which minimizes the total mitigation costs of reaching a specified climate goal, all associations between output variables are essentially a reflection of what is cheapest. For example, in a scenario where substantial residual emissions remain at net-zero and are offset by correspondingly large amounts of negative emissions, reducing gross emissions to zero must have been more expensive than continuing to emit and offsetting with negative emissions. The most cost-effective outputs for scenarios are also based on the assumptions of individual models, including the availability and cost of technologies.

To further explore this relationship between negative emissions and other parameters, the underlying structure of the IAMs is important to consider: some of the SR1.5 models are partial equilibrium models (e.g., POLES ADVANCE) while others are general equilibrium (e.g. AIM-CGE 2.0 and 2.1) or hybrid models (e.g., MESSAGE-GLOBIOM 1.0) that link the two (Huppmann, Kriegler, et al., 2018). Additionally, certain scenarios have conditions that limit the amount or type of negative emissions technology used, such as EMF33_1.5C_limbio, which sets a limit of 100 EJ/year for the amount of bioenergy from BECCS, cellulosic fuels, and hydrogen (Huppmann, Kriegler, et al., 2018). Supplementary Figure A.9 shows the scenario ranges for residual emissions, non-biomass renewable energy share, and electrification for each model. These ranges demonstrate how the structure and assumptions of individual models affect the scenario outputs (Bistline, 2021; Jaxa-Rozen & Trutnevyte, 2021): for example, GCAM scenarios tend to have systematically higher residual emissions and lower amounts of non-biomass renewable energy and electrification than those of other models (Supplementary Figure A.9). Such model

differences are visible in comparing individual scenarios, but the output ranges are more sensitive to the scenario constraints than on the models (Supplementary Figure A.10).

1.3 Discussion

In addition to renewable and net-zero targets, "electrify everything" has become an explicit policy goal in a growing number of places (Mingle, 2020), particularly regarding heating and cooking in the residential and commercial sectors (Deason & Borgeson, 2019; Sugiyama, 2012) and light-duty transportation (Needell, McNerney, Chang, & Trancik, 2016; Zhang & Fujimori, 2020). In contrast, in most net-zero scenarios, electricity accounts for less than half (median 48.5%) of final energy (Fig. 1.1e), including in the OECD and EU region (Fig. 1.2c). Although electricity makes up a greater fraction of final energy in all net-zero scenarios than it does today (~15% today), in some regions and cases electricity remains less than 30% of final energy used (Fig. 1.2c). This emphasizes that IAMs project considerable ongoing use of solid, liquid, and gaseous fuels in hard-to-electrify sectors (such as construction, agriculture, aviation and shipping) even when emissions are net-zero (Supplementary Figure A.11). In this context, lower levels of final energy use per capita is one of the more robust trends of 1.5°C scenarios. Meanwhile, our finding that electricity is somewhat less prevalent at the net-zero point in scenarios with lower warming may reflect the additional time available for end uses to electrify in less ambitious (higher warming) scenarios (Fig. 1.1e and 1.1b).

Although the current carbon intensity of final energy (~81 Mt CO_2/EJ) declines drastically in many net-zero scenarios (Fig. 1.1d), the absolute quantity of residual emissions remains substantial in many of the scenarios—as often as not >10 Gt CO_2

globally in the net-zero year (Fig. 1.3). This translates into prodigious quantities of negative emissions required, with perhaps proportional social, techno-economic, and biophysical challenges (Fuss et al., 2014; Hepburn et al., 2019; P. Smith et al., 2016). But we also find that both the residual emissions and the negative emissions required to offset them are not evenly distributed across world regions (Figs. 1.2d and 1.3b), which may have important implications for human development and equity (Pozo, Galán-Martín, Reiner, Mac Dowell, & Guillén-Gosálbez, 2020). In particular, net-zero scenarios frequently show substantial negative emissions from land use in the Latin America region but the bulk of residual emissions occurring in other regions (Fig. 1.3b). Although the magnitude of negative emissions is not strongly related to the composition of the energy system, those scenarios with greater quantities of negative emissions from BECCS seem to also have greater levels of final energy demand and lower shares of non-biomass renewables (e.g., solar, wind, hydro; Fig. 1.4e). In contrast, the scenarios with greater negative emissions from land use (e.g., afforestation; represented by orange color in Figure 1.4f) also have higher final energy demand, but have higher shares of non-biomass renewables (Fig. 1.4f). This reflects a logical trade-off in the availability of bioenergy and land-based carbon storage and suggests that the balance in IAMs outputs is being influenced by the level of future energy demand. However, it should be noted that prior studies have found that the value of negative emissions from BECCS will be more important than the value of generated electricity (Mathilde Fajardy et al., 2021; Muratori, Calvin, Wise, Kyle, & Edmonds, 2016).

Finally, the relationships between energy use, GDP, and likely warming amount show that energy use is often limited in net-zero scenarios, especially for scenarios that limit warming to a greater extent (Fig. 1.1a). The median final energy consumption in global net-

zero scenarios is 521 (range 227-857) EJ, compared to 416 EJ in 2018 (IEA, 2019). Given that global population is expected to reach nearly 9.5 billion by 2064 (median net-zero year) in SSP2 (Samir & Lutz, 2016), if per capita energy use remains constant at ~55 GJ/person, total final energy consumption will approach 523 EJ in 2064 – approximately equal to the net-zero scenario level. If instead per capita energy use continues to increase by about 0.16 GJ/person per year, as it did from 1971-2018 on average (IEA, 2019; *World Development Indicators*, 2019), total final energy consumption will approach 588 EJ in 2064 – 67 EJ above the net-zero scenario level. So, in order to limit final energy use to ~521 EJ in the median net-zero year, mean global per-capita energy use would have to remain nearly constant.

The process-based IAMs considered here have proven extraordinarily useful for articulating the overall shape of long-term mitigation pathways at a macro-regional to global scale, but they are also limited in many ways that might influence our understanding of net-zero on a more detailed level. For example, because IAMs are designed to focus on larger-scale trends, they tend to have lower technological, temporal, and spatial resolutions compared with detailed energy system models (Bistline et al., 2020; Gambhir, Butnar, Li, Smith, & Strachan, 2019) and do not consider the broad range of societal dynamics and political economy factors that can drive national emissions reduction strategies. Their strength in comprehensiveness is therefore balanced by limits to the detail in which they can represent regional or technological details that may be very relevant for actual strategy making, particularly with regard to rapid and disruptive technological change (e.g., management of electricity grids with high penetration of variable renewables, electric cars, greater digitalization, and hydrogen utilization pathways in heavy industry). Some studies

have shown that because of this lower spatiotemporal detail, IAMs may be underestimating the role of variable renewables such as solar PV (Creutzig et al., 2017; Gambhir, Butnar, et al., 2019). Furthermore, in this study we do not explicitly consider the detailed aspects of the agriculture, forestry, and other land use (AFOLU) sector and non-CO_2 emissions; however, these aspects are accounted for in the IAM frameworks themselves, which consistently include the linkages and tradeoffs between AFOLU and non-CO_2 emissions. The global full-economy representation provided by IAMs in this context make them important tools in understanding pathways to net-zero greenhouse gas emissions balance as foreseen in Article 4 of the Paris Agreement. For all of these reasons, the net-zero scenarios we analyze here certainly do not reflect many of the details that will characterize net-zero emissions energy systems in the real world, but IAMs nonetheless remain critical bridges between more detailed energy systems models and long-term projections of climate change.

In the time since the SR1.5 database was released, increased efforts have been made to improve the model representation of key technologies, such as carbon-neutral liquid fuels, long-term storage of variable renewable energy, and negative emissions strategies. Given that these scenarios show liquid fuels remaining prevalent in the existing net-zero scenarios, such modeling improvements will be important to monitor going forward. The relationship between higher residual emissions and corresponding higher amounts of negative emissions in warmer scenarios points toward reducing residual emissions as a target for policy improvement, since negative emissions strategies are required to offset any amount of residual emissions at net-zero. Reliance on massive amounts of future negative emissions poses substantial risk, given that there is still considerable uncertainty

surrounding the feasibility of negative emissions technologies at such large scales (Fuss et al., 2014; P. Smith et al., 2016). Policies that support carbon-neutral fuels and technologies now would in turn reduce the amount we must rely on large amounts of negative emissions to avoid harmful levels of warming in the future. Our findings thus represent an opportunity to assess emerging policies and energy trends in the context of longer-term global goals of limiting climate change.

1.4 Methods

Data source. All of the model scenarios analyzed as part of this study were obtained from the public 1.5˚C Scenario Database (the SR1.5 database), hosted by the International Institute for Applied Systems Analysis (IIASA) through a process facilitated by the Integrated Assessment Modelling Consortium (doi: 10.5281/zenodo.3363345 | url: data.ene.iiasa.ac.at/iamc-1.5c-explorer). The model outputs in the database were generated by the various Integrated Assessment Models (IAMs) listed in Supplementary Table S1, and compiled by the Integrated Assessment Modeling Consortium (IAMC) (Huppmann, Kriegler, et al., 2018; Huppmann, Rogelj, et al., 2018). The full scenario set was curated as part of the IPCC Special Report of Global Warming of 1.5°C, Chapter 2 on mitigation pathways and details of the models and scenarios are detailed in the Technical Annex of the Chapter. The processes are described in more detail by Huppmann et al. (Huppmann, Kriegler, et al., 2018; Huppmann, Rogelj, et al., 2018). In this paper we use version r2.0 of the all regions dataset. The 177 scenarios we assess here were produced by 7 main models (with 16 individual model variations), and thus are not truly independent of each other since each IAM has its own assumptions built into the model framework.

While an updated scenario database is being developed for the upcoming IPCC Sixth Assessment Report (AR6), our analysis is specifically about the characteristic of the net-zero energy system at the point of net-zero, and not the pathway up to that point. The broader insights of net-zero energy system characteristics gained from our analysis are thus valuable and we expect they won't differ significantly in subsequent analyses of the next generation of (AR6) scenarios. Moreover, although recent developments in the power sector, e.g. renewables, have been faster than expected, the observed values for 2019-2020 are still within the range of the SR1.5 scenarios. For example, in 2020, approximately 2.94 EJ was generated from solar electricity (IEA, 2021) and the SR1.5 scenario outputs for Secondary Energy|Electricity|Solar range from 0.17-6.6 EJ, with a median value of 1.76 EJ and a mean value of 2.4 EJ. For wind energy, approximately 5.88 EJ was generated in 2020 (IEA, 2021), and the SR1.5 scenario outputs for Secondary Energy|Electricity|Wind range from 0.97-23.6 EJ, with a median value of 7.4 EJ and a mean value of 6.9 EJ.

IAMs have a long and sometimes controversial history in their efforts to characterize emissions pathways with the aim of mitigating climate change. The IAMs here are primarily what would be considered as complex "process-based" IAMs, as opposed to simpler "cost-benefit" IAMs that primarily simulate climate-economy relationships to estimate the social cost of carbon (Fisher-Vanden & Weyant, 2020).

They use a variety of over-arching modelling methods including linear programming, partial- and computable general equilibrium, and recursive-dynamic formulations. The models used tend to represent macro-economic regions, comprising large countries and trading blocs, ranging from a few to tens of regions with inter-regional trade of commodities, such as fuels and biomass. This regional information was aggregated in the

IPCC SR1.5 process to a common 5-region definition (as above) to facilitate comparison. Temporal resolution is typically at 5 or 10-year timesteps, which is good for determining the levels of investments required, whilst abstractions need to be made to ensure that reliability of electricity systems remains plausible, such as ensuring that enough flexible reserve is available to meet peak electricity demands.

Scenarios representing climate policy tend to be implemented using carbon budget constraints that limit the cumulative carbon emissions over a period such that warming does not pass the desired level, e,g. 2°C. Further scenario-related constraints may limit a wide range of parameters, such as technological options and shares, rates of change and diffusion, etc.

The IAMs whose scenarios we assess here do not include feedbacks from climate impacts and damages, despite the fact that some studies have shown these could be substantial (K. Calvin & Bond-Lamberty, 2018; Woodard, Davis, & Randerson, 2018). Rather the models are designed to inform mitigation efforts and have relatively simplistic representations of the Earth system (K. Calvin & Bond-Lamberty, 2018). Some IAMs are beginning to include feedbacks between, for example, temperature changes and energy use(Katherine Calvin, Patel, et al., 2019), and more ambitious efforts are underway that will incorporate human energy, food and water systems into robust Earth system models (Katherine Calvin, Bond-Lamberty, et al., 2019; Collins et al., 2015).

Filtering and analysis of scenarios. Our analysis includes only scenarios that reach net-zero CO_2 emissions by the end of this century (year 2100). We define the net-zero emissions year for each scenario (i.e., the x-axis in Fig. 1.1b) as the first year that net global

CO_2 emissions were equal to or less than zero. Because each model produces parameter outputs at 5- or 10-year time steps, we interpolated annual data using second-order polynomials.

We only consider CO_2 and not CH_4 or N_2O for several reasons. First, many of the current net-zero policy targets are for net-zero CO_2 specifically (J. Rogelj et al., 2021). Results from this analysis will therefore be relevant to those policies in the context of net-zero CO_2. Second, entirely eliminating CH_4 or N_2O emissions will entail development of new technologies, particularly for removing these gases from the atmosphere (R. B. Jackson, Solomon, Canadell, Cargnello, & Field, 2019), such that there are not yet practicable pathways to net-zero for these gases (J. Rogelj et al., 2021). Third, N_2O is primarily related to agriculture, and our analysis is focused on the energy system.

The scenarios are categorized into 6 regions (global and the five world regions defined in the SR1.5 database) and 3 consolidated levels of end-of-century global warming, based on the wider set determined in the IPCC report:

- 1.5˚C, which includes "below 1.5˚C," "1.5˚C return with low overshoot," "1.5˚C return with high overshoot";
- 2°C, which includes "lower 2.0˚C" and "higher 2.0˚C," and;
- >2°C, which corresponds to the category "above 2.0˚C". These scenarios have >50% likelihood of exceeding global mean temperature change of 2.0˚C by 2100, with no set upper bound of temperature change.

These global warming outcomes are primarily characterized by the "likely" (>50% chance) of reaching the specified temperature level by 2100. Further sub-categories of "overshoot"

scenarios, based on the peak-warming and then return to a stabilization temperature help identify between scenarios that rely on substantial amounts of net-negative emissions.

The output variables for IAMs in the SR1.5 database are not entirely consistent; some models have extensive lists of outputs and regional and sectoral breakdowns, while others have comparatively few outputs and are missing some variables altogether. Our analysis therefore relies only on those IAM scenarios that include all output variables required for our analysis (177 out of 202 total net-zero emissions scenarios; see Supplementary Table S1). Our interest in including as many scenarios as possible had to be balanced against our interest in exploring more detailed geographical and technological characteristics. Our analysis used the following 7 output variables: (1) CO_2 emissions (total net, energy and industrial processes net, AFOLU net), (2) Population, (3) GDP (PPP), (4) Primary energy, direct equivalent (total, fossil, nuclear, solar, wind, hydro, biomass), (5) Carbon Sequestration through BECCS, (6) Carbon price, and (7) Final energy (total and share from electricity). Residual CO_2 emissions were calculated by adding the residual emissions from energy and industrial processes (and, if applicable, the residual AFOLU emissions) to the amount of carbon sequestration from BECCS in the net-zero year via the following equations:

If 'Emissions|CO2|Energy and Industrial Processes' is *positive* at net-zero:

- 'Emissions|CO2|Residual Fossil' = 'Emissions|CO2| Energy and Industrial Processes' + 'Carbon Sequestration|CCS|Biomass'

If 'Emissions|CO2|Energy and Industrial Processes' is *negative* at net-zero:

- ‘Emissions|CO2|Residual Fossil’ = ‘Emissions|CO2| Energy and Industrial Processes’ + ‘Carbon Sequestration|CCS|Biomass’ + ‘Emissions|CO2|AFOLU’

Additional context for policymakers. Around the world, countries and jurisdictions are adopting energy policies that mandate high levels of renewable or zero-carbon electricity in the next few decades (IEA, 2020; Ross & Damassa, 2015). For example, in the U.S., 14 states (California, Colorado, Hawaii, Maine, Maryland, Massachusetts, Nevada, New Mexico, New Jersey, New York, Oregon, Vermont, Virginia, and Washington) have laws requiring that >50% of electricity come from renewables such as wind, solar and biomass (but often excluding large-scale hydropower). Such goals are consistent with our analysis of net-zero scenarios generated by IAMs: renewables (including hydro) account for >50% of all primary energy in 74% of the net-zero scenarios.

However, many locations have pledged or mandated 100% renewable electricity and/or 100% net-zero emissions economy-wide by 2050, including the proposed EU Climate Law, and laws or government orders in the U.S. states of Hawaii, New York, Washington, and California. Although details of these plans vary, it is noteworthy that very few of the net-zero scenarios reflect these goals at the macro region level. This is due to the way that sources and sinks, from energy and land use sectors, and between CO_2 and non-CO_2 sources, are optimized over much larger spatial extents including the influence of inter-regional trade, rather than policies that are enacted at state- and country-level. For example, the share of primary energy derived from renewables in the first year of net-zero or net-negative emissions is <80% in all but 2 of the 177 scenarios (Fig. 1.1c). Similarly, emissions in the OECD and EU region remain net-positive in more than half of the net-zero

scenarios (pink points in Fig. 1.2d). Thus, we advise caution when interpreting these results, to note that aforementioned zero-carbon energy policies are not necessarily over-ambitious or inconsistent with global and macro-regional IAM scenarios, because other nearby places and regions (e.g., Middle East and Africa), are likely to still be net-positive at the point at which global CO_2 emissions hit net-zero (Figure 1.2d).

1.5 Figures and Tables

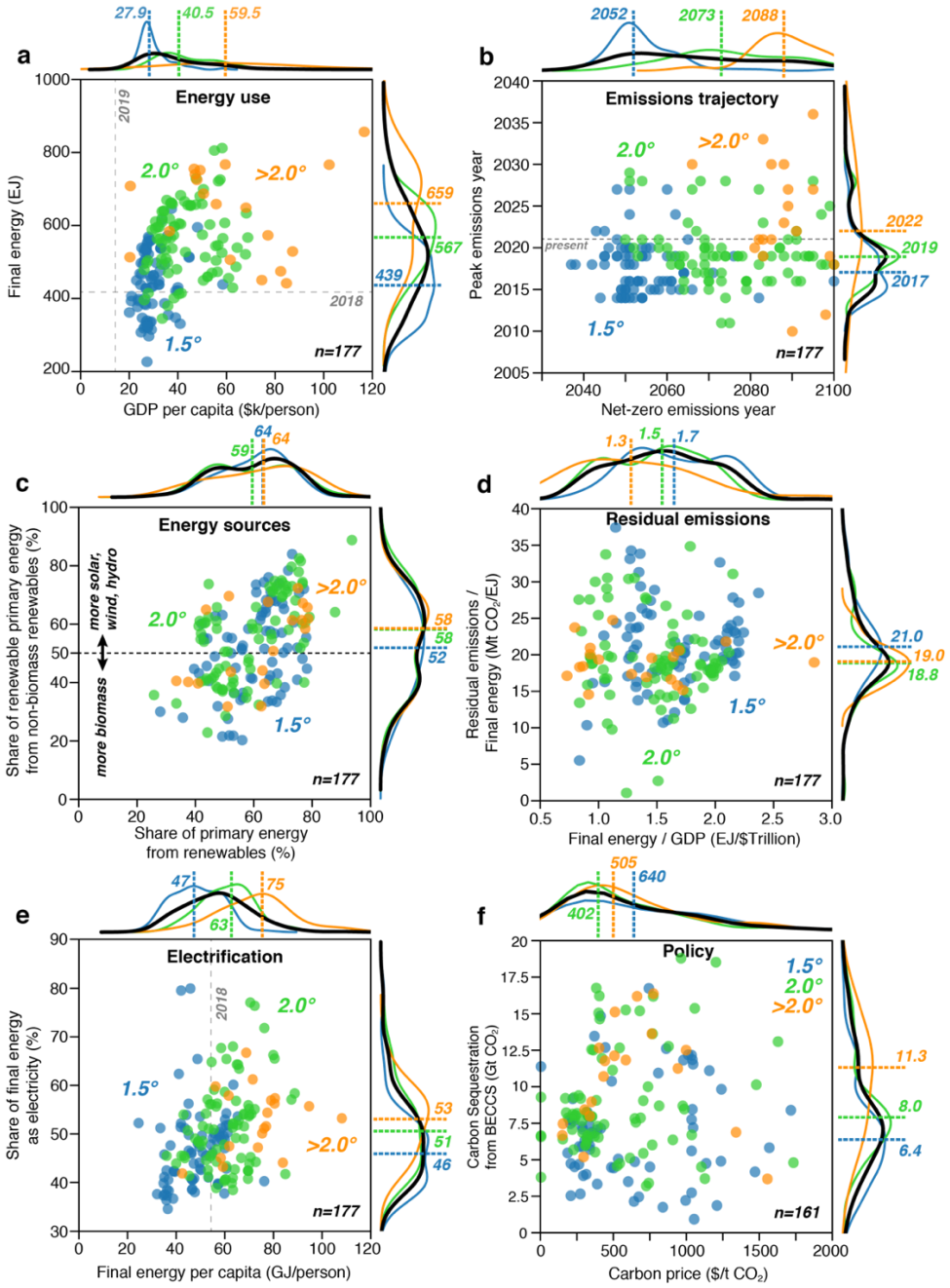

Figure 1.1 | Global net-zero emissions energy systems. Scenarios that reach net-zero emissions show differences in energy use (**a**), emissions trajectory (**b**), energy sources (**c**), residual emissions (**d**), electrification (**e**), and policy (**f**), particularly with respect to warming levels (blue = <1.5˚C, green = <2.0˚C, orange = >2.0˚C). Points represent individual scenarios, with frequency of scenarios shown along each axis for each warming level (colors corresponding to warming levels) and for all scenarios (black). Colored dashed lines and values indicate medians for warming groups, with colors corresponding to warming groups. Gray dashed lines indicate reference values for the year shown in gray.

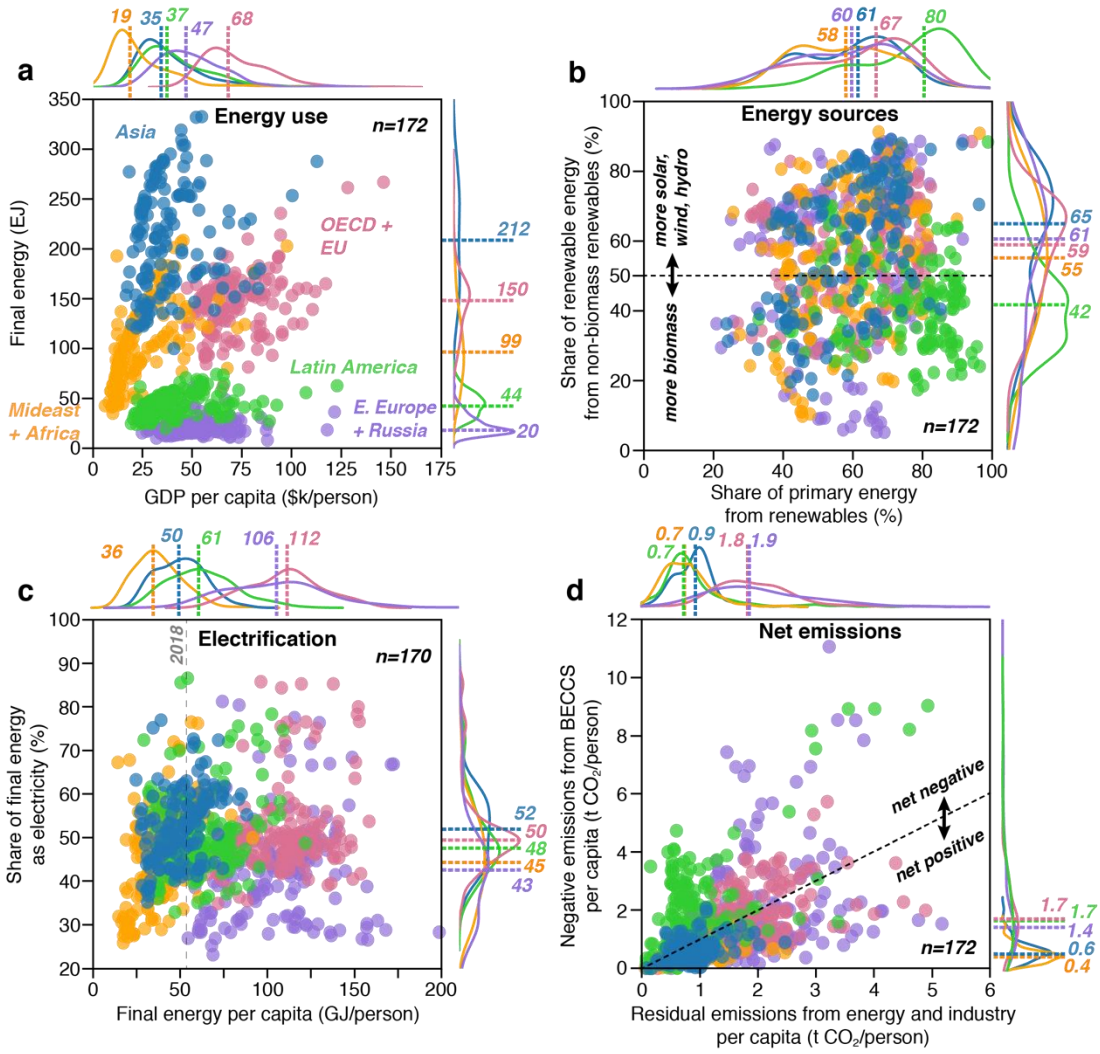

Figure 1.2 | Characteristics of regional energy systems and emissions when global emissions reach net-zero. Scenarios that reach net-zero emissions globally (n=175 scenarios with all regions) show regional differences in energy use (**a**), energy sources (**b**), electrification (**c**), and net emissions (**d**). Points represent individual scenarios, with frequency of scenarios shown along each axis for each region (Asia = blue, Latin America = green, Middle East+Africa = orange, OECD+EU countries = pink, and Eastern Europe+Russia = purple). Colored dashed lines and values indicate medians for each region.

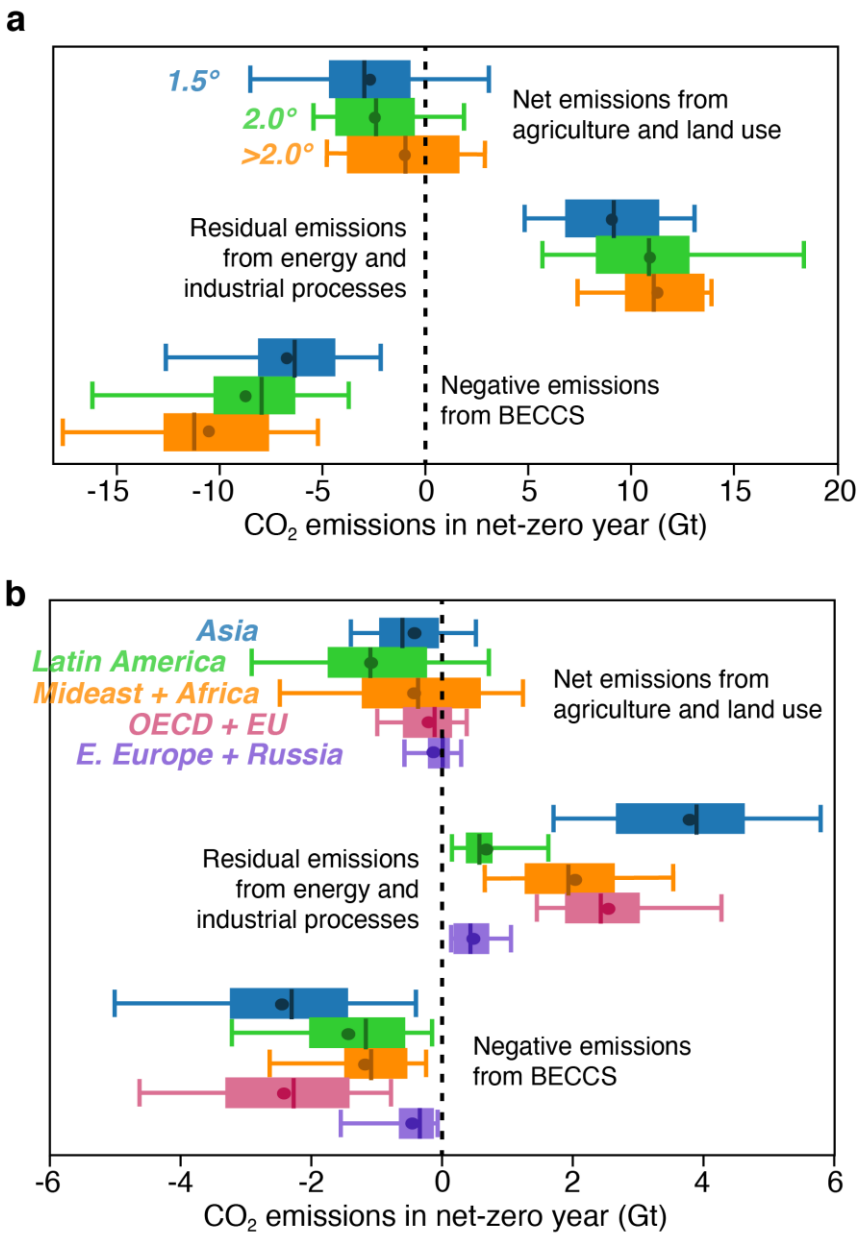

Figure 1.3 | Residual and negative emissions when global emissions reach net-zero. Residual and negative emissions in net-zero scenarios show global differences across different warming levels (**a**) and regions (**b**). In each case, the boxes show the range from 25th to 75th percentiles, whiskers show the 5th and 95th percentiles, and the lines and circles within the boxes denote the median and mean values, respectively.

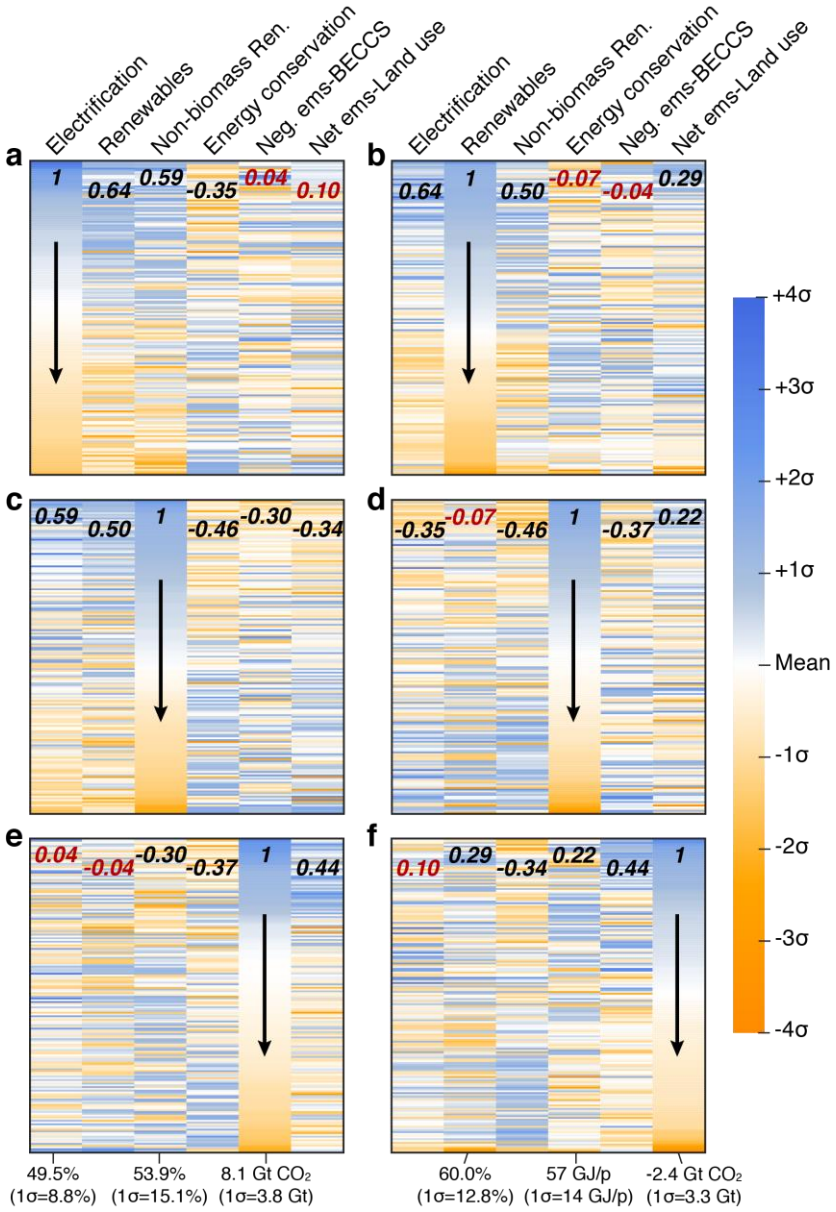

Figure 1.4 | Relative characteristics of scenarios in the year in which global emissions reach net-zero. "Electrification" is the share of final energy consumed as electricity. "Renewables" is the share of primary energy supplied by biomass, solar, wind, hydroelectricity, and geothermal. "Non-biomass ren." is the share of renewable energy sources provided by sources other than biomass. "Energy conservation" here reflects the inverse of final energy per capita, such that warmer colors indicate higher levels of energy consumption. "Negative ems-BECCS" is the total amount of negative emissions from bioenergy with carbon capture and storage. "Net ems-land use" is the net amount of global CO_2 emissions related to land use. Panels show scenario values (rows) sorted by (**a**) electrification, (**b**) renewables share, (**c**) non-biomass renewables share, (**d**) energy conservation, (**e**) negative emissions from BECCS, and (**f**) net land use emissions. Mean and standard deviation for parameters are shown below each column, and pairwise correlation coefficients (r) are shown in bold at the top of each column. Black r-values are statistically significant ($p < 0.05$), while red r-values are not.

Warming Category	Statistic	Final energy as electricity (%)	Primary Energy, Fossil (%)	Primary Energy, Nuclear (%)	Primary Energy, Renewable (%)	Renewable Energy, Non-biomass Renewables (%)	Final energy per capita (GJ/person)	Carbon seq., BECCS (Mt CO_2)	Net CO_2 emissions, land use (Mt CO_2)	Energy Intensity of GDP (EJ/ $Trillion)	Net-Zero Year
<1.5°C (n=77)	Median	46.1	32.6	4.8	63.5	51.9	47.4	6,356.8	-2,967.6	1.7	2052
	Mean	46.7	34.0	5.8	60.2	51.8	48.3	6,722.3	-2,696.9	1.7	2054
	Min	34.5	13.9	0	28.0	20.3	24.5	0	-13,477.0	0.8	2037
	Max	79.9	61.9	15.7	78.3	84.0	76.2	16,721.2	4,910.4	2.4	2100
2°C (n=81)	Median	50.9	34.2	4.8	59.4	58.4	62.8	7,977.4	-2,377.8	1.5	2073
	Mean	51.4	34.3	6.3	59.4	56.0	61.2	8,732.4	-2,462.1	1.5	2075
	Min	38.4	3.5	0.4	25.8	22.9	36.1	0	-17,152.1	0.8	2050
	Max	77.0	63.6	16.6	93.7	88.7	88.7	18,778.6	6,039.5	2.2	2100
>2°C (n=19)	Median	53.2	28.7	3.4	63.7	58.4	75.4	11,260.4	-962.1	1.3	2088
	Mean	52.6	31.2	7.3	61.5	53.3	73.0	10,505.6	-993.9	1.3	2088
	Min	41.8	18.3	0.2	33.5	31.8	42.5	3,721.0	-4,884.2	0.7	2066
	Max	66.7	51.7	23.4	78.7	72.3	108.1	16,355.9	5,410.9	2.9	2100
All (n=177)	Median	48.5	32.7	4.8	62.2	55.2	56.6	7,481.3	-2,503.8	1.6	2064
	Mean	49.5	33.8	6.2	60.0	53.9	56.8	8,048.3	-2,406.6	1.5	2067
	Min	34.5	3.5	0	25.8	20.3	24.5	0	-17,152.1	0.7	2037
	Max	79.9	63.6	23.4	93.7	88.7	108.1	18,778.6	6,039.5	2.9	2100
	F-stat	7.6	0.6	0.9	0.2	0.8	51.1	10.8	2.1	6.2	105.0
	p-value	<0.001	0.539	0.394	0.808	0.472	<0.001	<0.001	0.121	0.002	<0.001

Table 1.1 | Ranges of values in global scenario net-zero year. Median, mean, minimum, and maximum for each scenario group are shown for each variable. In the final two rows, the F-statistic from a one-way ANOVA test is shown for the "all scenarios" group, indicating the magnitude of variation between warming group means for that variable across all 177 scenarios. Statistical significance of the F-statistic is indicated by p-values (bottom row), with p-values <0.05 indicating that the variation between warming groups is statistically significant.

CHAPTER 2

Seaweed farming for climate change mitigation

The text of this chapter is adapted from:

DeAngelo, J., B.T. Saenz, I.B. Arzeno-Soltero, C. Frieder, M.C. Long, J. Hamman, K.A. Davis, and S.J. Davis. Economic and biophysical limits to seaweed farming for climate change mitigation. Nature Plants **9**, 45–57 (2023). https://doi.org/10.1038/s41477-022-01305-9

2.1 Introduction

Reaching net-zero CO_2 emissions will entail drastically reducing fossil fuel emissions and offsetting any residual emissions by removing carbon from the atmosphere (i.e. negative emissions) (Davis et al., 2018; DeAngelo et al., 2021; Fankhauser et al., 2022; Fuss et al., 2014; T. Gasser, Guivarch, Tachiiri, Jones, & Ciais, 2015). Biomass-based technologies may help on both fronts, by supplying carbon-neutral alternatives to fossil fuels (Reid, Ali, & Field, 2020; Vardon, Sherbacow, Guan, Heyne, & Abdullah, 2022) and providing negative emissions via enhancement of natural sinks (Griscom et al., 2017) and/or bioenergy with carbon capture and storage (Hanssen et al., 2020). However, numerous studies have questioned whether terrestrial biomass can provide either energy or negative emissions at the scales required in many climate mitigation scenarios, often owing to limited land and water resources (M. Fajardy & Mac Dowell, 2017; Heck, Gerten, Lucht, & Popp, 2018; P. Smith et al., 2016). This has driven surging interest in ocean-based carbon dioxide removal, including via cultivated macroalgae (seaweed), which would not require inputs of land or freshwater and might have environmental co-benefits (e.g., (AIEEP, 2021; Bach et al., 2021; Duarte et al., 2017; Froehlich et al., 2019; Gao et al., 2021; Gattuso et al., 2021; Krause-

Jensen & Duarte, 2016; NASEM, 2021; Wu et al., 2022)). Seaweed products might also help to lower greenhouse gas emissions, for example by reducing methane emissions from ruminants (Breanna M. Roque et al., 2019), and replacing fossil fuels (Freeman & von Keitz, 2017) and emissions-intensive agricultural products (Hong et al., 2021).

Seaweed has been successfully farmed in some places for centuries, and used for food, animal feed, and in more modern times, cosmetics, medicine, fertilizer, and biofuels (Aitken, Bulboa, Godoy-Faundez, Turrion-Gomez, & Antizar-Ladislao, 2014; Buschmann et al., 2017; Ghadiryanfar, Rosentrater, Keyhani, & Omid, 2016; Soleymani & Rosentrater, 2017). Production of seaweed for food increased 6% per year from 2000-2018 (FAO, 2020b) and seaweed harvest totaled ~1 million tons of carbon worldwide in 2018 (FAO, 2020b). In comparison, climate scenarios that limit warming to 1.5˚ or 2˚C generally require more than 1 gigaton of carbon (i.e. >3.67 Gt CO_2) to be removed annually from the atmosphere in the year CO_2 emissions reach net-zero (DeAngelo et al., 2021). To contribute to such climate goals, seaweed farming must therefore expand tremendously, and in turn contend with large uncertainties in the productivity of different types of seaweed in different places, the net costs of farming, the magnitude of emissions avoided or carbon sequestered, and the potential for undesirable ecological impacts. Recent studies of seaweed farming have examined localized opportunities and dynamics in particular regions (Bach et al., 2021; Gao et al., 2021; Hadley, Wild-Allen, Johnson, & Macleod, 2015), made rough estimates of the global potential (de Ramon N'Yeurt, Chynoweth, Capron, Stewart, & Hasan, 2012; Froehlich et al., 2019; Gattuso et al., 2021; Lehahn, Ingle, & Golberg, 2016), and modeled the Earth system response to gigaton-scale production (Wu et al., 2022). Yet the productivity, costs, and potential climate benefits of such farming are

spatially heterogeneous and scale-dependent, and the key sensitivities and trade-offs important to investors and decision makers have not been comprehensively evaluated. Here, we use coupled biophysical and technoeconomic models to systematically assess the economic costs and potential climate benefits of seaweed farming, testing their sensitivity across large ranges in individual variables and comparing different product pathways.

Details of our analytic approach are described in the *Methods*. In summary, we use outputs from a newly-developed biophysical model (G-MACMODS) (Arzeno-Soltero et al., 2022; Frieder et al., 2022) to estimate potential harvest of four different seaweed types (tropical red, tropical brown, temperate red, and temperate brown; Supplementary Fig. B.1) at a resolution of 1/12° (~9 km at the equator) globally. Nutrients are a key constraint on seaweed growth. G-MACMODS assumes that nitrogen is the limiting nutrient and we model two idealized scenarios: an "ambient" nutrient scenario that computes growth based on observed, climatological surface nitrate concentrations, and a "limited nutrient" scenario that computes growth rate based on ambient nitrate concentrations, but limits algal biomass increases so as not to exceed the magnitude of local natural (upward) nitrate supply as estimated by a high-resolution simulation of the Community Earth System Model (Harrison, Long, Lovenduski, & Moore, 2018). Based on the simulated yields, we then calculate spatially-explicit costs per ton of seaweed harvested and either costs per ton of GHG emissions avoided (when used as food, feed, or for biofuels) or costs per ton of carbon removed from the atmosphere as a carbon dioxide removal (CDR) strategy. Given the large uncertainty in technoeconomic parameters, we perform a Monte Carlo simulation with n=5,000 for each nutrient scenario, assuming uniform distributions of each variable. Technoeconomic variables include (1) farming costs (e.g., capital cost, harvest costs), (2)

for carbon sequestration, the fraction of sunk seaweed carbon sequestered for > 100 years in the deep sea, and (3) for GHG emissions mitigation, the net cost and net emissions of seaweed transported and converted into a product (Table 2.1; see Supplementary Tables B.1 and B.2 for listings of all variables and relevant sources). We test the model sensitivity to seaweed yield by sampling from a normal distribution of seaweed yield uncertainty for each Monte Carlo simulation. Additionally, because seaweed draws carbon from the surface ocean dissolved inorganic carbon pool (which does not maintain instantaneous equilibrium with the atmosphere) and because large-scale seaweed farming can reduce natural carbon uptake by phytoplankton via nutrient competition, we include a variable representing the net efficiency of seaweed growth in reducing atmospheric CO_2 ("atmospheric removal fraction"; Supplementary Table B.1). Our approach is predicated on large uncertainties associated with most of the variables we analyze, not only in the future but also the present (the relatively few costs reported in the literature are location- and/or species-specific), as well as our primary goal of informing future research by identifying relative differences, sensitivities and trade-offs that are robust across our simulations.

2.2 Results

Seaweed production cost

The maps in Figure 2.1 show the range of modeled seaweed production costs (i.e. $ per ton of harvested dry weight prior to transport) in different regions under the ambient nutrient scenario and assuming the most-productive type of seaweed is grown in each grid cell (Supplementary Fig. B.2 shows analogous costs for limited nutrient scenario). Minimum modeled costs (Figs. 2.1a, d) thus reflect high levels of seaweed growth (ambient

nutrients) and very low assumed costs of farming, whereas the maximum costs in Supplementary Fig. B.2c and B.2f reflect lower levels of seaweed growth in most areas (limited nutrients) and high-end cost assumptions. Since our ability to accurately assess the role of nutrient constraints as a determinant of yield is a major driver of total uncertainty in cost, our results are thereby likely to encompass a wide range of outlooks, including substantial future reductions in farming costs related to technological breakthroughs, returns to scale, and boosted productivity (e.g., autonomous farms, depth cycling, artificial upwelling, and offshore integrated multi-trophic aquaculture (Gao, Beardall, et al., 2022; Gao, Gao, Fu, Li, & Xu, 2022)).

Although the spread in average cost in the 1% of ocean area where costs are lowest (labels beneath each panel) range from $190-$2,790 per ton of dry weight (tDW) seaweed yield, regional patterns of production costs are relatively consistent across cost simulations (Fig. 2.1). For example, the equatorial Pacific, Gulf of Alaska, and southeastern edge of South America are consistently among the lowest cost areas to produce seaweed (yellow and green shading in Fig. 2.1), and there are large swaths of ocean that cannot produce seaweed for <$2,000/tDW in any case (areas shaded blue in Fig. 2.1). These patterns reflect the combination of seaweed productivity and the associated number of harvests (Supplementary Figs. B.3 and B.4, respectively). Higher harvest costs can erode the cost advantage of highly productive areas: for example, despite having much lower seaweed yields per unit area, the North Pacific's lower harvest costs lead to production costs that are often similar to those in the Equatorial Pacific (Fig. 2.1 and Supplementary Fig. B.3). Moreover, because transportation of harvested seaweed is not included in the at-farm production costs but rather in the post-cultivation costs (see *Methods*), some areas of open

ocean far from ports have low at-farm production costs. On average, the costs of seeded line, total harvest costs, and capital costs (including mooring costs) dominate total production costs, representing 56(32-92)%, 19(4-38)%, and 17(3-33)% across seaweed types, respectively (Supplementary Fig. B.5).

Finally, since global seaweed yield is reduced in simulations that limit nutrient availability to natural vertical nutrient fluxes, the production costs in the 1% of ocean area with the lowest cost are much higher ($350-$7,150 per ton of dry weight; Supplementary Fig. 2.2) than in simulations in which seaweed is allowed to use all ambient nutrients. This suggests that without methods to enhance nutrient availability (e.g., depth cycling, artificial upwelling, or offshore integrated multi-trophic aquaculture (Gao, Beardall, et al., 2022; Gao, Gao, et al., 2022)), limiting seaweed yields to maintain surface ocean nutrient levels might be cost-prohibitive except in the most optimistic technoeconomic scenarios.

Net cost of climate benefits

The maps in Figure 2.2 show net costs of different climate benefits from farmed seaweed. We choose to show costs when propagating the most optimistic assumptions (5th percentile costs) from ambient nutrient simulations to reflect low-cost results that might be achieved with economies of scale (Supplementary Figs. B.6 and B.7 show results under limited nutrients and for median net costs, respectively). We define the cost to sequester carbon via sinking seaweed as the $/t$CO_2$ removed from the atmosphere for at least 100 years, assuming no other economic value. In contrast, costs of emissions avoided by using produced seaweed for food, feed or biofuel are given in units of $/t$CO_2$-eq and in each case reflect seaweed production, transportation and conversion costs, and the product's market

value as well as the CO_2-equivalent GHG emissions (CH_4 and N_2O assuming GWP_{100}) displaced by the product net of any emissions related to transportation and processing (see *Methods*). When calculating GHG emissions avoided, we assume that products made from seaweed can directly replace conventional food (pulses, vegetables, fruits, oil crops, and cereals), feed (oil crops and cereals), and fuels, thereby avoiding GHG emissions from industrial agriculture practices or CO_2 emissions from fossil fuel combustion (Hong et al., 2021). For example, if seaweed is used for food and replaces some amount of vegetables in a person's diet, then the GHG emissions associated with the production of those vegetables that the seaweed replaces are counted as avoided emissions.

In the lowest-cost 1% ocean areas, the average cost is much higher per ton of carbon sequestered by sinking seaweed ($540/t$CO_2$) than per ton of CO_2-eq emissions avoided—regardless of whether the seaweed is used for food ($20/t$CO_2$-eq), animal feed ($140/tCO_2-eq), or biofuel ($320/t$CO_2$-eq). The substantial cost difference between sequestration by sinking and emissions avoided by products is most influenced by the products' market value and the potential to avoid non-CO_2 GHGs, despite the higher cost and emissions required to transport harvested seaweed to port.

In particular, the non-CO_2 GHG emissions that could be avoided by using seaweed for either food consumed by humans or feed consumed by animals effectively multiply the potential climate benefits of a ton of seaweed carbon, whereas the climate benefits of either sinking or converting seaweed to biofuels are constrained by the carbon present in the seaweed itself. Yet carbon sequestration is nonetheless favored in some locations given the high costs of transporting seaweed back to the nearest port (e.g., areas of the equatorial

Pacific that are shaded yellow and green in Fig. 2.2a and blue in Figs. 2.2c; see also Supplementary Fig. B.8).

Key sensitivities

Figure 2.3 shows the relative importance of all variables in generating spread in our Monte Carlo estimates of production costs and net costs of climate benefits, focusing on the lowest-cost areas (Supplementary Fig. B.9 shows the same results for limited nutrient simulations). These results emphasize which variables are most important to achieving very low costs. Low production costs are most sensitive to seaweed yields, followed by the cost of seeded line (secondary line with seaweed seedlings that is wrapped around a structural rope, or nets for some temperate red seaweeds; yellow in Fig. 2.3a) and capital costs (e.g., boats, harvest machines, buoys, anchors, and other lines; green in Fig. 2.3a). Together, seaweed yield and seeded line cost account for >89% of the uncertainty in production costs in the places where costs are lowest, and costs are never below $400/tDW in simulations where seeded line is assumed to cost >$1 per meter.

Costs of carbon sequestered are quite sensitive to production costs (incl. all parameters shown in Fig. 2.3a), but the most important parameter aside from production costs and yield is the fraction of the seaweed carbon that corresponds to equivalent carbon removal from the atmosphere (light green in Fig. 2.3b). Although this fraction has generally been assumed to be 1, recent studies have shown that air-sea fluxes of CO_2 may not keep pace with carbon uptake by growing seaweed and, among other mechanisms that reduce efficiency, nutrient competition from farmed seaweed may diminish natural carbon uptake and export accomplished by phytoplankton (Bach et al., 2021; Wu et al., 2022). The

atmospheric removal fraction accounts for >24% of the variation in sequestration costs in the places where costs are lowest, and costs are never below \$400/tCO_2 sequestered unless the removal fraction is assumed to be >0.6 (Figs. 2.3b and 2.3e).

Our estimates of cost per GHG emissions avoided are most sensitive to the assumed magnitude of CO_2-equivalent emissions avoided by a seaweed product (light blue in Fig. 2.3c). The product avoided emissions accounts for >38% of the variation in costs per emissions avoided in the places where costs are lowest, and costs are never more than \$700/tCO_2-eq avoided in simulations where the product avoided emissions are assumed to be >4.25 tCO_2-eq/tDW seaweed (Figs. 2.3c and 2.3f). Yet production costs remain important, and low costs of emissions avoided (<\$200/ tCO_2-eq) can be achieved even when the avoided emissions are <1 tCO_2-eq/tDW if seaweed production costs are very low (Figs. 2.3c and 2.3f).

Costs and benefits of large-scale farming seaweed

Figure 2.4 shows the cumulative potential of GHG emissions avoided or carbon sequestered in the 1% of ocean areas with the lowest costs, shaded with costs per ton based on the 5^{th} percentile of 5,000 ambient nutrient cost simulations (i.e. reflecting optimistically high seaweed yield, low farming costs, and large climate benefits from replacement of agricultural products; Supplementary Figs. B.10 and B.11 shows results for median costs and limited nutrient scenario). No matter the scenario or percentile, in the 1% of areas with the lowest costs, the costs per ton of CO_2 sequestered are always higher than the costs per ton of CO_2-eq emissions avoided. In the optimistic case depicted in Figure 2.4, 1 Gt of CO_2-eq emissions might be avoided or 1 Gt of CO_2 sequestered by farming

0.025% and 0.110% of lowest-cost ocean areas, respectively, (roughly 90,000 km^2 and 400,000 km^2 or close to the areas of Portugal and Zimbabwe, respectively) at an average profit of \$50/tCO_2-eq emissions avoided or at an average cost of \$480/tCO_2 sequestered. In limited nutrient simulations with optimistic cost assumptions (Supplementary Fig. B.11a, B.11b), the lowest-cost ocean area that might be required to reach 1 Gt CO_2-eq avoided emissions or 1 Gt CO_2 sequestered annually is 0.035% and 0.100% for avoided emissions and sequestration, respectively, or roughly 130,000 km^2 and 360,000 km^2, with associated costs of \$30/tCO_2-eq avoided and \$830/tCO_2 sequestered. Average costs at the median of Monte Carlo simulations for both nutrient scenarios rise substantially to \$110-310/tCO_2-eq emissions avoided or \$1,120-\$2,090/tCO_2 sequestered, respectively (Supplementary Figs. B.10, B.11a, B.11b). These costs increase to \$140-420/tCO_2-eq at 3 Gt CO_2-eq avoided and to \$1,190-2,280/tCO_2 at 3 Gt CO_2 sequestered annually, requiring ocean areas of 0.085-0.100% and 0.285-0.410% for avoided emissions and sequestration, respectively (roughly 310,000-360,000 km^2 and 1,030,000-1,480,000 km^2). Moreover, climate benefits increase approximately linearly with area up to 1% of ocean area, reaching totals of >29 Gt CO_2-eq avoided or >9 CO_2 sequestered annually in the ambient nutrient simulations and >19 Gt CO_2-eq avoided or >8 CO_2 sequestered annually in the limited nutrient simulations.

Supplementary Figure B.12 shows the locations of the lowest cost areas in Figure 2.4, which, for sequestration, are concentrated in the equatorial Pacific and Gulf of Alaska, and for avoided emissions products include additional areas offshore of Argentina, the Korean Peninsula, and New Zealand as well as areas of the North and Norwegian Seas. Importantly, we estimate that perhaps 10-15% of lowest cost areas for sequestration and 40-45% of lowest cost areas for avoided emissions are either in highly-trafficked shipping lanes or

part of existing marine protected areas (see *Methods*), which could present challenges for seaweed farming in these areas.

Despite being a small percentage of global ocean area, farming 0.025% of the global ocean area (~90,000 km^2) would represent over a thirty-fold increase in the area of current seaweed farming (~2,700 km^2; (FAO, 2020a, 2020b; Hwang, Yotsukura, Pang, Su, & Shan, 2019)). Thus, producing seaweed in the lowest cost areas to reach 1 Gt CO_2-eq of emissions avoided or 1 Gt CO_2 sequestered by 2050 would entail the area farmed to increase by roughly 12% or 18% per year, respectively, compared to the 2000-2018 seaweed farming industrial growth rate of 6% (FAO, 2020b). Achieving the same level of climate benefits from seaweed by 2030 increases the implied expansion rate of farms to roughly 42% or 64% per year for emissions avoided or carbon sequestered, respectively. Note that these areas and industry growth rates reflect the minimum that might be required for gigaton-scale climate impact, since the ambient nutrient scenario assumes that all surface ocean nutrients are available for seaweed growth. In the limited nutrient scenario, reaching 1 Gt CO_2-eq of emissions avoided in the lowest-cost areas by 2050 might require ~130,000 km^2, which would represent nearly a 50-fold increase in the area currently farmed and would entail a 14% annual growth rate.

2.3 Discussion

Our results suggest that it might be possible to sequester >1 $GtCO_2$ at costs as low as \$480/tCO_2 if nearly all seaweed carbon corresponds directly to an amount of CO_2 removed from the atmosphere, production costs are reduced to near the lowest published costs (Camus, Infante, & Buschmann, 2019; van den Burg, van Duijn, Bartelings, van Krimpen, &

Poelman, 2016) (e.g., seeded line and capital costs of <$0.40/m and $3,300/ha, respectively), and/or seaweed yields are high (e.g., >6,000 tDW/km^2 for tropical reds and >2,000 tDW/km^2 for temperate browns). Nonetheless, $480/t$CO_2$ is comparable to the $500-600 t/$CO_2$ costs of direct air capture (DAC) reported by the company Climeworks (Temple, 2021) (but much more than $94-$232 DAC costs estimated by Keith et al. (Keith, Holmes, St. Angelo, & Heidel, 2018)). Sequestration costs also rise sharply if the assumed atmospheric removal fraction or seaweed yield decreases or if production costs increase (Supplementary Figs. B.7 and 10, Fig. 2.3e). In comparison, >1 GtCO_2-eq emissions might be avoided at a profit of $50/t$CO_2$-eq if similarly low production costs are achieved and seaweed products avoid emissions of >3 tCO_2-eq/tDW (e.g., by displacing vegetables, legumes, or soy from some regions). Although the cost per emission avoided is typically higher if seaweed is instead used for biofuels (Fig. 2.2; Supplementary Figs. B.6, B.7), such fuels may command a substantial "green premium" as countries seek to decarbonize aviation and long-distance transportation of freight (Christopher Bataille et al., 2020; Davis et al., 2018; Gray, McDonagh, O'Shea, Smyth, & Murphy, 2021; Vardon et al., 2022).

Although it is thus conceivable that farmed seaweed could feasibly deliver globally-relevant climate benefits, our modeling and cost estimates are subject to important caveats and limitations. First, modeled economic parameter ranges are broad, spanning a relatively small number of divergent data points from publicly available datasets and scientific literature. In some cases, these ranges were extended downward to reflect potential future cost reductions that were not represented by existing data. Better constraining these cost ranges for both current and future scenarios would improve the model and reduce uncertainty. Similarly, future work could analyze in greater detail the specific types and

scale of agricultural or energy products that might be displaced by seaweed and their GHG emissions. Although the relative benefits of avoiding different GHG emissions versus sequestering carbon for different periods of time are beyond the scope of our analysis, they may be important to investors and decision makers. For example, in many potentially low-cost seaweed production regions, the time scale of sunk carbon that remains "sequestered" in the deep ocean is less than 100 years; if CDR accounting requires multi-century sequestration, the cost of seaweed-based CDR may become prohibitively high.

There are also large sources of uncertainty that deserve further exploration in the future. For example, we find that estimated costs per ton of CO_2-eq emissions avoided or CO_2 sequestered are highly sensitive to both the nutrient scenario (ambient vs. limited nutrients, Figure 2.2 and Supplementary Fig. B.6) and yield uncertainty within each nutrient scenario. Nutrient reallocation from competition between farmed seaweed and phytoplankton is also a critical dynamic that warrants analysis in the context of a fully coupled earth system model, since farming seaweed at gigaton-scales would likely diminish natural carbon uptake by phytoplankton and therefore reduce the net drawdown of atmospheric CO_2 (Berger, Bopp, Ho, & Kwiatkowski, 2022). Moreover, our climate benefit calculations do not include particulate seaweed biomass that may be exported to the deep sea prior to harvest (analogous to sinking ~5% of the harvested biomass (Krause-Jensen & Duarte, 2016)), and we also do not consider any potential non-CO_2 GHG emissions from the seaweed cultivation process. The G-MACMODS model also assumes that nitrogen is the limiting macronutrient for seaweed growth (and micronutrients are supplemented by farming techniques), and while nitrogen limits production in large parts of the ocean, phosphorus might be more limiting in some regions. Finally, we must continue to evaluate

the potential consequences to ocean ecosystems and biogeochemical cycles before seriously considering farming and/or sinking gigatons of seaweed (Wu et al., 2022).

Despite these uncertainties and limitations, our analysis supports continued research, development, and demonstration of the potential for seaweed farming to produce meaningful climate benefits. Specifically, our model highlights the most important targets for research and innovation. Biophysical factors such as death (including disease, pests, weather events) and exudation rates are not well-established and may substantially alter projected seaweed yields (Arzeno-Soltero et al., 2022); regional biogeochemical and Earth system feedbacks could similarly undermine the efficacy of sinking seaweed carbon; and low or narrow demand for seaweed products could limit the potential to offset land-use and fossil GHG emissions. Finally, although some seaweed innovators are focused on farm designs that reduce labor and transportation costs, our results suggest that the keys to maximizing yield with low production costs are seeded line and basic farm equipment like boats, buoys, and anchors. But even if seed and capital costs are minimized, seaweed CDR seems likely to be more expensive than alternatives like direct air capture, and it is not clear that there are viable and large markets for seaweed products. These factors, combined with the challenges inherent to verification and monitoring as well as the potential for ecosystem disruption, suggest that expansion of seaweed cultivation should be approached with caution. The outlook for a massive scale-up of seaweed climate benefits is thus decidedly murky, but our findings can help direct research, investments, and decision making to clear the waters.

2.4 Methods

Monte Carlo analysis

Seaweed production costs and net costs of climate benefits were estimated based on outputs of the biophysical and technoeconomic models described below. The associated uncertainties and sensitivities were quantified by repeatedly sampling from uniform distributions of plausible values for each cost and economic parameter (n=5,000 for each nutrient scenario from the biophysical model, for a total of n=10,000 simulations; see Supplementary Figs. B.14, B.15) (Bryant & Lempert, 2010; Lawrence, Haasnoot, & Lempert, 2020; Lempert, Groves, Popper, & Bankes, 2006; Lindroos, Rydén, Langørgen, Pursiheimo, & Pikkarainen, 2019; Rozenberg, Davis, Narloch, & Hallegatte, 2015; Vermeulen et al., 2013). Parameter importance across Monte Carlo simulations (Fig. 2.3 and Supplementary Fig. B.9) was determined using decision trees in LightGBM, a gradient-boosting machine learning framework.

Biophysical Model

G-MACMODS is a nutrient-constrained, biophysical macroalgal growth model with inputs of temperature, nitrogen, light, flow, wave conditions, and amount of seeded biomass (Broch & Slagstad, 2012; Hadley et al., 2015), that we use to estimate annual seaweed yield per area (either in tons of carbon or tons of dry weight biomass per km^2 per year) (Arzeno-Soltero et al., 2022; Frieder et al., 2022). In the model, seaweed takes up nitrogen from seawater, and that nitrogen is held in a stored pool before being converted to structural biomass via growth (Droop, 1983). Seaweed biomass is then lost via mortality, which includes breakage from variable ocean wave intensity. The conversion from stored

nitrogen to biomass is based on the minimum internal nitrogen requirements of macroalgae, and the conversion from biomass to units of carbon is based on an average carbon content of macroalgal dry weight (~30%) (Duarte, 1992). The model accounts for farming intensity (sub-grid-scale crowding) and employs a conditional harvest scheme, where harvest is optimized based on growth rate and standing biomass (Arzeno-Soltero et al., 2022).

The G-MACMODS model is parameterized for four types of macroalgae: temperate brown, temperate red, tropical brown, and tropical red. These types employed biophysical parameters from genera that represent over 99.5% of present-day farmed macroalgae (Eucheuma, Gracilaria, Kappahycus, Sargassum, Porphyra, Saccharina, Laminaria, Macrocystis) (FAO, 2020a). Environmental inputs were derived from satellite-based and climatological model output mapped to 1/12-degree global resolution, which resolves continental shelf regions. Nutrient distributions were derived from a 1/10-degree resolution biogeochemical simulation led by the National Center for Atmospheric Research (NCAR) and run in the Community Earth System Model (CESM) framework (Harrison et al., 2018).

Two nutrient scenarios were simulated with G-MACMODS and evaluated using the technoeconomic model analyses described below: the "ambient nutrient" scenario where seaweed growth is computed using surface nutrient concentrations without depletion or competition, and "limited nutrient" simulations where seaweed growth is limited by an estimation of the nutrient supply to surface waters (computed as the flux of deep-water nitrate through a 100-m depth horizon). For each Monte Carlo simulation in the economic analysis, the technoeconomic model randomly selects either the 5^{th}, 25^{th}, 50^{th}, 75^{th}, or 95^{th}

percentile G-MACMODS seaweed yield map from a normal distribution to use as the yield map for that simulation. Figures and numbers reported in the main text are based on the ambient nutrient scenario; results based on the limited nutrient scenario are shown in Supplementary Figures.

Technoeconomic model

We estimate the net cost of seaweed-related climate benefits by first estimating all costs and emissions related to seaweed farming, up to and including the point of harvest at the farm location, then estimating costs and emissions related to the transportation and processing of harvested seaweed, and finally estimating the market value of seaweed products and either carbon sequestered or GHG emissions avoided.

Production costs and emissions. Spatially-explicit costs of seaweed production ($/tDW) and production-related emissions (tCO_2/tDW) are calculated based on ranges of capital costs ($/km^2), operating costs (incl. labor, $/km^2), harvest costs ($/km^2), and transport emissions per distance traveled (tCO_2/km) in the literature (Table 2.1, Supplementary Tables B.1 and B.2); annual seaweed biomass (tDW/km^2, for the preferred seaweed type in each grid cell), line spacing, and number of harvests (species-dependent) from the biophysical model; as well as datasets of distances to the nearest port (km), ocean depth (m), and significant wave height (m).

Capital costs are calculated as:

$$c_{cap} = c_{capbase} + \left(c_{capbase} \times (k_d + k_w)\right) + c_{sl} \quad (1)$$

where c_{cap} is the total annualized capital costs per km^2, $c_{capbase}$ is the annualized capital cost

per km^2 (e.g., cost of buoys, anchors, boats, structural rope) prior to applying depth and wave impacts, k_d and k_w are the impacts of depth and waviness on capital cost, respectively, each expressed as a multiplier between 0 and 1 modeled using our Monte Carlo method and applied only to grid cells where depth > 500m and/or significant wave height > 3m, respectively, and c_{sl} is the total annual cost of seeded line calculated as:

$$c_{sl} = c_{slbase} \times p_{sline} \quad (2)$$

where c_{slbase} is the cost per meter of seeded line, and p_{sline} is the total length of line per km^2, based on the optimal seaweed type grown in each grid cell.

Operating and maintenance costs are calculated as:

$$c_{op} = c_{ins} + c_{lic} + c_{lab} + c_{opbase} \quad (3)$$

where c_{op} is the total annualized operating and maintenance costs per km^2, c_{ins} is the annual insurance cost per km^2, c_{lic} is the annual cost of a seaweed aquaculture license per km^2, c_{lab} is the annual cost of labor excluding harvest labor, and c_{opbase} is all other operating and maintenance costs.

Harvest costs are calculated as:

$$c_{harv} = c_{harvbase} \times n_{harv} \quad (4)$$

where c_{harv} is the total annual costs associated with harvesting seaweed per km^2, $c_{harvbase}$ is the cost per harvest per km^2 (including harvest labor but excluding harvest transport), and n_{harv} is the total number of harvests per year.

Costs associated with transporting equipment to the farming location are calculated as:

$$c_{eqtrans} = c_{transbase} \times m_{eq} \times d_{port} \quad (5)$$

where $c_{eqtrans}$ is total annualized cost of transporting equipment, $c_{transbase}$ is the cost to transport 1 ton of material 1km on a barge, m_{eq} is the annualized equipment mass in tons, and d_{port} is the ocean distance to the nearest port in km.

The total production cost of growing and harvesting seaweed is therefore calculated as:

$$c_{prod} = \frac{(c_{cap}) + (c_{op}) + (c_{harv}) + (c_{eqtrans})}{s_{dw}} \quad (6)$$

where $\boldsymbol{c_{prod}}$ is total annual cost of seaweed production (growth + harvesting), c_{cap} is as calculated in eq. (1), c_{op} is as calculated in eq. (3), c_{harv} is as calculated in eq. (4), $c_{eqtrans}$ is as calculated in eq. (5), and s_{dw} is the dry weight of seaweed harvested annually per km^2.

Emissions associated with transporting equipment to the farming location are calculated as:

$$e_{eqtrans} = e_{transbase} \times m_{eq} \times d_{port} \quad (7)$$

where $e_{eqtrans}$ is the total annualized CO_2 emissions in tons from transporting equipment, $e_{transbase}$ is the CO_2 emissions from transporting 1 ton of material 1km on a barge, m_{eq} is the annualized equipment mass in tons, and d_{port} is the ocean distance to the nearest port in km.

Emissions from maintenance trips to/from the seaweed farm are calculated as:

$$e_{mnt} = \left((2 \times d_{port}) \times e_{mntbase} \times \left(\frac{n_{mnt}}{a_{mnt}} \right) \right) + (e_{mntbase} \times d_{mnt}) \quad (8)$$

where e_{mnt} is total annual CO_2 emissions from farm maintenance, d_{port} is the ocean distance

to the nearest port in km, n_{mnt} is the number of maintenance trips per km^2 per year, a_{mnt} is the area tended to per trip, d_{mnt} is the distance traveled around each km^2 for maintenance, and $e_{mntbase}$ is the CO_2 emissions from traveling 1km on a typical fishing maintenance vessel (e.g. a 14m Marinnor vessel with 2x310hp engines) at an average speed of 9 knots (16.67 km/h), resulting in maintenance vessel fuel consumption of 0.88 l/km (Aitken et al., 2014; Johnson, 2011).

Total emissions from growing and harvesting seaweed are therefore calculated as:

$$e_{prod} = \frac{(e_{eqtrans}) + (e_{mnt})}{s_{dw}} \quad (9)$$

where e_{prod} is total annual emissions from seaweed production (growth + harvesting), $e_{eqtrans}$ is as calculated in eq. (7), e_{mnt} is as calculated in eq. (8), and s_{dw} is the dry weight of seaweed harvested annually per km^2.

Market value and climate benefits of seaweed. Further transportation and processing costs, economic value, and net emissions of either sinking seaweed in the deep ocean for carbon sequestration or converting seaweed into usable products (biofuel, animal feed, pulses, vegetables, fruits, oil crops, and cereals) are calculated based on ranges of transport costs ($/tDW/km), transport emissions (tCO_2-eq/t/km), conversion cost ($/tDW), conversion emissions (tCO_2-eq/tDW), market value of product ($/tDW), and the emissions avoided by product (tCO_2-eq/tDW) in the literature (Table 2.1). Market value is treated as globally homogenous and does not vary by region. Emissions avoided by products were determined by comparing estimated emissions related to seaweed production to emissions from non-seaweed products that could potentially be replaced by

seaweed (including non-CO_2 greenhouse gas emissions from land use) (Hong et al., 2021). Other parameters used are distance to nearest port (km), water depth (m), spatially-explicit sequestration fraction (%) (Siegel, DeVries, Doney, & Bell, 2021), and distance to optimal sinking location (km; cost-optimized for maximum emissions benefit considering transport emissions combined with spatially-explicit sequestration fraction; see *Distance to sinking point calculation* section below). Each Monte Carlo simulation calculates the cost of both CDR via sinking seaweed and GHG emissions mitigation via seaweed products.

For seaweed CDR, after the seaweed is harvested, it can either be sunk in the same location in which it was grown or be transported to a more economically favorable sinking location where more of the seaweed carbon would remain sequestered for 100 years (see *Distance to optimal sinking point* at the end of *Methods*). Immediately post-harvest, the seaweed still contains a large amount of water, requiring a conversion from dry mass to wet mass for subsequent calculations (Arzeno-Soltero et al., 2022):

$$s_{ww} = \frac{s_{dw}}{0.1} \tag{10}$$

where s_{ww} is the annual wet weight of seaweed harvested per km^2 and s_{dw} is the annual dry weight of seaweed harvested per km^2.

The cost to transport harvested seaweed to the optimal sinking location is calculated as:

$$c_{swtsink} = c_{transbase} \times d_{sink} \times s_{ww} \tag{11}$$

where $c_{swtsink}$ is the total annual cost to transport harvested seaweed to the optimal sinking location, $c_{transbase}$ is the cost to transport 1 ton of material 1km on a barge, d_{sink} is the distance in km to the economically-optimized sinking location, and s_{ww} is the annually-

harvested seaweed wet weight in t/km^2 as in eq. (10).

The cost associated with transporting replacement equipment (e.g., lines, buoys, anchors) to the farming location and hauling back used equipment at the end of its assumed lifetime (1 year for seeded line, 5-20 years for capex by equipment type) in the sinking CDR pathway are calculated as:

$$c_{eqtsink} = \left(c_{transbase} \times (2 \times d_{sink}) \times m_{eq}\right) + \left(c_{transbase} \times d_{port} \times m_{eq}\right) \quad (12)$$

where $c_{eqtsink}$ is the total annualized cost to transport both used and replacement equipment, $c_{transbase}$ is the cost to transport 1 ton of material 1km on a barge, m_{eq} is the annualized equipment mass in tons, d_{sink} is the distance in km to the economically-optimized sinking location, and d_{port} is the ocean distance to the nearest port in km. We assume that the harvesting barge travels from the farming location directly to the optimal sinking location with harvested seaweed and replaced (used) equipment in tow (incl. used seeded line and annualized mass of used capital equipment), sinks the harvested seaweed, returns to the farm location, and then returns to the nearest port (see Supplementary Fig. B.16). These calculations assume the shortest sea-route distance (see *Distance to optimal sinking point*).

The total value of seaweed that is sunk for CDR is therefore calculated as:

$$v_{sink} = \frac{\left(v_{cprice} - \left(c_{swtsink} + c_{eqtsink}\right)\right)}{s_{dw}} \quad (13)$$

where $\boldsymbol{v_{sink}}$ is the total value (cost, if negative) of seaweed farmed for CDR in $/tDW, v_{cprice}

is a theoretical carbon price, $c_{swtsink}$ is as calculated in eq. (11), $c_{eqtsink}$ is as calculated in eq. (12), and s_{dw} is annually-harvested seaweed dry weight in t/km^2. We do not assume any carbon price in our Monte Carlo simulations (v_{cprice} is equal to zero), making v_{sink} negative and thus representing a net cost.

To calculate net carbon impacts, our model includes uncertainty in the efficiency of using the growth and subsequent deep-sea deposition of seaweed as a CDR method. The uncertainty is expected to include the effects of reduced phytoplankton growth from nutrient competition, the relationship between air-sea gas exchange and overturning circulation (collectively hereafter referred to as the "atmospheric removal fraction"), and the fraction of deposited seaweed carbon that remains sequestered for at least 100 years. The total amount of atmospheric CO_2 removed by sinking seaweed is calculated as:

$$e_{seqsink} = k_{atm} \times k_{fseq} \times \frac{tC}{tDW} \times \frac{tCO_2}{tC} \quad (14)$$

where $e_{seqsink}$ is net atmospheric CO_2 sequestered annually in tons per km^2, k_{atm} is the atmospheric removal fraction, and k_{fseq} is the spatially-explicit fraction of sunk seaweed carbon that remains sequestered for at least 100 years (Siegel et al., 2021).

The emissions from transporting harvested seaweed to the optimal sinking location are calculated as:

$$e_{swtsink} = e_{transbase} \times d_{sink} \times s_{ww} \quad (15)$$

where $e_{swtsink}$ is the total annual CO_2 emissions from transporting harvested seaweed to the optimal sinking location in tCO_2/km^2 , $e_{transbase}$ is the CO_2 emissions (tons) from transporting 1 ton of material 1km on a barge (tCO_2/t-km), d_{sink} is the distance in km to the

economically-optimized sinking location, and s_{ww} is the annually-harvested seaweed wet weight in t/km^2 as in eq. (10). Since the unit for $e_{transbase}$ is tCO$_2$/t-km, the emissions from transporting seaweed to the optimal sinking location are equal to $e_{transbase} \times d_{sink} \times s_{ww}$, and the emissions from transporting seaweed from the optimal sinking location back to the farm are equal to 0 (since the seaweed has been deposited already, so seaweed mass to transport is now 0). Note that this does not yet include transport emissions from transport of equipment post-seaweed-deposition (see eq. 16 below and Supplementary Fig. B.16).

The emissions associated with transporting replacement equipment (e.g., lines, buoys, anchors) to the farming location and hauling back used equipment at the end of its assumed lifetime (1 year for seeded line, 5-20 years for capex by equipment type) (Aitken et al., 2014; Camus et al., 2019) in the sinking CDR pathway are calculated as:

$$e_{eqtsink} = \left(e_{transbase} \times (2 \times d_{sink}) \times m_{eq}\right) + \left(e_{transbase} \times d_{port} \times m_{eq}\right) \quad (16)$$

where $e_{eqtsink}$ is the total annualized CO$_2$ emissions in tons from transporting both used and replacement equipment, $e_{transbase}$ is the CO$_2$ emissions from transporting 1 ton of material 1km on a barge, m_{eq} is the annualized equipment mass in tons, d_{sink} is the distance in km to the economically-optimized sinking location, and d_{port} is the ocean distance to the nearest port in km. We assume that the harvesting barge travels from the farming location directly to the optimal sinking location with harvested seaweed and replaced (used) equipment in tow (incl. used seeded line and annualized mass of used capital equipment), sinks the harvested seaweed, returns to the farm location, and then returns to the nearest port.

These calculations assume the shortest sea-route distance (see *Distance to optimal sinking point*).

Net CO_2 emissions removed from the atmosphere by sinking seaweed are thus calculated as:

$$e_{remsink} = \frac{\left(e_{seqsink} - \left(e_{swtsink} + e_{eqtsink}\right)\right)}{s_{dw}} \quad (17)$$

where $e_{remsink}$ is the net atmospheric CO_2 removed per ton of dry weight seaweed, $e_{seqsink}$ is as calculated in eq. (14), $e_{swtsink}$ is as calculated in eq. (15), $e_{eqtsink}$ is as calculated in eq. (16), and s_{dw} is annually-harvested seaweed dry weight in t/km^2.

Net cost of climate benefits.

Sinking. To calculate the total net cost and emissions from the production, harvesting, and transport of seaweed for CDR, we combine the cost and emissions from the sinking-pathway cost and value modules. The total net cost of seaweed CDR per dry weight ton of seaweed is calculated as:

$$c_{sinknet} = c_{prod} - v_{sink} \quad (18)$$

where $c_{sinknet}$ is the total net cost of seaweed for CDR per dry weight ton harvested, c_{prod} is the net production cost per ton DW as calculated in eq. (6), and v_{sink} is the net value (or cost, if negative) per ton seaweed DW as calculated in eq. (13).

The total net CO_2 emissions removed per dry weight ton of seaweed is calculated as:

$$e_{sinknet} = e_{remsink} - e_{prod} \quad (19)$$

where $e_{sinknet}$ is the total net atmospheric CO_2 removed per dry weight ton of seaweed harvested annually (tCO_2/tDW/year), $e_{remsink}$ is the net atmospheric CO_2 removed via seaweed sinking annually as calculated in eq. (17), and e_{prod} is the net CO_2 emitted from production and harvesting of seaweed annually as calculated in eq. (9). For each Monte Carlo simulation, locations where $e_{sinknet}$ is negative (i.e., net emissions rather than net removal) are not included in subsequent calculations since they would not be contributing to CDR in that location under the given scenario. Note that these net emissions cases only occur in areas far from port in specific high-emissions scenarios. Even in such cases, most areas still contribute to CO_2 removal (negative emissions), so costs from locations with net removal are included.

Total net cost is then divided by total net emissions to get a final value for cost per ton of atmospheric CO_2 removed:

$$c_{pertonsink} = \frac{c_{sinknet}}{e_{sinknet}} \tag{20}$$

where $c_{pertonsink}$ is the total net cost per ton of atmospheric CO_2 removed via seaweed sinking ($/$tCO_2$ removed), $c_{sinknet}$ is total net cost per ton seaweed DW harvested as calculated in eq. (18) ($/tDW), and $e_{sinknet}$ is total net atmospheric CO_2 removed per ton seaweed DW harvested as calculated in eq. (19) (tCO_2/tDW).

GHG emissions mitigation. Instead of sinking seaweed for CDR, seaweed can be used to make products (incl. but not limited to food, animal feed, and biofuels). Replacing convention products with seaweed-based products can result in "avoided emissions" if the emissions from growing, harvesting, transporting, and converting seaweed into products is

less than the total greenhouse gas emissions (incl. non-CO_2 GHGs) embodied in conventional products that seaweed-based products replace.

When seaweed is used to make products, we assume it is transported back to the nearest port immediately after being harvested. The annualized cost to transport the harvested seaweed and replacement equipment (e.g., lines, buoys, anchors) is calculated as:

$$c_{transprod} = \frac{\left(c_{transbase} \times d_{port} \times \left(s_{ww} + m_{eq}\right)\right)}{s_{dw}} \quad (21)$$

where $c_{transprod}$ is the annualized cost per ton DW seaweed to transport seaweed and equipment back to port from the farm location, $c_{transbase}$ is the cost to transport 1 ton of material 1 km on a barge, m_{eq} is the annualized equipment mass in tons, d_{port} is the ocean distance to the nearest port in km, s_{ww} is the annual wet weight of seaweed harvested per km^2 as calculated in eq. (10), and s_{dw} is the annual dry weight of seaweed harvested per km^2.

The total value of seaweed that is used for seaweed-based products is calculated as:

$$v_{product} = v_{mkt} - \left(c_{transprod} + c_{conv}\right) \quad (22)$$

where $v_{product}$ is the total value (cost, if negative) of seaweed used for products ($/tDW), v_{mkt} is how much each ton of seaweed would sell for given the current market price of conventional products that seaweed-based products replace ($/tDW), $c_{transprod}$ is as calculated in eq. (21), and c_{conv} is the cost to convert teach ton of seaweed to a usable product ($/tDW).

The annualized CO_2 emissions from transporting harvested seaweed and equipment

back to port are calculated as:

$$e_{transprod} = \frac{\left(e_{transbase} \times d_{port} \times \left(s_{ww} + m_{eq}\right)\right)}{s_{dw}} \quad (23)$$

where $e_{transprod}$ is the annualized CO_2 emissions per ton DW seaweed to transport seaweed and equipment back to port from the farm location, $e_{transbase}$ is the CO_2 emissions from transporting 1 ton of material 1km on a barge, m_{eq} is the annualized equipment mass in tons, d_{port} is the ocean distance to the nearest port in km, s_{ww} is the annual wet weight of seaweed harvested per km^2 as calculated in eq. (10), and s_{dw} is the annual dry weight of seaweed harvested per km^2.

Total emissions avoided by each ton of harvested seaweed DW are calculated as:

$$e_{avprod} = e_{subprod} - \left(e_{transprod} + e_{conv}\right) \quad (24)$$

where e_{avprod} is total CO_2-eq emissions avoided per ton of seaweed DW per year (incl. non-CO_2 GHGs using a Global Warming Potential (GWP) time period of 100 years), $e_{subprod}$ is the annual CO_2-eq emissions avoided per ton seaweed DW by replacing a conventional product with a seaweed-based product, $e_{transprod}$ is as calculated in eq. (23), and e_{conv} is the annual CO_2 emissions per ton seaweed DW from converting seaweed into usable products. $e_{subprod}$ was calculated by converting seaweed DW to caloric content (USDA, 2020) for food/feed and comparing emissions intensity per kcal to agricultural products (Hong et al., 2021), or by converting seaweed DW into equivalent biofuel content with a yield of 0.25 tons biofuel per ton DW (Roesijadi, Jones, Snowden-Swan, & Zhu, 2010) and dividing the CO_2 emissions per ton fossil fuel by the seaweed biofuel yield.

To calculate the total net cost and emissions from the production, harvesting, transport, and conversion of seaweed for products, we combine the cost and emissions from the product-pathway cost and value modules. The total net cost of seaweed for products per dry weight ton is calculated as:

$$c_{prodnet} = c_{prod} - v_{product} \quad (25)$$

where $c_{prodnet}$ is the total net cost per dry weight ton of seaweed harvested for use in products, c_{prod} is the net production cost per ton DW as calculated in eq. (6), and $v_{product}$ is the net value (or cost, if negative) per ton DW as calculated in eq. (22).

The total net CO_2-eq emissions avoided per dry weight ton of seaweed used in products is calculated as:

$$e_{prodnet} = e_{avprod} - e_{prod} \quad (26)$$

where $e_{prodnet}$ is the total net CO_2-eq avoided per dry weight ton of seaweed harvested annually (tCO_2/tDW/year), e_{avprod} is the net CO_2-eq emissions avoided by seaweed products annually as calculated in eq. (24), and e_{prod} is the net CO_2 emitted from production and harvesting of seaweed annually as calculated in eq. (9). For each Monte Carlo simulation, locations where $e_{prodnet}$ is negative (i.e., net emissions rather than net emissions avoided) are not included in subsequent calculations since they would not be avoiding any emissions in that scenario.

Total net cost is then divided by total net emissions avoided to get a final value for cost per ton of CO_2-eq emissions avoided:

$$c_{pertonprod} = \frac{c_{prodnet}}{e_{prodnet}} \quad (27)$$

where $c_{pertonprod}$ is the total net cost per ton of CO_2-eq emissions avoided by seaweed products ($/t$CO_2$-eq avoided), $c_{prodnet}$ is total net cost per ton seaweed DW harvested for products as calculated in eq. (25) ($/tDW), and $e_{prodnet}$ is total net CO_2-eq emissions avoided per ton seaweed DW harvested for products as calculated in eq. (26) (tCO_2/tDW).

Parameter ranges for Monte Carlo simulations

For technoeconomic parameters with two or more literature values (see Supplementary Table B.1), we assumed that the maximum literature value reflected the 95th percentile and the minimum literature value represented the 5th percentile of potential costs or emissions. For parameters with only one literature value, we added +- 50% to the literature value to represent greater uncertainty within the modeled parameter range. Values at each end of parameter ranges were then rounded prior to Monte Carlo simulations as follows: capital costs, operating costs, and harvest costs to the nearest \$10,000/km^2, labor costs and insurance costs to the nearest \$1,000/km^2, line costs to the nearest \$0.05/m, transport costs to the nearest \$0.05/t/km, transport emissions to the nearest 0.000005 tCO_2/t/km, maintenance transport emissions to the nearest 0.0005 tCO_2/km, product avoided emissions to the nearest 0.1 tCO_2-eq/tDW, conversion cost down to the nearest \$10/tDW on the low end of the range and up to the nearest \$10/tDW on the high end of the range, and conversion emissions to the nearest 0.01 tCO_2/tDW.

We extended the minimum range values of capital costs to \$10,000/km^2 and transport emissions to 0 to reflect potential future innovations, such as autonomous floating farm

setups that would lower capital costs and net-zero emissions boats that would result in 0 transport emissions. To calculate the minimum value of \$10,000/km^2 for a potential autonomous floating farm, we assumed that the bulk of capital costs for such a system would be from structural lines and floatation devices, and we therefore used the annualized structural line (system rope) and buoy costs from Camus et al. (2019) (Camus et al., 2019) rounded down to the nearest \$5,000/km^2. The full ranges used for our Monte Carlo simulations and associated literature values are shown in Supplementary Table B.1.

Distance to optimal sinking point

Distance to the optimal sinking point was calculated using a weighted distance transform (path-finding algorithm, modified from code by Omar Richardson (2020) (Richardson, 2020)) that finds the shortest ocean distance from each seaweed growth pixel to the location at which the net CO_2 removed is maximized (incl. impacts of both increased sequestration fraction and transport emissions for different potential sinking locations) and the net cost is minimized. This is not necessarily the location in which the seaweed was grown, since the fraction of sunk carbon that remains sequestered for 100 years is spatially heterogeneous(Siegel et al., 2021). For each ocean grid cell, we determined the cost-optimal sinking point by iteratively calculating equations 11-20 and assigning d_{sink} the distance calculated by weighted distance transform to each potential sequestration fraction 0.01-1.00 in increments of 0.01. With the exception of transport emissions, the economic parameter values used for these calculations were the averages of unro unded literature value ranges - we assumed that the maximum literature value reflected the 95th percentile and the minimum literature value represented the 5th percentile of potential costs or

emissions, or for parameters with only one literature value, we added +- 50% to the literature value to represent greater uncertainty within the modeled parameter range. For transport and maintenance transport emissions, we extended the minimum values of the literature ranges to zero to reflect potential net-zero emissions transport options and used the mean values of the resulting ranges. The d_{sink} that resulted in minimum net cost per ton CO_2 for each ocean grid cell was saved as the final d_{sink} map, and the associated sequestration fraction value that the seaweed is transported to via d_{sink} was assigned to the original cell where the seaweed was farmed and harvested (Supplementary Fig. B.19). If the cost-optimal location to sink using this method was the same cell where the seaweed was harvested, then d_{sink} was 0km and the sequestration fraction was not modified from its original value (Supplementary Fig. B.18).

Comparison of gigaton-scale sequestration area to previous estimates

Previous related work estimating the ocean area suitable for macroalgae cultivation (Froehlich et al., 2019) and/or the area that might be required to reach gigaton-scale carbon removal via macroalgae cultivation (Froehlich et al., 2019; Gao, Beardall, et al., 2022; Wu et al., 2022) has yielded a wide range of results, primarily due to differences in modeling methods. For example, Gao et al. (2022) (Gao, Beardall, et al., 2022) estimate that 1.15 million km^2 would be required to sequester 1Gt of CO_2 annually when considering carbon lost from seaweed biomass/sequestered as POC and rDOC, and assume that the harvested seaweed is sold as food such that the carbon in the harvested seaweed is not sequestered. The area (0.4 million km^2) required to sequester 1 Gt CO_2 in our study assumes that all harvested seaweed is sunk to the deep ocean to sequester carbon.

Additionally, a preprint by Wu et al. (2022) (Wu et al., 2022) estimates that roughly 12 Gt CO_2 could be sequestered annually via macroalgae cultivation in approximately 20% of the world ocean area (i.e., 1.67% ocean area per Gt CO_2), which is a much larger area per Gt CO_2 than our estimate of 0.110% ocean area. This notable difference arises for several reasons—including differences in yield (yields in the Wu et al. preprint are around 500 tDW/year in the highest-yield areas, whereas yields in our cheapest sequestration areas from G-MACMODS average 3,400 tDW/km^2/year)—that arise from differences in model methodology. First, Wu et al. model temperate brown seaweeds, while our study considers different seaweed types, many of which have higher growth rates, and uses the most productive seaweed type for each ocean grid cell. The G-MACMODS seaweed growth model we use also has a highly optimized harvest schedule, includes luxury nutrient uptake (a key feature of macroalgal nutrient physiology), and does not directly model competition with phytoplankton during seaweed growth. Finally, tropical red seaweeds (the seaweed type in our cheapest sequestration areas) grow year-round, while others – like the temperate brown seaweeds modeled by Wu et al. – only grow seasonally. These differences all contribute to higher productivity in our model leading to a smaller area required for gigaton-scale CO_2 sequestration compared to Wu et al (2022) (Wu et al., 2022).

Conversely, the ocean areas we model for seaweed-based CO_2 sequestration or GHG emissions avoided are much larger than the 48 million km^2 that Froehlich et al. (2019) (Froehlich et al., 2019) estimate is suitable for macroalgae farming globally. Although our maps show productivity and costs everywhere, the purpose of our modeling was to evaluate where different types of seaweed grow best and how production costs and

product values vary over space, in order to highlight the lowest-cost areas (which are often the highest-producing areas) under various techno-economic assumptions.

Comparison of seaweed production costs to previous estimates

Although there are not many estimates of seaweed production costs in the scientific literature, our estimates for the lowest-cost 1% area of the ocean ($190-$2,790/tDW) are broadly consistent with previously published results: seaweed production costs reported in the literature range from $120-$1,710/tDW (Camus et al., 2019; Capron et al., 2020; Correa et al., 2016; van den Burg et al., 2016), but are highly dependent on assumed seaweed yields. For example, Camus et al. (2019) (Camus et al., 2019) calculate a cost of $870/tDW assuming minimum yield of 12.4 kgDW/m of cultivation line (equivalent to 8.3 kgDW/m^2 using 1.5m spacing between lines). Using the economic values from Camus et al. (2014) but with our estimates of average yield for the cheapest 1% production cost areas (2.6 kgDW/m^2) gives a much higher average cost of $2,730/tDW. Contrarily, van den Burg et al. (2016) (van den Burg et al., 2016) calculate a cost of $1,710/tDW using a yield of 20 tDW/hectare (i.e. 2.0 kg/m^2). Instead, assuming our average yields from lowest-cost areas (i.e. 2.6 kgDW/m^2 or 26 tDW/hectare) would decrease the cost estimated by Van den Burg et al. (2016) to $1,290/tDW. Most recently, Capron et al. (2020) (Capron et al., 2020) calculate an optimistic scenario cost of $120/tDW based on an estimated yield of 120 tDW/hectare (12 kg/m^2; over 4.5 times higher than the average yield in our lowest-cost areas). Again, instead assuming the average yield in our lowest-cost areas would raise Capron et al.'s production cost to $540/tDW (between the $190-$880/tDW minimum to median production costs in the cheapest 1% areas from our model; Fig. 2.1a,b).

Data Sources

Seaweed biomass harvested. We use global, spatially-explicit data for seaweed biomass harvest potential under both ambient and limited nutrient scenarios from the G-MACMODS seaweed growth model, presented in Arzeno-Soltero et al. (2023).

Fraction of deposited carbon sequestered for 100 years. We use data from Siegel et al. (2021) interpolated to 1/12-degree grid resolution.

Distance to nearest port. We use the Distance from Port V1 dataset from the Global Fishing Watch interpolated to 1/12-degree grid resolution.

Significant wave height. We use data for annually averaged significant wave height from the European Center for Medium-range Weather Forecasts (ECMWF) interpolated to 1/12-degree grid resolution.

Ocean depth. We use data from the General Bathymetric Chart of the Oceans (GEBCO).

Shipping lanes. We use data of Automatic Identification System (AIS) signal count per ocean grid cell, interpolated to 1/12-degree grid resolution. We define a major shipping lane grid cell as any cell with $>2.25 \times 10^8$ AIS signals, a threshold that encompasses most major trans-Pacific and trans-Atlantic shipping lanes as well as major shipping lanes in the Indian Ocean, North Sea, and coastal routes worldwide.

Marine Protected Areas (MPAs). We use data from the World Database on Protected Areas (WDPA) and define a MPA as any protected ocean area >20 km^2.

2.5 Figures and Tables

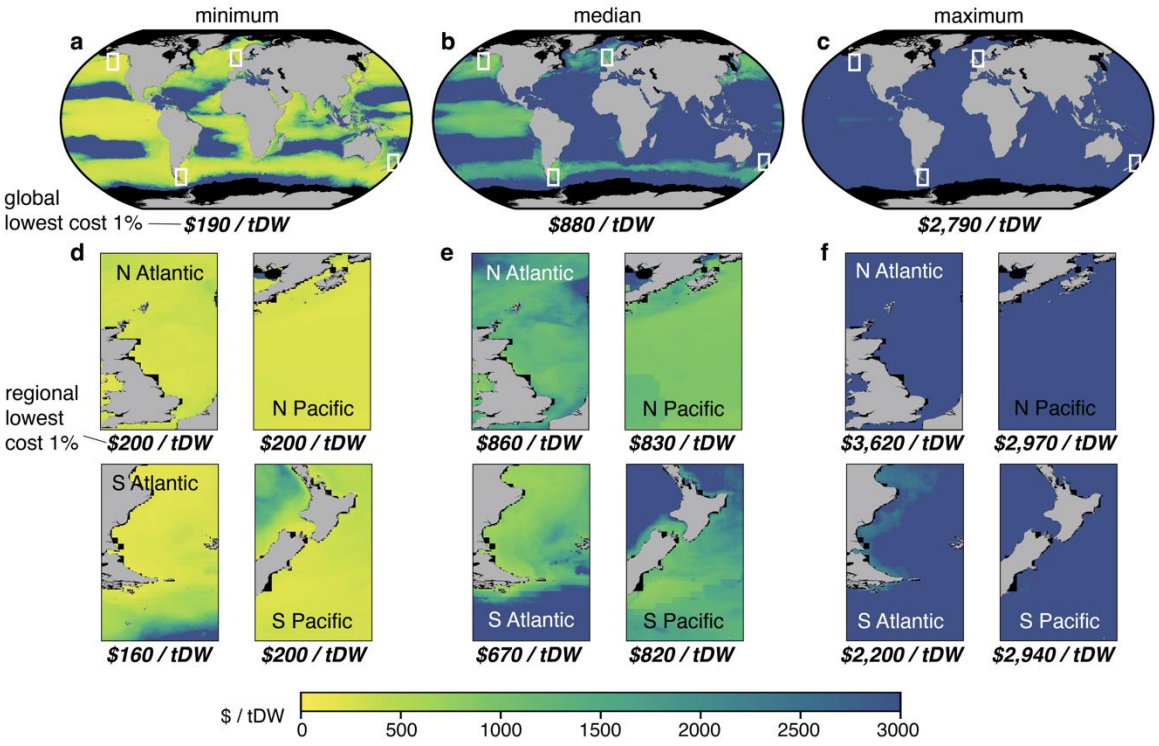

Figure 2.1 | Seaweed production costs. Estimated seaweed production costs vary considerably depending on assumed costs of farming capital, seeded lines, labor, and harvest (transport of harvested seaweed is not included). Across ambient nutrient simulations, average farming cost in the 1% of global ocean areas with lowest cost ranges from $190/tDW (**a**) to $2,790/tDW (**c**), with a median of $880/tDW (**b**). Regional insets (**d-f**) reveal small-scale features in particularly low-cost areas. Supplementary Fig. B.2 shows maps for limited nutrient simulations.

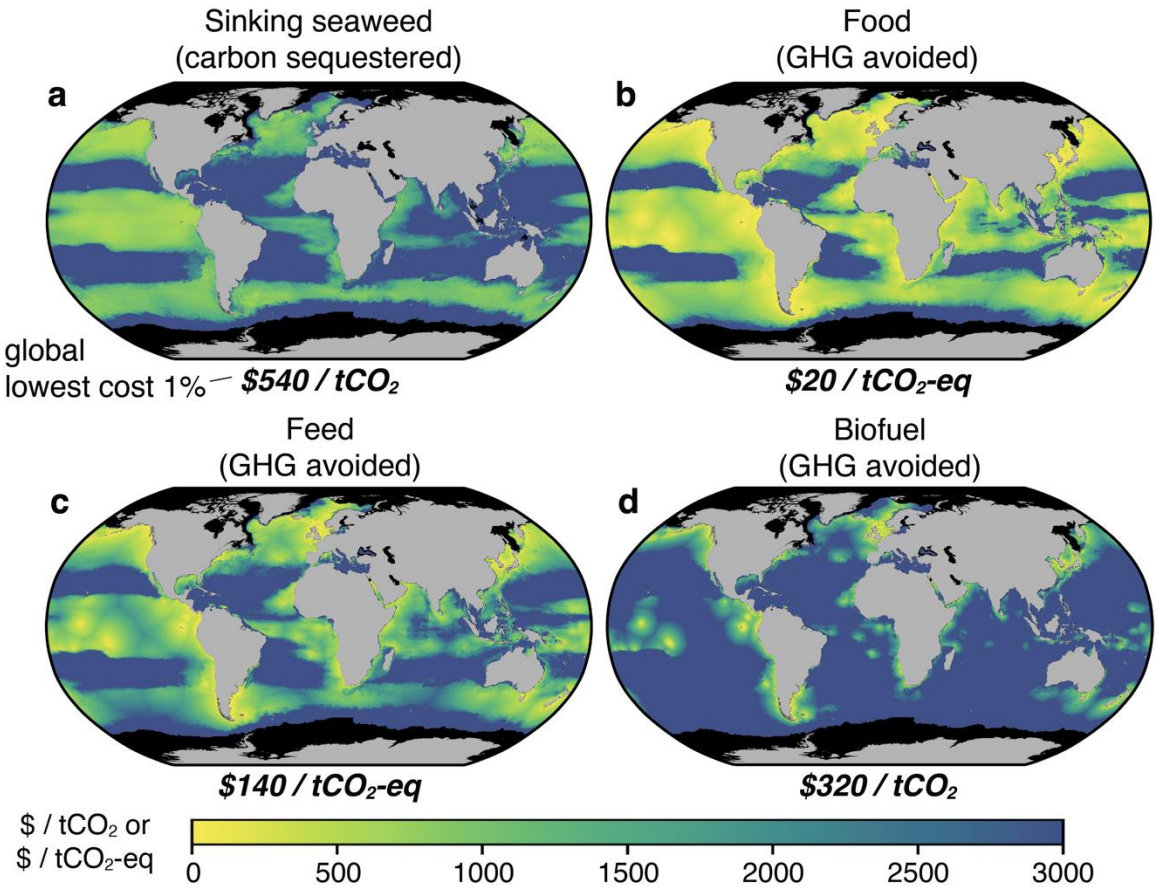

Figure 2.2 | Net cost of potential seaweed climate benefits. Costs of using farmed seaweed to sequester carbon or avoid GHG emissions vary in space according to estimated production costs as well as spatially-explicit differences in the costs and net emissions of transportation, sinking or conversion, and replacement of conventional market alternatives with seaweed products. Differentiation between seaweed product groups (**b**-**d**) is based on emissions avoided by seaweed products and market value for each product type. Maps show costs when propagating the most optimistic assumptions (5th percentile costs) from ambient nutrient simulations. Average cost in the 1% of global ocean areas with lowest cost ranges from \$20/tCO_2-eq avoided when seaweed is used for food (**b**) to \$540/tCO_2 sequestered by sinking seaweed (**a**). Supplementary Figs. B.6 and B.7 show maps for limited nutrient simulations and median costs, respectively.

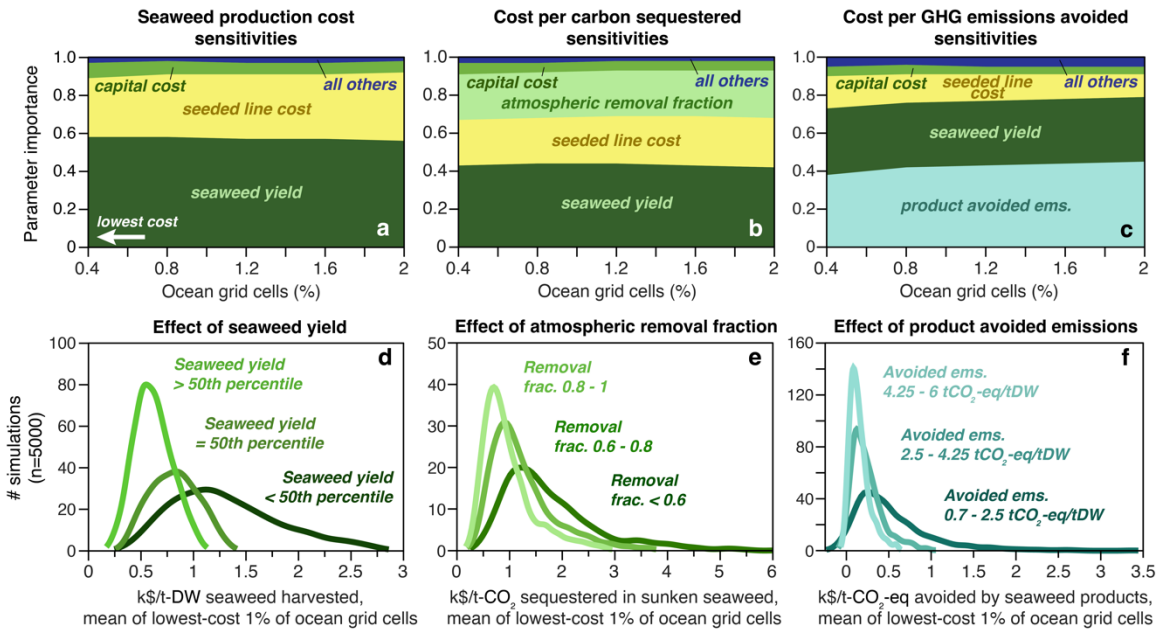

Figure 2.3 | Key cost sensitivities of seaweed production and climate benefits. Across Monte Carlo simulations in the 2% of ocean grid cells where costs are lowest, estimated seaweed production cost is especially sensitive to the seaweed yield amount and seeded line cost (**a**), whereas costs of carbon sequestration (**b**) and GHG emissions avoided (**c**) are strongly influenced by the fraction of seaweed carbon that corresponds to an equivalent amount removed from the atmosphere and the assumed emissions avoided by seaweed products, respectively, in addition to seaweed yield and seeded line cost. Panels **d**-**f** show kernel density plots for the most important parameters in the cheapest 1% ocean areas, showing that the lowest production and climate benefit costs depend upon seaweed yield being at or above the median of potential seaweed yields (**d**), an assumed atmospheric removal fraction of >0.6-0.8 (**e**), and avoided emissions >2.5 tCO_2-eq/tDW (**f**). Supplementary Fig. B.9 shows cost sensitivities in limited nutrient simulations.

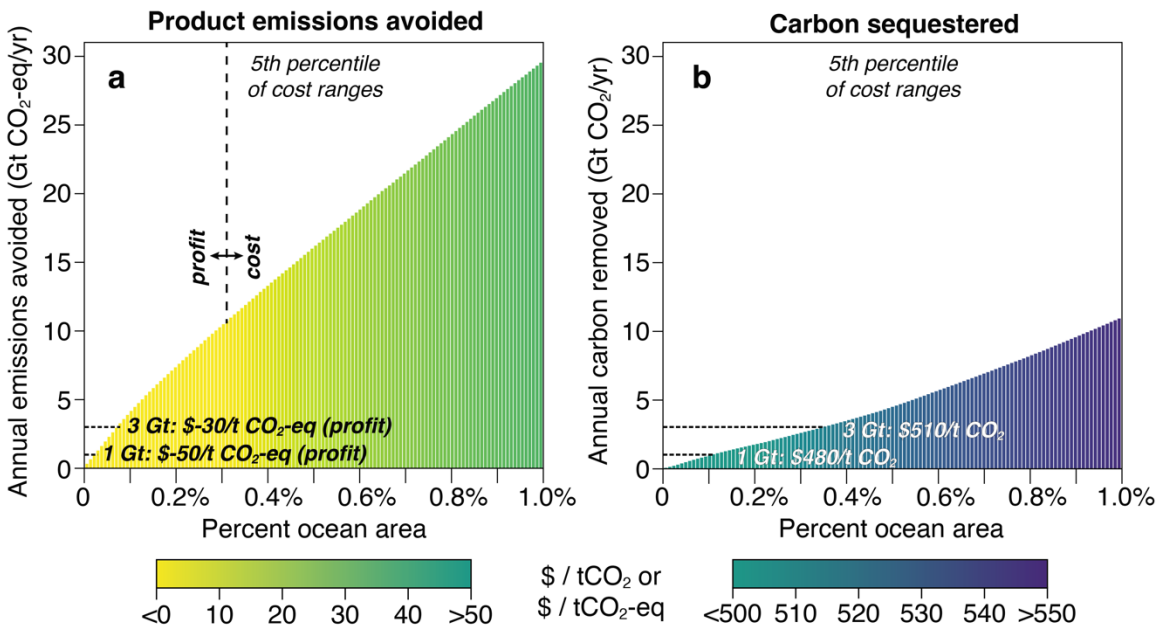

Figure 2.4 | Cumulative potential climate benefits of large-scale seaweed farming. Total GHG emissions avoided (**a**) or carbon sequestered (**b**) each year could reach gigaton-scales if seaweed were farmed over large areas of the ocean. Bars show the potential climate benefits as a function of the lowest-cost ocean area (0.1% of ocean area is roughly 360,000 km^2, nearly the area of Germany and 130 times the total area of current seaweed farms), and colors indicate the average cost (or profit) per tCO_2-eq emissions avoided or tCO_2 sequestered using optimistically low net costs (5th percentile) from ambient nutrient simulations. Supplementary Figs. B.10 and B.11 show cumulative potential and costs at the median and in limited nutrient simulations.

Table 2.1 | Ranges of selected variables used in our technoeconomic analysis.

Variable	Unit	Model Range	Values reported in literature
Capital costs	$/km^2/year	10,000 – 1,000,000	929,676 (van den Burg et al., 2016) 550,000 – 950,000 (Capron et al., 2020) 375,910 (Correa et al., 2016) 210,580 (Camus et al., 2019)
Seeded line cost (includes hatchery costs)	$/m	0.05 – 1.45	1.38 (van den Burg et al., 2016) 0.13 (Camus et al., 2019)
Harvest costs (includes harvest labor, excludes harvest transport)	$/km^2/harvest	120,000 – 400,000	381,265 (Camus et al., 2019) 138,000 (van den Burg et al., 2016)
Transport cost per ton of material (includes loading/unloading costs)	$/t/km	0.1 – 0.35	0.225 (van den Burg et al., 2016)
Transport emissions per ton of material	tCO_2/t/km	0 – 0.000045	0.00003 (Aitken et al., 2014)
Maintenance boat emissions	tCO_2/km	0 – 0.0035	0.0023653 (calculated using methods from (Aitken et al., 2014; Johnson, 2011))

Atmospheric removal fraction	fraction (unitless)	0.4 – 1	0.4 – 0.75 (Berger et al., 2022) 0.5 (global average, from preliminary experiment by authors using (Harrison et al., 2018) informed by (Bach et al., 2021))
Seaweed market value for product end-use	$/tDW	400 – 800	Food: 500-800 (dried seaweed wholesale price from ("Dried Seaweed Price," 2022)) Feed: 400-500 (values per ton dry animal feed and soybean meal from (USDA, 2022; van den Burg et al., 2016), assuming a direct replacement with dry seaweed) Fuel: 430 (dried seaweed price for bioethanol production, calculated based on bioethanol yield per ton seaweed (0.25) and average of 2021-2022 historical E85 fuel prices ($3.76/GGE) from (U.S.DOE, 2022), modeled range 400-500) Not product-specific: 400 (dried seaweed market price of $400/tDW from (Buschmann et al., 2017))

GHG emissions avoided by replacement with seaweed product	tCO_2-eq/tDW	0.7 – 6.0	Food: 1-6 (considering global average emissions from GHGs per kcal for pulses, vegetables, fruits, oil crops, and cereals, from (Hong et al., 2021)) Feed: 1-3.1 (considering global average emissions from GHGs per kcal for oil crops and cereals, +- 50% uncertainty, from (Hong et al., 2021)) Fuel: 0.7-1 (assuming 3.2-3.5 tCO_2/t fossil fuel by fuel type from (EIA, 2021) and 0.25 t bioethanol/tDW yield from (Roesijadi et al., 2010), and energy density equivalence conversions by fuel type)

CHAPTER 3

Net-zero emissions food systems

3.1 Introduction

Feeding a growing global population without further damaging the environment is one of the key challenges of the coming decades. Over the past 60 years, growing demand for food was met via the expansion of industrialized agriculture (The Green Revolution), which led to increased crop yields and new crop varieties that fed most of the world even as population doubled (Pingali, 2012; Tilman, 1998). However, these successes in crop production relied heavily on higher application rates of synthetic nitrogen fertilizer, leading to a seven-fold increase in fertilizer use from the 1960s to the 1990s (Tilman, 1998) which in turn led to an increase in nutrient pollution and greenhouse gas (GHG) emissions (though still lower net GHG emissions than would have occurred without the yield gains of the Green Revolution (Burney, Davis, & Lobell, 2010)). And despite steadily-improving crop yields, agriculture is still the major driver of deforestation and terrestrial biodiversity loss, particularly in the tropics (Jaureguiberry et al., 2022; Ortiz, Outhwaite, Dalin, & Newbold, 2021; Pendrill et al., 2022).

Today, agricultural systems are responsible for 1/3 of global greenhouse gas emissions (Crippa et al., 2021; Hong et al., 2021) and over 80% of deforestation (UNCCD, 2022). The food system is the core of the broader agricultural sector and caused 18.5 Gt CO_2-eq emissions in 2017 (Figure 3.1) (Crippa et al., 2021; Hong et al., 2021). Even if we successfully eliminated all GHG emissions from energy and industry today (including energy inputs into the food system), roughly 14 Gt CO_2-eq emissions – over 23% of total

anthropogenic GHG emissions – would remain from land-based emissions and waste (Figure 3.1). A substantial share of food system emissions are particularly hard-to-abate compared to other emitting sectors (e.g., short-haul transportation), including area sources of powerful non-CO_2 GHGs (e.g., methane and N_2O) that result from the fundamental chemistry of food production and are therefore intimately linked to modern agricultural practices (Crippa et al., 2021; Hong et al., 2021; Rosa & Gabrielli, 2023). Moreover, even where clear and technically feasible solutions to agricultural emissions already exist, the socio-economic and political barriers to action are often daunting (e.g, deforestation), and some of the largest sources of agricultural emissions are in developing regions without strong governance regarding land-use practices (Hong et al., 2021; Searchinger et al., 2019).

These challenges to mitigating food system emissions will continue to grow with increasing population and affluence, and the impacts of climate change on agriculture may increasingly undermine progress in agricultural production for many crops and regions (Jägermeyr et al., 2021; Ortiz et al., 2021). Yet despite agriculture's substantial contribution to global GHG emissions, it is not yet clear how to reduce the full scope of agricultural emissions to a point compatible with climate stabilization or even net-zero emissions. Several recent studies have highlighted opportunities for reducing emissions from parts of the food system (Rosa & Gabrielli, 2023; Soofi, Manshadi, & Saucedo, 2022), while others have focused largely on the carbon sequestration potential of agriculture to reduce food system emissions (Costa et al., 2022). Additionally, representation of agriculture and land-use in integrated assessment models is improving but still lacks detail and consistency, particularly with regard to yield projections and the assumed rates of land-use change for

carbon removal (e.g., afforestation, expansion of energy cropland area for BECCS) (Turner, Field, Lobell, Sanchez, & Mach, 2018).

Here we review the prospect of transitioning to a net-zero emissions food system and discuss the unique challenges associated with eliminating agricultural emissions. We assess the technical potential of mitigation solutions for different hard-to-abate processes, the role of both demand- and supply-side measures to reduce emissions, and priorities for research and policy action.

3.2 Food system outputs

A functional food system must meet the basic nutritional needs of the population while also upholding the pillars of food security: availability, accessibility, utilization, and stability (FAO, 2014). As population and affluence grow, demand for more emissions-intensive foods and luxury goods (e.g., beef, highly-processed foods) are also expected to increase (Searchinger et al., 2019; Tilman et al., 2011). Demand for food will increasingly compete for land with emissions mitigation strategies like bioenergy and nature-based carbon removal (Riahi et al., 2017; Stehfest et al., 2019) and with the need to preserve and restore natural habitats.

In this section we describe several necessary nutritional outputs of the food system, their current and projected GHG emissions through mid-century, and the key uncertainties of projected demand for food and other agricultural products. This overview of food system outputs is non-exhaustive; indeed, many other dietary components (e.g., micronutrients) are important to a well-balanced diet in the long-term. Our aim is not to undertake a fully comprehensive assessment of a healthy diet but rather to provide background on dietary

components that make up the majority of food demand and therefore also account for the bulk of current and potential future food-related emissions. We also do not cover the scope of luxury food goods like alcohol, stimulants, spices, and processed foods. Finally, we note that any long-term demand predictions for agricultural commodities have large error bars and associated uncertainties, but by outlining a range of potential outcomes, we hope to provide a framework by which to evaluate the relative contribution of different commodities to future food system emissions and highlight the largest sources of uncertainty across different projections.

1. Calories and Carbohydrates

The primary goal of the food system is to provide dietary calories, which are largely supplied by carbohydrates: the USDA recommends that carbohydrates should supply 45-65% of daily calories (USDA & USDHHS, 2020). Staple crops (e.g., cereal and grain crops like wheat, rice, maize) are a major source of dietary carbohydrates globally (Falcon, Naylor, & Shanker, 2022; FAO, 2022; Slavin & Carlson, 2014). In 2017, cereals accounted for 54% of total caloric agricultural production (including feed and biofuels) (Hong et al., 2021) and made up 45% of total caloric food supply globally (FAO, 2022), causing nearly 8 Gt of CO_2-eq GHG emissions (Crippa et al., 2021; Hong et al., 2021). Projections of demand for staple crops by 2050 vary widely due to uncertainties in mid-century population (especially in Sub-Saharan Africa) and inconsistent incorporation of income elasticity of food demand into overall projections (Falcon et al., 2022). Estimates of total food demand in 2050 range from <45% to >55% increase relative to 2019 with a median of 51% (Falcon et al., 2022). Projections for rice and maize consumption change are particularly variable:

rice ranges from 4% to 33% increase relative to 2019, while maize ranges from 24% to 64% (Falcon et al., 2022). Assuming a 2050 population of 10 billion and no changes to the emissions intensity of food production, emissions from cereal crops alone would reach 12 Gt CO_2-eq annually (Crippa et al., 2021; Hong et al., 2021).

Other important sources of dietary carbohydrates (in addition to grains) include vegetables, fruits, milk, and milk products (Slavin & Carlson, 2014). Additional sources of calories include meat (8% of total caloric food supply in 2017), sugar and other sweeteners (8%), fruits and vegetables (7% combined), milk (5%), pulses (2%), and oilcrops (2%) (FAO, 2022). Although it only accounted for 0.6% of total caloric agricultural production, beef caused over 3 Gt CO_2-eq GHG emissions in 2017 (17% of food system total emissions) (Hong et al., 2021). Chicken, by comparison, is much less emissions-intensive: it accounted for 0.7% of total caloric agricultural production and caused 0.2 Gt CO_2-eq emissions (1% of food system total emissions). In scenarios with a 2050 population of 10 billion, demand for beef is projected to grow by 19-50% relative to 2019, while demand for chicken is projected to grow by 46-131% (Falcon et al., 2022). An increase of 19% for beef and 131% for chicken would cause annual emissions of 3.8 and 0.6 Gt CO_2-eq, respectively, by 2050.

2. Protein

Dietary protein consists of many different amino acids, the balance of which is important for human health (Falcon et al., 2022; FAO, 2013; Wolfe, Baum, Starck, & Moughan, 2018). Amino acids serve numerous essential functions in the body, including the maintenance of both structural and functional proteins that break down over time (FAO, 2013; Wolfe et al., 2018). Amino acids can be classified as dietary essential (essential

amino acids, EAA) and dietary non-essential (non-essential amino acids, NEAA). EAAs must be supplied through dietary intake because they either cannot be synthesized by the human body or cannot be synthesized at the rate required to meet nutritional requirements. NEAAs can be synthesized by the body and therefore are not required to be fully supplied by dietary intake (Wolfe et al., 2018). There is ongoing debate about the optimal amount of protein intake in a healthy adult diet, but most research indicates a range of 0.8 – 0.9 grams of protein per kg body weight or 10-35% of daily caloric intake as protein (Falcon et al., 2022; Phillips, 2012; Wolfe et al., 2018) which could be supplied solely by plant sources of protein.

The largest sources of dietary protein in the global food supply are wheat, rice, milk, poultry, pork, vegetables, and maize (FAO, 2022). 2050 demand projections for wheat fall between 30-35% growth relative to 2019, while rice ranges from 4% to 33% increase and poultry from 46-131% (Falcon et al., 2022). Pork demand is projected to increase 16-39% by 2050 relative to 2019. An increase of 131% for poultry and 39% for pork would cause 0.6 and 2.0 Gt CO_2-eq emissions, respectively, in 2050.

3. Fats

Dietary fats are essential macronutrients that serve many roles in the human body (e.g., energy storage, structural unit formation for cellular membranes, and vitamin absorption) (Bajželj, Laguzzi, & Röös, 2021; Falcon et al., 2022). The Food and Agriculture Organization of the United Nations (FAO) recommends that fats make up 20-35% of total daily energy intake (Bajželj et al., 2021). Major sources of dietary fat in the global food supply include pork, oilseeds, milk, poultry, butter, grains, and beef (Bajželj et al., 2021; FAO, 2022). From

a food demand perspective, vegetable fats (oils) are characterized by a high degree of substitution: many different crops produce oil, so the demand for any particular oil crop is highly sensitive to changes in price (Falcon et al., 2022). Due to this high degree of substitution and its high oil yield per hectare, palm oil could have an even larger demand increase than soybean oil by 2050 (Falcon et al., 2022). Among animal fats, pork is the largest source, accounting for 13% of total fat supply quantity in 2017 (FAO, 2022). Projections for 2050 pork demand range from 16-39% increase relative to 2019 (Falcon et al., 2022). At the higher end of the range with a 39% increase, pork would cause 2.0 Gt CO_2-eq emissions in 2050.

3.3 Levers for mitigating food system emissions

Given the growing demand for agricultural products and the hard-to-abate emissions associated with producing those products, the *Pale* identity (Hong et al., 2021) is a useful tool for quantitatively exploring levers to reduce food system emissions at scale. It is an agriculture-specific adaptation of the Kaya identity and expresses food system emissions as a function several underlying drivers:

$$E = P\left(\frac{A}{P}\right)\left(\frac{L}{A}\right)\left(\frac{E}{L}\right) = Pale \quad (28)$$

Where E represents the flux of agricultural GHG emissions, P is the population, A is the total agricultural production, and L is the agricultural land area. In the righthand-most side of the equation, $a = A/P$ is per-capita agricultural production, $l = L/A$ is the land-use intensity of agricultural production (i.e., the inverse of yield), and $e = E/L$ is the emissions intensity of land use (Hong et al., 2021). For the purposes of assessing food system emissions

specifically (as opposed to all agricultural emissions), we use a version of the *Pale* decomposition that excludes emissions from timber harvest but includes emissions from waste as well as energy and industry inputs to the food system (e.g., fuel for tractors, electricity for pumping irrigation water, synthetic fertilizer production, etc.).

The *Pale* identity drivers can be understood conceptually as demand ($a = A/P$), yields (inverse of $l = L/A$), and emissions associated with farming practices ($e = E/L$). In this section we discuss the potential for each of these drivers to act as levers for emissions mitigation, the current state of technologies to reduce the magnitude of each driver, and the challenges and opportunities for scaling solutions globally.

1. Decrease demand – changes to *what* and *how much* food we produce

a. Dietary shifts

Shifting diets to include a higher proportion of low-emissions-intensity foods and therefore reduce demand for the most emissions-intensive foods would in turn reduce the average emissions intensity of overall food demand. Figure 3.2 shows the potential for decreased demand from dietary shifts to reduce food system emissions. 2017 emissions from beef, dairy, pork, and chicken are shown in the top-right corner of each panel (Crippa et al., 2021; Hong et al., 2021), with contours representing the decreased emissions resulting from some percentage of the highest per-capita consumers reducing their consumption by some percent. Uneven distances between contours (e.g., contours that are more closely spaced toward the top left corner of each panel) indicate inequitable per-capita consumption of that product and a higher Gini coefficient (White, 2000). Beef (panel A), for example, has a Gini coefficient of 0.54, indicating inequitable consumption with

much higher per-capita consumption concentrated in just a handful of countries (the top three beef consuming countries per-capita are Argentina, the United States, and Brazil) (FAO, 2022).

This inequity of per-capita consumption is evident in the potential to mitigate emissions from shifting diets away from beef: if the top 15% of per-capita beef consumers worldwide reduced their beef intake by 30% (represented on panel A as point (70, 85)), annual beef emissions would be approximately 2.6 Gt CO_2-eq – nearly 0.5 Gt less than the original 3.1 Gt CO_2-eq emissions from beef. Panel D, on the other hand, shows that the emissions mitigation from the complete elimination of chicken consumption would only reduce emissions by 0.23 Gt – less than half of the mitigation potential from the top 15% of beef consumers reducing beef consumption by just 30%. These relationships indicate that reducing demand for beef is a powerful lever to reduce food system emissions, since even fractional changes in consumption from a subset of the population would have an outsized emissions mitigation impact compared to other animal-based sources of nutrition.

Reducing demand for emissions-intensive foods does not mean that people would then simply eat less food – those calories would need to be replaced by other foods. The net emissions mitigation impact of a diet shift to less emissions-intensive foods is therefore the sum of the emissions reduction from shifting away from one food plus the additional emissions resulting from increased consumption of another. For a highly emissions-intensive food like beef, shifting to alternative sources of calories will almost always still lower the average emissions intensity of food demand. One exception to this is sheep and goat meat, which have a higher average emissions intensity than beef (Hong et al., 2021).

Supplementary Figure C.1 shows the net emissions resulting from a replacement of beef with mass-equivalent pulses (legumes), the food group with the next-highest emissions intensity after beef (Hong et al., 2021). Compared to Figure 3.2A, which shows the emissions reduction from lower beef consumption but not the emissions associated with replacement calories, replacing beef with pulses in a diet still has significant emissions benefits. Take, for instance, the example point previously discussed for Figure 3.2A: 15% of the top beef-eating population eating 30% less beef, as indicated by point (70%, 85%) in panel A. This shift showed a 0.5 Gt CO_2-eq emissions reduction from baseline without considering the replacement of those beef calories with another food source. For the same shift away from beef but now replacing that beef with mass-equivalent pulses, Supplementary Figure C.1 shows that net emissions reductions would still be nearly 0.4 Gt CO_2-eq compared to baseline.

b. Plant-based and synthetic meats

Instead of shifting demand from meat to less emissions-intensive sources of nutrients that have significantly different texture and flavor, there are increasing options on the market for plant-based or synthetic (cultured) meats. These plant-based or cultured options are typically less emissions-intensive to produce compared to their traditional agriculturally-sourced counterparts while aiming to reproduce the same texture and flavor, making diet shifts away from meat easier for larger portions of the population (Rubio, Xiang, & Kaplan, 2020). Some well-known brands of the newest generation of plant-based meats are Impossible™ Foods and Beyond Meat®, both of which have released full life cycle assessments (LCAs) of their products' environmental impact and GHG emissions. Plant-based meat production on average uses 32% less energy, requires 97% less land, and

causes 88% less greenhouse gas emissions compared to beef (Rubio et al., 2020). Cultured cell-based meat also uses significantly less land compared to conventional beef, but it requires 35% more energy per unit of production (Rubio et al., 2020). However, given that most beef emissions are caused by land-use and enteric fermentation (Hong et al., 2021), cultured meat still causes 75% less greenhouse gas emissions than conventional beef (Rubio et al., 2020).

Willingness to try plant-based meat is relatively high in several large markets (China, India, the United States), but concerns over taste, texture, price, and level of food processing still pose barriers for broader consumer acceptance and market scalability (Rubio et al., 2020). Cultured cell-based meat faces similar barriers to scale, with some consumers also citing the "unnatural" nature of cultured meat as "unappealing" (Rubio et al., 2020). There is, however, a willingness to try cultured meat among the majority of consumers in the US (Wilks & Phillips, 2017), and omnivores are more likely to report willingness to purchase cultured meat compared to vegans or vegetarians (Rubio et al., 2020; Wilks & Phillips, 2017). Although a substantial demand shift from conventional meat to plant-based or synthetic meat is not likely to occur quickly, there are spaces within the existing market to serve smaller but growing subsets of the population who are open to purchasing meat alternatives (Rubio et al., 2020).

c. Reduce food loss and waste

Reducing food loss and waste is a way to directly impact the total demand for agricultural production. Food loss occurs on the supply-side from damage or spoilage prior to reaching retails or consumers, while food waste occurs on the demand-side from

spoilage or disposal by retailers or consumers (FAO, 2019; Hegwood et al., 2023; Quested, O'Connor, & Forbes, 2021). Approximately 24% of all food calories produced are ultimately lost or wasted (Kummu et al., 2012; Searchinger et al., 2019). By mass, around 14% of food is lost prior to the retail stage (FAO, 2019), while 11% is wasted in households, 5% is wasted in food service, and 2% is wasted in retail (Quested et al., 2021), amounting to about 1/3 of total food mass produced that is lost or wasted. Emissions from food loss during processing (liquid and solid) as well as post-consumer food waste incineration, methane from landfills, and wastewater account for 1.7 Gt CO_2-eq emissions (Crippa et al., 2021), or 9% of total food system emissions (Figure 3.1). Over 90% of those 1.7 Gt CO_2-eq emissions are from retail and consumer household waste (Crippa et al., 2021). On top of those direct emissions, there are emissions associated with producing that lost or wasted food, such that reducing food loss and waste would also reduce the emissions caused by producing the food in the first place. Total emissions from both the production and disposal of lost or wasted food is approximately 5.6 Gt CO_2-eq – over 9% of total anthropogenic GHG emissions.

Food loss and waste are caused by multiple underlying drivers, among which are poor infrastructure, lack of awareness of the food waste problem, concerns about possible risks of consuming food that may be spoiled, poor supply and demand planning, and marketing strategies (Hanson et al., 2019). Reductions to food loss and waste may also have significant rebound effects that offset up to 71% of emissions mitigation, whereby decreased demand causes lower food prices, resulting in more food purchased and consumed (Hegwood et al., 2023). However, there would still be a net reduction in total food loss and waste even with the maximum potential rebound effects taken into account,

and more access to cheaper food would improve food security for many populations (Hegwood et al., 2023). Both food loss and waste can be reduced by improvements to packaging and storage (Hanson et al., 2019; Poore & Nemecek, 2018), and efforts to reduce food loss should be prioritized for the most emissions-intensive foods like beef, dairy, and rice (Hanson et al., 2019). Moreover, efforts to educate and inform the public about the need to reduce household food waste should be prioritized in higher-income countries (where food waste is the larger issue) and efforts to implement better storage and supply chain practices to reduce food loss should be prioritized in lower-income countries (where food loss is the larger issue) (Hanson et al., 2019).

Even with significant reductions, some amount of food loss and waste may be unavoidable. This residual food waste can potentially be repurposed as animal feed, reducing both the emissions from its disposal and displacing demand and emissions for feed crops (Torok, Luyckx, & Lapidge, 2021). Regulatory frameworks still largely prohibit using human food waste for animal feed or limit the types of waste that can be used; however, with appropriate processing and safety practices, it is possible to effectively integrate food waste into existing commercial feed production systems, as evidenced by the successful food-waste-to-pig-feed industry in Japan (Torok et al., 2021). Commercial food waste can also be processed via anaerobic digestion to create both a soil amendment and biomethane, which could be used to replace of fossil methane in a variety of applications (Levis & Barlaz, 2011).

2. Sustainable intensification – changes to *how* we produce food

a. Closing yield gaps

Improving yields is essential to meet growing food demand without causing further land-use change. Yield gaps – differences between observed yields and potential yields given current best agricultural practices – persist in many areas due to nutrient and/or water limitations (Foley et al., 2011; Mueller et al., 2012; Ray, Mueller, West, & Foley, 2013; Schils et al., 2018). Yield gaps are especially prevalent among cereal crops worldwide (Foley et al., 2011; Mueller et al., 2012; Schils et al., 2018). Increased irrigation alone could close cereal yield gaps in 16% of underachieving areas, and increased nutrient application alone could close cereal yield gaps in 73% of underachieving areas. Together, improved irrigation and nutrient management can close cereal yield gaps in all underperforming areas to within 75% of attainable yields and result in a 29% global production increase from existing cropland (Mueller et al., 2012). However, it is also important to prioritize resource input efficiency to minimize nitrogen and phosphorus runoff and avoid exacerbating water scarcity. There is also a potential tradeoff between the goal of reducing N_2O emissions from soils and increasing nutrient application to close yield gaps (Kim, Giltrap, & Sapkota, 2023). Targeted strategies to both improve input efficiency in regions with nutrient overuse (e.g., China) and increase nutrient application in regions with nutrient deficiencies (e.g., Eastern Europe) could close yield gaps to with 75% of attainable yields while minimizing net changes to total nutrient inputs (Mueller et al., 2012).

The potential to close yield gaps is important to consider when projecting whether future crop demand can be met without additional land-use change. Figure 3.3 shows historical global average cereal yields (FAO, 2023) and yield projections through 2050 from Integrated Assessment Model (IAM) scenarios (orange, green, and blue lines from 2020-2050) (Byers et al., 2022). Yield projections include an uncertainty range calculated from

potential climate impacts on average cereal yields (Jägermeyr et al., 2021), which are not directly modeled by IAM scenarios. Theoretical yields that would be required to meet projected food demand without additional land-use change after 2030 are also included (red dot indicating mean demand increase assuming a population of 10 billion by 2050, with whiskers representing high and low demand increase potential for same population) (Falcon et al., 2022). Finally, the historical yield trend is shown as a dashed black line. It is important to note that regional and crop-specific differences in yield trends, drivers, and climate impacts will be important for developing targeted intensification/adaptation strategies but are likely not well-represented by global averages. Following the historical trend results in a 2050 yield closest to the maximum IAM scenario projection with adverse climate impacts. If we expect yields to continue improving along the historical trend for the next 30 years, this might indicate that IAMs underestimate the rate of yield improvements on average. However, even if we assume cereal yield gaps can be closed to within 75% of attainable yields globally by 2050, the resulting 29% production increase would result in a 2050 yield slightly below what would be expected from the historical trend, indicating that additional technological and agronomic management practices will likely be required to meet projected food demand without additional land-use change or dietary shifts (red point with uncertainty whiskers in Figure 3.3). Moreover, fundamental differences in assumptions among individual IAMs regarding the rate of technological innovation, improved agronomy practices, and land-use/land-use change all lead to lead to high uncertainty of yield drivers (e.g., total crop production and cropland/pasture area) (Stehfest et al., 2019). A more consistent and comprehensive representation of biogeochemical-agronomic feedbacks in IAMs would improve confidence in both the

robustness of future yield projections and the degree to which improved management and technologies would impact yield trends (Stehfest et al., 2019; Van Zeist et al., 2020).

b. Slow-release fertilizers

Additional yield gains can be achieved by implementing new technologies and farming practices beyond those required to close yield gaps. Crop genetic engineering, for example, has potential to increase yields by improving resilience to abiotic stress, optimizing photosynthesis, and improving nitrogen use efficiency (Baily-Serres, Parker, Ainsworth, Oldroyd, & Schroeder, 2019). However, the timeline for developing improved crop varieties is long compared to other yield improvement strategies, and research indicates that nearly 90% of yield increases for U.S. maize since 2005 were due to climate and agronomy rather than crop genetic improvements (Rizzo et al., 2022). Another potential technology is slow-release nitrogen fertilizer, which (as the name suggests) releases nitrogen more slowly than conventional fertilizers and in a pattern that more closely matches the crop nitrogen uptake for physiological functions (Guertal, 2009; Li, Cheng, Lu, & Lu, 2021). Because of these properties, slow-release fertilizer only requires a single application per growing season, which can improve both yields and nitrogen use efficiency (Li et al., 2021; Wesołowska et al., 2021) and potentially reduce soil GHG emissions and nutrient leaching (Guertal, 2009; Wesołowska et al., 2021). Synthetic slow-release fertilizers can be separated into two main categories: chemically reacted slow-release products and physically coated slow-release products. Chemically reacted slow-release nitrogen fertilizers are created from urea that has been chemically reacted into a form that is slower to release into soil, examples of which include urea formaldehyde (UF) and isobutylidene diurea (IBDU) (Guertal, 2009). Physically-coated slow-release fertilizers are slow-releasing

because of a physical coating around the fertilizer material, which is typically made of sulfur, wax, and/or plastic resin. Examples of physically coated slow-release nitrogen fertilizers include sulfur-coated urea and resin-coated urea (Guertal, 2009).

Slow-release fertilizers have existed for many years but are typically not used for large-scale commercial farming due to much higher up-front costs (Lawrencia et al., 2021; Li et al., 2021; Wesołowska et al., 2021). Sulfur-coated and resin-coated fertilizers can be up to 2 and 3 times more expensive, respectively, than conventional fertilizers (Wesołowska et al., 2021). In some cases, yield gains and labor savings from using slow-release fertilizers could offset most of the costs over time or even lead to cost-savings (Li et al., 2021), although it is not clear to what extent these potential cost savings could scale for larger commercial applications. Additionally, most polymer-based coatings are not biodegradable, and regulations in many regions restrict the use of non-biodegradable physical coatings to limit environmental impacts (Lawrencia et al., 2021; Wesołowska et al., 2021). Natural polymer coatings are being developed with the goal of creating a fully biodegradable coating option, but the technology is still in its early stages; natural polymers presently lack sufficient mechanical integrity to form an effective coating unless they are mixed with other (non-biodegradable) materials (Lawrencia et al., 2021). Ultimately, to facilitate the broader adoption of slow-release fertilizers, targeted research is needed to bring biodegradable coating materials down the cost curve and improve their mechanical integrity.

c. Improving farming practices

Management practices such as cover cropping (Jian, Du, Reiter, & Stewart, 2020; Marcillo & Miguez, 2017; Oldfield, Bradford, & Wood, 2019; Pittelkow et al., 2015; Vendig et

al., 2023) and cropping rotation diversification (Nunes, van Es, Schindelbeck, Ristow, & Ryan, 2018; M. E. Smith et al., 2023) can also effectively boost yields. Cover cropping is the practice of growing a non-cash crop on otherwise bare or fallow soil to reduce soil erosion and improve soil quality (Marcillo & Miguez, 2017; Vendig et al., 2023). Yield gains from cover cropping are likely the direct result of increased soil organic carbon (SOC) concentrations, which can lead to yield gains of up to 24% with legume cover crops specifically (Nunes et al., 2018; Vendig et al., 2023). Because they are not cash-crops, cover crops incur additional costs from purchasing and planting, which poses a barrier to widespread adoption; however, utilizing cover crops that can be grazed by cattle could help to offset costs while still ultimately improving specific crop yields, thereby generating higher returns (Schomberg et al., 2014). Increasing crop rotational diversity is the practice of growing multiple crop species in a rotation sequence in the same field and can lead to yield benefits that increase over time, particularly for cereals with lower levels of nitrogen inputs (M. E. Smith et al., 2023). Low- or no-tillage (Dittmer, Darby, Goeschel, & Adair, 2020; MacLaren et al., 2022; Mathers et al., 2023; Nunes et al., 2018; Pittelkow et al., 2015; Powlson et al., 2014) has unclear impacts on yields, with some studies indicating it improves yields under certain conditions (e.g., in dry regions with rainfed agriculture) while others indicate is has a negligible or even slightly negative yield impact. In summary, additional yield gains are possible by implementing improved management practices, but both the opportunity cost and upfront costs of such practices still pose barriers to widespread adoption. Organizations should prioritize research and demonstration of applications with co-benefits that can help offset costs or even lead to cost savings when combined with the resulting yield increases.

3. Emissions reduction, re-allocation, and suppression – changes to *how* and *where* we produce food

Reducing the emissions associated with farming is a particularly challenging goal: emissions originate from area sources (as opposed to point sources) that are intimately linked to modern agricultural practices and fundamental chemistry (Clark et al., 2020; Crippa et al., 2021; Hong et al., 2021; Rosa & Gabrielli, 2023; Tilman et al., 2011). Based on the *Pale* identity (eq. 28), food systems cannot reach net-zero emissions without significantly reducing the emissions intensity of farming, and any amount by which emissions intensity is not reduced must be ultimately offset with equivalent GHG removal. Strategies for reducing emissions intensity can be broadly categorized as either reduction or suppression, and a combination of both strategies is essential to reduce the emissions intensity of food production at a global scale.

a. Reduction

Reduction strategies involve changes to *how* we grow food to reduce farming process emissions. A high-priority reduction strategy is the decarbonization of energy and industry inputs to agricultural systems (Rosa & Gabrielli, 2023; Soofi et al., 2022). Emissions from energy and industry caused 4.6 Gt CO_2-eq emissions in 2017 – a quarter of the food system total (Crippa et al., 2021; Hong et al., 2021). System-wide electrification of on-farm energy uses (e.g., electric tractors) (Soofi et al., 2022) combined with zero-carbon electricity and heat generation could eliminate a total of 3 Gt CO_2-eq emissions from production, packaging, retail, and households (Crippa et al., 2021). Of the remaining 1.6 Gt CO_2-eq emissions, 0.87 Gt is from fossil fuel combustion for food transport and 0.76 Gt is from

industrial process emissions (Crippa et al., 2021). Electrification of short- and medium-haul transport is viable with current technologies, and long-haul transport (e.g., heavy trucking, shipping, and aviation) can be decarbonized via fuel-swapping with carbon-neutral liquid fuels (Bergero et al., 2023; Davis et al., 2018). Industrial process emissions include emissions from steel and synthetic fertilizer production. Steel production emissions can be reduced through use of electric arc furnaces, process heat fuel-switching, efficiency improvements, and biomass-derived or hydrogen reductants, while fertilizer production emissions can be reduced by using electrolytic hydrogen production instead of steam methane reformation (Davis et al., 2018).

On-farm emissions can also be reduced by improving manure management practices. Most manure management emissions are from liquid manure systems (lagoons), which are the primary systems used by farms with large manure volumes (Aguirre-Villegas & Larson, 2017; Owen & Silver, 2015). Smaller farms primarily use solid manure management systems, which have comparatively lower GHG emissions due to higher aeration rates (Aguirre-Villegas & Larson, 2017; Chadwick et al., 2011; Owen & Silver, 2015). For permitted facilities that handle large amounts of manure, switching from liquid to solid manure management systems may not be feasible given constrains to manure storage and application timing that are required to maintain water and air quality (Aguirre-Villegas & Larson, 2017). However, it is possible to reduce emissions from manure lagoons by more than 50% via anaerobic digestion (Aguirre-Villegas & Larson, 2017).

b. Suppression

Suppression strategies are technical innovations that inhibit the formation of GHG emissions from farming practices. Suppression is particularly important for emissions that result from biogeochemical processes inherent to food production, such as enteric fermentation, release of N_2O from soils, and methane from rice cultivation (Crippa et al., 2021; Hong et al., 2021; Rosa & Gabrielli, 2023). Methane formation from enteric fermentation naturally occurs during ruminant digestion and acts as a metabolic hydrogen sink (Beauchemin, Ungerfeld, Eckard, & Wang, 2020; Janssen, 2010; McCauley et al., 2020; Ungerfeld, 2020). An effective metabolic hydrogen sink helps to maintain both rumen pH and the kinetic favorability of digestion chemistry (Beauchemin et al., 2020; Janssen, 2010; McCauley et al., 2020; Ungerfeld, 2020). However, methane release from the digestive system is a net energy loss – if ruminants could instead utilize the excess hydrogen instead of releasing it as methane, they could get up to 12% more energy out of the same mass of food (Glasson et al., 2022).

Methods for suppressing methane formation during ruminant digestion include feed additives and vaccines that directly inhibit methanogens in the rumen (Glasson et al., 2022; Honan, Feng, Tricarico, & Kebreab, 2022; A. Patra, Park, Kim, & Yu, 2017; A. K. Patra, 2012; Reisinger et al., 2021; B.M. Roque et al., 2019). Seaweed feed additives containing high amounts of bromoform (e.g., *Asparagopsis taxiformis sp.*) have been shown to reduce ruminant methane emissions by up to 95% without adverse impacts to volatile fatty acid production (B.M. Roque et al., 2019), although more research is needed to rule out any long-term effects to cattle health or growth beyond 5-6 months of treatment. The active compounds in seaweed feed additives are also metabolized quickly, so consistent feeding

with the feed additives would be needed to keep seeing emissions mitigation benefits (Ungerfeld, 2020). Moreover, if methanogenesis is inhibited in the long term, it may be necessary to enhance alternate metabolic hydrogen sinks to stabilize rumen pH and digestion reaction kinetics (Ungerfeld, 2020). Adding fumarate to cattle feed (or any compound with a redox potential higher than CO_2) is a possible method to enhance alternate hydrogen sinks and maintain metabolic hydrogen flow (Ungerfeld, 2020).

Soil N_2O emissions are a result of nitrification and denitrification, and N_2O emissions increase with increased rates of synthetic fertilizer application (Butterbach-Bahl, Baggs, Dannenmann, Kiese, & Zechmeister-Boltenstern, 2013; Graham, Wortman, & Pittelkow, 2017). In the absence of innovative suppression methods, a tradeoff therefore exists between mitigating soil N_2O emissions and yield gains. Integrated nutrient management (INM) is a potential soil emissions suppression method that aims to synchronize crop demand with nutrient availability through a combination of organic, inorganic, and biological soil amendments (Graham et al., 2017). By synchronizing crop demand for nutrients with nutrient availability in soils, INM increases nitrogen use efficiency which thereby reduces excess nitrogen in soils, which can theoretically reduce N_2O emissions without sacrificing yields. Although effectiveness and mitigation potential vary widely across studies, in general, INM treatments with low C:N ratios tend to be the most effective at reducing N_2O emissions compared to treatments with higher C:N ratios or organic amendments alone (Graham et al., 2017). Other potential soil amendments include biochar and organic fertilizers: biochar can lower N_2O emissions rates by facilitating electron transfer to denitrifying organisms in the soil (Cayuela et al., 2013), and organic fertilizers (e.g., manure) can lower N_2O emissions by increasing the relative abundance of denitrifying

microorganisms that favor complete denitrification to N_2 gas over incomplete denitrification to N_2O (Lazcano, Zhu-Barker, & Decock, 2021).

Methane emissions from rice cultivation caused 0.86 Gt CO_2-eq emissions in 2017, nearly 5% of the food system total (Figure 3.1) (Hong et al., 2021). Agronomic management practices such as controlled irrigation – irrigation techniques such as alternate wetting and drying (AWD) or drip irrigation that minimize anaerobic growing conditions – can help to reduce rice methane emissions (Mallareddy et al., 2023), but the benefits are highly dependent on site-specific environmental conditions and have tradeoffs with yield gains (Cho et al., 2022). Recent innovations in biochemical methods have strong potential for methane suppression: cellulose acetate coated ethephon, a type of slow-release plant growth regulator with strong inhibitory effects on methanogenesis, has been shown to reduce rice paddy methane emissions by up to 90% without negatively impacting yields (Cho et al., 2022).

4. Interventions for removing residual emissions

Even with decreased demand and ambitious improvements to yields and emissions intensity of farming, it will be extremely difficult to fully eliminate GHG emissions from the global food system. In order to reach net-zero emissions, any residual emissions must therefore be offset by an equivalent amount of GHG removal. Figure 3.4 summarizes the amount of GHG removal that would be required to reach net-zero emissions as a function of *Pale* identity drivers under different demand scenarios (Falcon et al., 2022). As indicated by moving from the top right corner toward the bottom left corner of each panel, reductions in the land intensity of production (l/a) and emissions intensity of land use (e/l) result in

lower food system emissions and therefore lower amounts of GHG removal that would be required compared to baseline. For example, in a low-food-demand scenario for 2050 (Figure 3.4, panel C) where food-driven land-use change stops after 2030 and 50% of beef consumption shifts to chicken, food system emissions are reduced from 26 Gt to 9 Gt CO_2-eq (represented by the white square point). Further reductions in (e/l) through emissions reduction and suppression methods and/or further reductions in (l/a) by yield improvements and land restoration could result in even lower amounts of residual emissions and therefore less GHG removal required to reach net-zero.

Carbon dioxide removal (CDR) is the main form of GHG removal that exists today, though not yet near the scale required to reach gigaton-scale removal and sequestration. Different approaches to CDR vary widely in their efficacy, durability, and price (Chay et al., 2022; Wenger, D'Alessandro, & Wright, 2022). CDR methods can be loosely categorized on a spectrum ranging from "nature-based" to "engineered". Examples of methods at or near the "nature-based" end of the spectrum include afforestation or reforestation, seaweed farming and sinking, and ocean iron fertilization (OIF) (Chay et al., 2022). Methods that fall at or near the "engineered" end of the spectrum include bioenergy with carbon capture and storage (BECCS) and direct air capture and storage (DAC) (Chay et al., 2022). Most CDR methods are a combination of "nature-based" and "engineered" in that they enhance or mimic natural carbon sinks through innovative technology and engineering techniques (Wilcox, Kolosz, & Freeman). Examples of these methods that fall somewhere in the middle of the spectrum include enhanced weathering (EW), ocean alkalinity enhancement (OAE), biomass carbon removal and storage (BiCRS), and biochar (Chay et al., 2022; Wilcox et al.). Enhanced weathering in agricultural soils may have significant co-benefits for crop yields

(Beerling et al., 2023; Edwards et al., 2017), but further research and demonstration is needed to determine if potential co-benefits can reliably scale for multiple crop types and climates. Whether nature-based or engineered or some combination of both, in order for the climate impact of CDR to effectively offset residual emissions, the durability of carbon removal and storage must be at least as long as the average atmospheric lifetime of any residual emissions it is used to offset. Otherwise, a low-durability removal is essentially a delayed re-emission of the original residual GHG. Durability varies widely by CDR approach and is (with a few exceptions) directly related to cost (Wenger et al., 2022). Increased deployment of CDR that is expensive today will continue to bring the technology down cost curves (McQueen et al., 2021), although it is unclear just how low costs can get, particularly for engineered methods (Davis et al., 2018).

Methane removal technologies are still in early stages of development compared to CDR (R.B. Jackson et al., 2021). Due to methane's relatively short atmospheric lifetime but high radiative forcing, the main benefit of methane removal is the potential to limit temperature overshoot above climate targets (R.B. Jackson et al., 2021; Ming et al., 2022). Methods for methane removal include photocatalysis in solar updraft towers, zeolite catalysis in direct air capture structures, enhancement of natural hydroxyl and chlorine sinks, and methanotrophic bacteria (R.B. Jackson et al., 2021; Ming et al., 2022). Some of these methods could be cheaper at scale per ton CO_2-eq than CDR and may have co-benefits to air-quality, and crop yields. However, the cheapest potential method – enhancement of natural chlorine sinks – poses such significant risks to human health that it should only be considered in extremely remote areas if at all (Ming et al. 2022). Methane capture by zeolite in DAC devices and subsequent removal via thermal catalysis is a safer method that

can potentially take advantage of DAC scaling to minimize additional infrastructure costs (Ming et al. 2022), but the lower concentration of methane in ambient air compared to CO_2 may make co-removal in the same device difficult. Photocatalysis on surfaces can potentially remove other non-CO_2 GHGs, like N_2O, though much more research is needed on technical potential and costs (Ming et al. 2022).

3.4 Summary and Conclusions

Achieving net-zero emissions in the global food system is a particularly daunting task due to the share of area-source non-CO_2 GHG emissions that are fundamentally linked to modern agricultural practices. Shifting diets away from beef would have an outsized impact on decreasing the average emissions intensity of caloric production, while reducing food loss and waste may increase food security through microeconomic rebound effects in addition to emissions mitigation. Closing yield gaps is a top priority for sustainable intensification, and targeted strategies to improve input efficiency in some regions while increasing nutrient application in others could close yield gaps with minimal net changes to total nutrient inputs. In order for slow-release fertilizers to contribute to sustainable intensification at scale, further research is needed into the development of cost-competitive, fully biodegradable options.

Increasing demand for food, combined with potential tradeoffs between yield gains and higher N_2O emissions, will ultimately drive the need for emissions suppression at the farm-level. Promising methods are being developed to suppress GHG emissions from enteric fermentation, soils, and rice paddies, although further research is needed to determine the long-term efficacy and scalability of solutions. Even with optimistic yield gains and

widespread on-farm emissions suppression, land-based emissions cannot reach zero unless we stop deforestation. At COP26, world leaders pledged to end deforestation by 2030 (Thomas Gasser, Ciais, & Lewis, 2022), and strict land-use policies should be put in place now to ensure the pledge is ultimately fulfilled. Finally, GHG removal will likely be required to offset some amount of particularly difficult-to-eliminate emissions, and new approaches for both methane removal and commercial CDR scalability are areas of active research. Creating a sustainable agriculture system that can feed the world without contributing to climate change will require coordinated efforts from both consumers and producers and consumers across multiple food and energy sectors, and we must rapidly scale up those efforts starting today.

3.5 Methods

2017 emissions (Figure 3.1). We used data from Hong et al. (2021) for the land-based components of food system emissions (including land-based agricultural emissions and land-use change) and data from Crippa et al. (2021) EDGAR-FOOD v6 for the energy, industry, and waste components of food system emissions. We only considered emissions directly related to the food system and thus excluded emissions from wood harvesting (timber). When allocating energy, industry, and waste emissions to agricultural product emissions from Hong et al., we used data from Poore and Nemecek (2018) for the commodity-specific proportion of emissions from land-based and non-land-based activities.

Dietary shifts (Figure 3.2). We used country-level per-capita food supply available for consumption data for beef, dairy, poultry, and chicken from the FAOSTAT food balances

(FAO, 2022). We calculated country-level total consumption by multiplying per-capita consumption with the population for each country. Global cumulative consumption was then calculated by summing the country-level totals, sorted from lowest to highest per-capita consumption. Total emissions for each food as a function of cumulative global consumption (y-axis of Figure 3.2 panels) were then calculated by scaling the total emissions for each food from Hong et al. (2021) to the percent increase in global cumulative consumption from each country's consumption. We then calculated the relationship between total emissions for each food and the corresponding cumulative population using polynomial curve-fitting. Finally, the resulting equation was then plotted as a function of fractional consumption (x-axis of Figure 3.2 panels). To determine the net emissions change resulting from replacing beef with mass-equivalent pulses (Supplementary Figure C.1), we first converted the mass of additional pulses to calories and then calculated the additional emissions that would be caused by increased caloric pulses consumption using the average emissions per kcal for pulses from Hong et al. (2021). We then added the associated pulses emissions to the avoided (negative) emissions from reduced beef consumption.

Yields and climate impacts (Figure 3.3). For plotting historical yield data, we used 1961-2020 cereal yield from FAOSTAT Food Production (FAO, 2023). For projecting future yields, we calculated the minimum, median, and maximum annual % increase in cereal yield from IPCC AR6 Integrated Assessment Model scenarios (Byers et al., 2022) that reach 2.0˚C or lower by 2100 and applied those rates of increase to the 2020 historical yield value from FAOSTAT. To calculate the climate impact uncertainty ranges, we used data on climate impacts by 2100 for rice, wheat, and maize from Figure 1 of Jägermeyr et al. (2021).

We converted this crop-specific data to minimum, average, and maximum potential climate impact for all cereals using a weighted average of the minimum, average, and maximum values from the individual cereal crops based on the fraction of total cereals production from each crop. The resulting minimum, mean, and maximum annual average % climate impacts on cereal yield were then added to the % increases in cereal yield from AR6 scenarios for a total of 9 yield-climate impact scenarios (each possible combination of min, median, max yield increase from AR6 scenarios and min, median, max climate impacts). Because data from Jägermeyr et al. (2021) is for the year 2099, the resulting net yield changes for 2099 were plotted and then linearly interpolated for years 2021-2098. The crop yield forecast values in Figure 3.3 for 2050 are from these interpolations.

The theoretical yield required to meet 2050 food demand without additional land-use change (red point and whiskers in Figure 3.3) was calculated based on several important assumptions: (1) that cereal demand on average would increase by the same percent as total average food demand from Falcon, Naylor, and Shanker (2022); (2) that 2050 population is 10 billion; and (3) that cropland for cereal production does not change beyond 2020. Cereal cropland area has fluctuated somewhat over the last 60 years (by approximately +12% from 1961-1980, -10% from 1980-2000, and +11% from 2000-2020) but on average has remained around 700 million hectares (Hong et al. 2021). It is possible that cereal demand on average will not increase by the same percentage as total food demand: specific cereal crops show large differences in projected demand by 2050 (Falcon, Naylor, and Shanker, 2022), but given the lack of specific data for wheat in Falcon, Naylor and Shanker (2022) and uncertain dynamics between different demand scenarios and commodity-specific demand, the average food % demand increase was assumed.

Emissions mitigation and the Pale identity (Figure 3.4). For projecting food system emissions in 2050, we used data on percent increases in total food demand and commodity-specific increases from Falcon, Naylor, and Shankar (2022), adjusted from the base period of 2019-2050 to 2017-2050 using FAO data on global caloric food production by product (FAO, 2023). The demand scenarios used from Falcon, Naylor, and Shankar (2022) were the minimum, average, and maximum % changes in total demand for a population of 10 billion people. We calculated the change in emissions for each food group by multiplying the resulting % changes in demand with total emissions for each food (calculated using data from Hong et al. (2021) and Crippa et al. (2021); see section on calculating 2017 emissions). To calculate the change in emissions from foods without projected demand changes in Falcon, Naylor, and Shanker (2022), we summed the 2017 emissions from foods that did have projected demand changes and subtracted the resulting sum from the total food system emissions (Hong et al., 2021; Crippa et al., 2021; see section on calculating 2017 emissions) to calculate the remaining emissions from all other foods in 2017. We then calculated the % change in demand for all other foods that would be required to result in the average food demand increase from Falcon, Naylor, and Shanker (2022) considering the % increases in foods with individual demand projections. We then calculated 2050 emissions from all other foods by multiplying the emissions from all other foods in 2017 by that % change that would be required to meet overall food demand increase in 2050. Finally, we summed the emissions from both groups (foods with defined % increases and all other foods) to calculate total food system emissions in 2050.

Next, we plotted the relationship between the resulting 2050 food system emissions, agricultural land area, and total food calories for each demand scenario using the Pale

identity (eq. 28). Total food calories demanded were calculated by multiplying 2017 food supply calories by the minimum, average, and maximum % change in total food demand for a population of 10 billion (Falcon, Naylor, and Shanker, 2022). Agricultural land area for each demand scenario was calculated assuming yields (average for all foods) increases linearly through 2050 and dividing the total food production amount (from Falcon, Naylor, and Shanker demand scenarios) by 2050 yield. The change in emissions that would result from stopping land use change after 2030 and shifting 50% of beef demand to (represented by square points in each Figure 3.4 panel) were calculated based on several assumptions: (1) that land-use change increase based on the linear average rate from historical data until 2030 and then remains constant; and (2) that 50% of caloric beef demand shifts to chicken but total food calories demanded in each scenario remains the same. Importantly, the yields that result from these assumptions are much higher than the yield that would be expected in 2050 if yield follows a linear increase trend, which is why the land-use intensity of production is lower than baseline for this scenario in all panels of Figure 3.4. This indicates that significant sustainable intensification would be required to meet caloric demand if land-use change for food stops by the end of the decade.

3.6 Figures

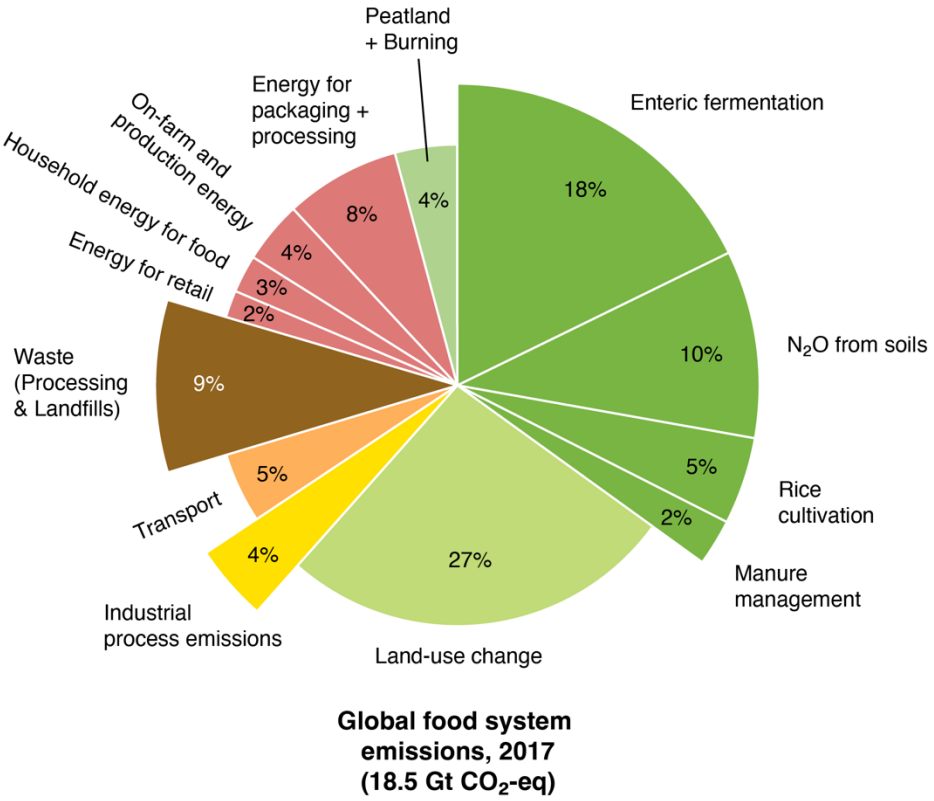

Figure 3.1 | 2017 Food system emissions. Emissions from the food system are caused by a combination of land-use change and land management (green wedges), energy inputs (red and orange wedges), industrial processes (yellow wedge), and waste (brown wedge). Wedges with a larger radius are particularly hard-to-abate from a technological/chemical perspective, though some smaller radius wedges might still be hard-to-abate for non-technical reasons (e.g., land-use change)

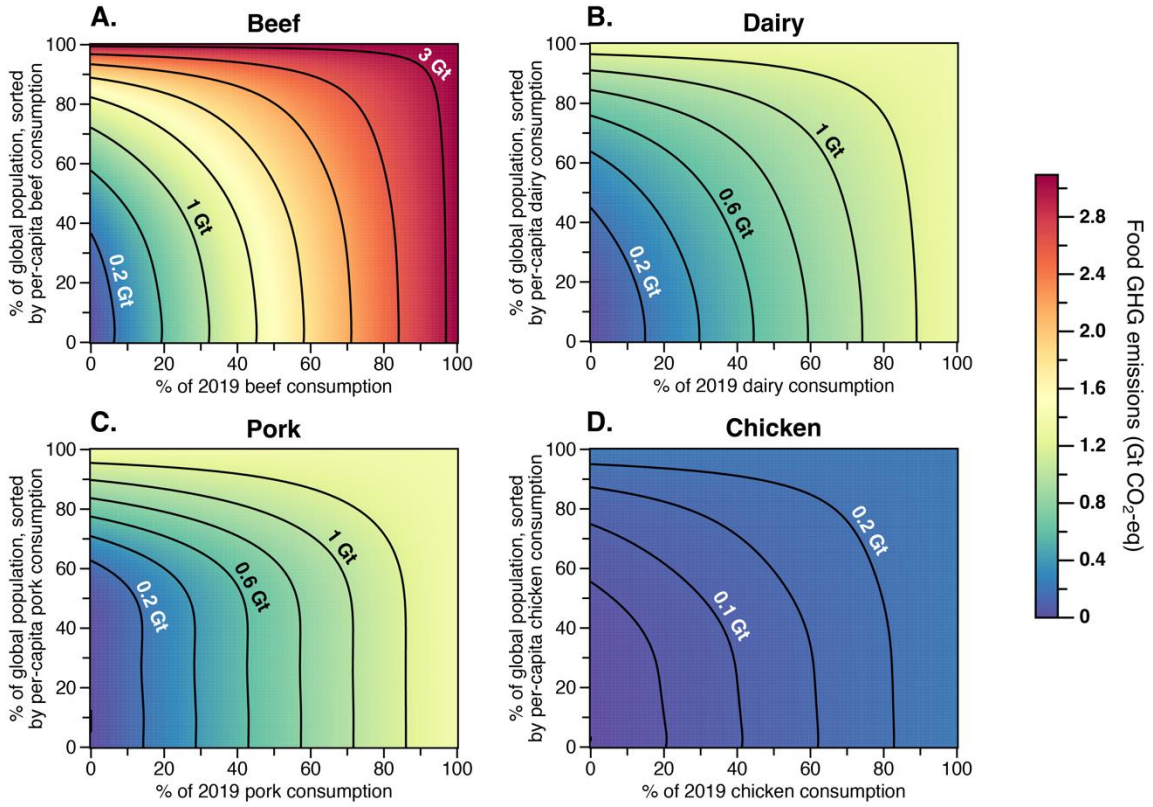

Figure 3.2 | Potential for dietary shifts to reduce food system emissions. Emissions from beef (**A**), dairy (**B**), pork (**C**), and chicken (**D**) in 2017 are shown as a function of the fraction of current consumption (x-axis) and the percentage of the population consuming that fraction of the food product, sorted top to bottom from highest to lowest national per-capita consumption (y-axis). 2017 emissions from each food product are thus represented by the values in the top-right corner of each panel, with contours representing the decreased emissions resulting from some percentage of the highest per-capita consumers reducing their consumption by some percent. For example, if the top 15% of per-capita beef consumers worldwide reduced their beef intake by 30% (represented on panel A as point (70, 85)), annual emissions from beef would be approximately 2.6 Gt CO2-eq, which is 0.5 Gt less than the original 3.1 Gt CO2-eq emissions from beef.

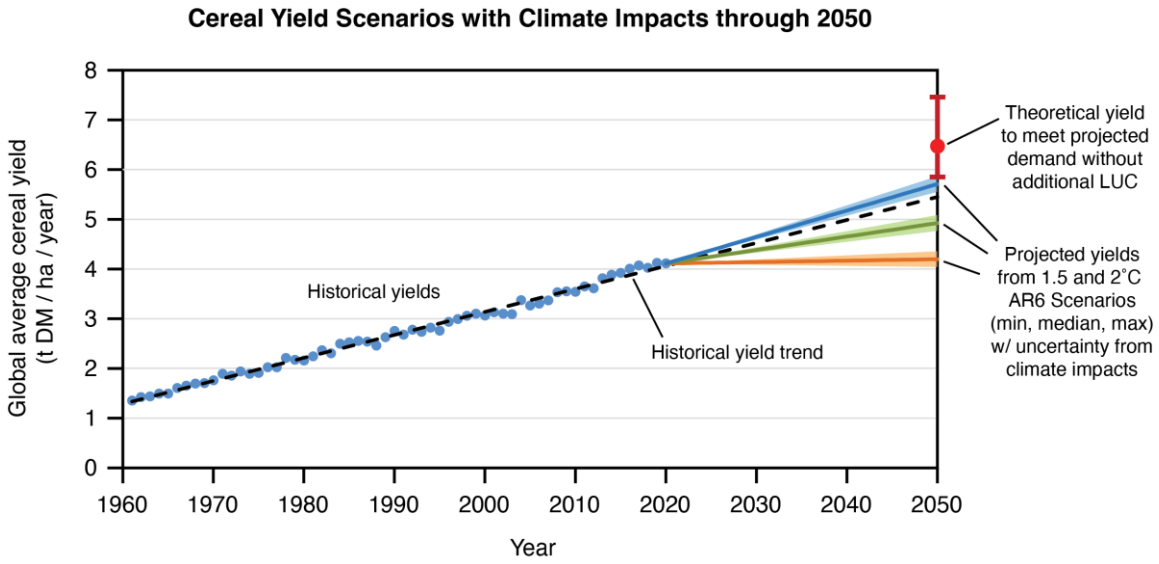

Figure 3.3 | Historical and projected cereal yields through 2050. Historical global average cereal yields (FAO, 2023) are shown as blue points, and yield projections through 2050 from Integrated Assessment Model (IAM) scenarios that limit mean end-of-century warming to 2˚C or less are shown as orange, green, and blue lines from 2020-2050 (Byers et al., 2022). Yield projections include an uncertainty range calculated from potential climate impacts on average cereal yields (Jägermeyr et al., 2021), which are not directly modeled by IAM scenarios. Theoretical yields that would be required to meet projected food demand without additional land-use change after 2030 are also included (red dot for mean demand increase assuming a population of 10 billion by 2050, with whiskers representing high and low demand increase potential for same population) (Falcon et al., 2022). The historical yield trend is shown as a dashed black line.

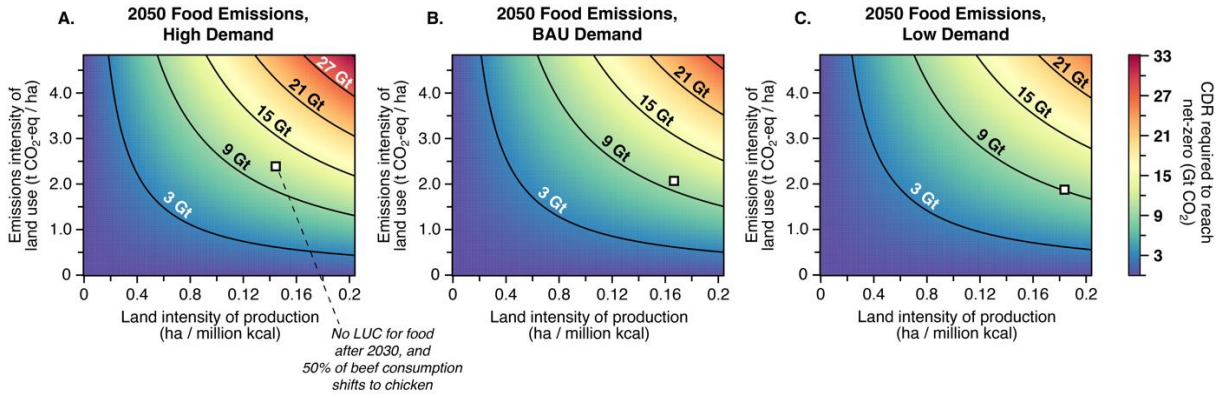

Figure 3.4 | Emissions mitigation levers for 2050 from the Pale identity. Total food system emissions in 2050 are shown as a function of the emissions intensity of land use (y-axis) and the land intensity of production (x-axis), with contours representing the amount of GHG removal to offset those residual emissions to reach net-zero. Each panel assumes a different food demand scenario from Falcon, Naylor, and Shanker (2022) with a 2050 population of 10 billion. White square points represent the total emissions that would result from a constant agricultural land area after 2030 and 50% of beef consumption shifting to a caloric-equivalent amount of chicken by 2050.

SUMMARY AND CONCLUSIONS

Supplying food and energy services to a growing global population without exceeding mean end-of-century warming of 2˚C will require massive systemic shifts to our agriculture and energy systems. The pace at which we make these shifts will determine how much we must rely on corresponding amounts of GHG removal to reach net-zero emissions and stabilize climate (Byers et al., 2022; Davis et al., 2018; DeAngelo et al., 2021; Matthews & Caldeira, 2008; Matthews et al., 2009). Even in the most ambitious mitigation scenarios, however, carbon removal by 2100 is often at the gigaton-scale annually (Byers et al., 2022; DeAngelo et al., 2021). Moreover, the amount of carbon removal is not evenly distributed across world regions, which has important implications for burden-sharing and equity (DeAngelo et al., 2021; Pozo et al., 2020). It is therefore essential to decarbonize as rapidly and comprehensively as possible while also scaling up technologies to remove excess GHGs from the atmosphere, particularly in developed nations that have caused the vast majority of historical cumulative emissions.

Reaching net-zero emissions in the energy system will entail rapid increases in renewable electricity generation, a massive scale-up in carbon-neutral liquid fuel production for use as drop-in fuel, and widespread electrification of energy services (Byers et al., 2022; Davis et al., 2018; DeAngelo et al., 2021). It will also potentially require large amounts of carbon capture and sequestration (CCS): in IAM scenarios that reach net-zero CO_2 emissions by 2100, about 1/3 of primary energy production still comes from fossil fuels on average when the energy system reaches net-zero emissions (DeAngelo et al., 2021). Development and deployment of CCS for existing fossil fuel energy generation

should therefore be prioritized now, in addition to early retirement of fossil fuel power plants without CCS capabilities (Fofrich et al., 2020). Emissions must also peak as soon as possible, and a rapid scale-up of carbon removal technologies is needed to reach the scales that might be required by end-of-century to offset residual emissions (Byers et al., 2022; DeAngelo et al., 2021).

In the context of reaching gigaton-scale carbon removal, nature-based strategies are appealing due to their lower energy and material requirements compared to engineered strategies. Marine nature-based methods, such as seaweed farming and sinking, also have advantages over land-based methods in that they do not require fertilizer or freshwater and do not need to compete for space with agriculture (Arzeno-Soltero et al., 2023; DeAngelo et al., 2023; Duarte et al., 2017; Froehlich et al., 2019). It is possible for seaweed farming and sinking to sequester carbon at gigaton-scales (Arzeno-Soltero et al., 2023; DeAngelo et al., 2023), but uptake of the nutrients required to grow such large amounts of seaweed would likely displace large amounts of phytoplankton growth and would therefore have significant negative impacts on ocean ecosystems. This competition with phytoplankton for nutrients would also negatively impact the net amount of carbon removed per ton of seaweed carbon grown, resulting in lower net additionality (Berger, Kwiatkowski, Ho, & Bopp, 2023). The cost per ton of CO_2 removed by growing and sinking seaweed could be as low as $480 in the cheapest areas, but this is still much higher than the optimistic target of $100 per ton that many carbon removal targets are aiming to achieve. The more economical climate benefit use for seaweed is as a substitute for agricultural products: if seaweed can sell at market prices displace demand for food, it could return a profit for each ton of CO_2-eq emissions avoided.

Using seaweed for food has such a high potential for avoiding emissions because modern agriculture is extremely emissions-intensive (Crippa et al., 2021; Hong et al., 2021). Rapid and sweeping changes are therefore needed to reduce food system emissions and eventually reach net-zero. On the demand side, shifting diets away from beef would have an outsized impact on decreasing the average emissions intensity of caloric production, while reducing food waste may increase food security through microeconomic rebound effects in addition to mitigating emissions. On the supply side, closing yield gaps is a top priority for sustainable intensification, and targeted strategies to improve input efficiency in some regions while increasing nutrient application in others could close yield gaps with minimal net changes to total nutrient inputs. Promising methods are being developed to suppress GHG emissions from enteric fermentation, soils, and rice paddies, although further research is needed to determine the long-term efficacy and scalability of solutions globally. Stopping deforestation is also a top priority, which will require aggressive policy action to enact strict land-use regulations. Without further land-use change, even more rapid yield gains and/or diet shifts to less land-intensive foods will be required to meet projected food demand.

Ultimately, achieving net-zero emissions energy and food systems by the end of this century will require accelerated and sweeping changes to existing systems. While it is certainly a daunting task, there are reasons to be optimistic about achieving this goal. Renewable energy is cost-competitive with fossil fuel energy sources most world regions (G. Luderer et al., 2022) and will likely continue to get cheaper, thanks to rapid technological progress and learning curves. The Inflation Reduction Act of 2022 was the US government's most ambitious piece of climate legislation to date, and it has the potential to

decrease US emissions economy-wide by nearly 50% by 2035 compared to 2005 levels (Bistline et al., 2023). Additionally, corporate investment in the climate-tech space is increasingly driving innovation and deployment of scalable low-carbon technologies (Surana et al., 2023). If we build on this momentum by scaling coordinated efforts to decarbonize energy and food systems, every bit of progress we make will contribute to better living conditions for future generations.

References

Aguirre-Villegas, H. A., & Larson, R. A. (2017). Evaluating greenhouse gas emissions from dairy manure management practices using survey data and lifecycle tools. *Journal of Cleaner Production, 143*, 169-179. doi:https://doi.org/10.1016/j.jclepro.2016.12.133

AIEEP. (2021). *Guidance for Ocean-Based Carbon Dioxide Removal Projects: A Pathway to Developing a Code of Conduct*. Retrieved from https://www.aspeninstitute.org/wp-content/uploads/files/content/docs/pubs/120721_Ocean-Based-CO2-Removal_E.pdf: https://www.aspeninstitute.org/wp-content/uploads/files/content/docs/pubs/120721_Ocean-Based-CO2-Removal_E.pdf

Aitken, D., Bulboa, C., Godoy-Faundez, A., Turrion-Gomez, J. L., & Antizar-Ladislao, B. (2014). Life cycle assessment of macroalgae cultivation and processing for biofuel production. *Journal of Cleaner Production, 75*. doi:10.1016/j.jclepro.2014.03.080

Arzeno-Soltero, I., Frieder, C., Saenz, B. T., Long, M., DeAngelo, J., Davis, S. J., & Davis, K. A. (2022). Biophysical potential and uncertainties of global seaweed farming. *preprint retrieved from EarthArXiv*. doi:https://doi.org/10.31223/X52P8Z

Arzeno-Soltero, I., Frieder, C., Saenz, B. T., Long, M., DeAngelo, J., Davis, S. J., & Davis, K. A. (2023). Large global variations in the carbon dioxide removal potential of seaweed farming due to biophysical constraints. *Communications Earth & Environment, 4*. doi:https://doi.org/10.1038/s43247-023-00833-2

Audoly, R., Vogt-Schilb, A., Guivarch, C., & Pfeiffer, A. (2018). Pathways toward zero-carbon electricity required for climate stabilization. *Applied Energy, 225*, 884-901.

Bach, L. T., Tamsitt, V., Gower, J., Hurd, C. L., Raven, J. A., & Boyd, P. W. (2021). Testing the climate intervention potential of ocean afforestation using the Great Atlantic Sargassum Belt. *Nature Communications, 12*(1), 2556. doi:10.1038/s41467-021-22837-2

Baily-Serres, J., Parker, J. E., Ainsworth, E. A., Oldroyd, G. E. D., & Schroeder, J. I. (2019). Genetic strategies for improving crop yields. *Nature, 575*, 109-118. doi:https://doi.org/10.1038/s41586-019-1679-0

Bajželj, B., Laguzzi, F., & Röös, E. (2021). The role of fats in the transition to sustainable diets. *The Lancet Planetary Health, 5*(9), E644-E653. doi:https://doi.org/10.1016/S2542-5196(21)00194-7

Bataille, C. (2019). Physical and policy pathways to net-zero emissions industry. *WIRES Wiley Interdisciplinary Reviews*, 1-20. doi:10.1002/wcc.633

Bataille, C., Waisman, H., Briand, Y., Svensson, J., Vogt-Schilb, A., Jaramillo, M., . . . Imperio, M. (2020). Net-zero deep decarbonization pathways in Latin America: Challenges and opportunities. *Energy Strategy Reviews*. doi:10.1016/j.esr.2020.100510

Beauchemin, K. A., Ungerfeld, E. M., Eckard, R. J., & Wang, M. (2020). Review: Fifty years of research on rumen methanogenesis: lessons learned and future challenges for mitigation. *Animal, 14*, s2-s16. doi:https://doi.org/10.1017/S1751731119003100

Beerling, D. J., Epihov, D. Z., Kantola, I. B., Masters, M. D., Reershemius, T., & Planavsky, N. J. (2023). Enhanced weathering in the U.S. Corn Belt delivers carbon removal with agronomic benefits. doi:https://doi.org/10.48550/arXiv.2307.05343

Berger, M., Bopp, L., Ho, D. T., & Kwiatkowski, L. (2022). *Assessing global macroalgal carbon dioxide removal potential using a high-resolution ocean biogeochemistry model*. Paper presented at the EGU General Assembly, Vienna, Austria.

Berger, M., Kwiatkowski, L., Ho, D. T., & Bopp, L. (2023). Ocean dynamics and biological feedbacks limit the potential of

macroalgae carbon dioxide removal. *Environmental Research Letters, 18*.

doi:https://doi.org/10.1088/1748-9326/acb06e

Bergero, C., Gosnell, G., Gielen, D., Kang, S., Bazilian, M., & Davis, S. J. (2023). Pathways to net-zero emissions from aviation. . *Nature Sustainability 6*, 404-414. doi:https://doi.org/10.1038/s41893-022-01046-9

Bistline, J. (2021). The importance of temporal resolution in modeling deep decarbonization of the electric power sector. *Environmental Research Letters*. doi:10.1088/1748-9326/ac10df

Bistline, J., Blanford, G., Brown, M., Burtraw, D., Domeshek, M., Farbes, J., . . . Jones, R. (2023). Emissions and energy impacts of the Inflation Reduction Act. *Science, 380*(6652), 1324-1327.

Bistline, J., Cole, W., Damato, G., DeCarolis, J., Frazier, W., Linga, V., . . . Young, D. (2020). Energy storage in long-term system models: a review of considerations, best practices, and research needs. *Progress in Energy, 2*, 039601.

Broch, O. J., & Slagstad, D. (2012). Modelling seasonal growth and composition of the kelp Saccharina latissima. *Journal of Applied Phycology*. doi:10.1007/s10811-011-9695-y

Bryant, B. P., & Lempert, R. J. (2010). Thinking inside the box: A participatory, computer-assisted approach to scenario discovery. *Technological Forecasting and Social Change*. doi:10.1016/j.techfore.2009.08.002

Burney, J. A., Davis, S. J., & Lobell, D. B. (2010). Greenhouse gas mitigation by agricultural intensification. *Proceedings of the National Academy of Sciences, 107*(26), 12052 - 12057. doi:https://doi.org/10.1073/pnas.0914216107

Buschmann, A. H., Camus, C., Infante, J., Neori, A., Israel, Á., Hernández-González, M. C., . . . Critchley, A. T. (2017). Seaweed production: overview of the global state of exploitation, farming and emerging research activity. *European Journal of Phycology*. doi:10.1080/09670262.2017.1365175

Butterbach-Bahl, K., Baggs, E. M., Dannenmann, M., Kiese, R., & Zechmeister-Boltenstern, S. (2013). Nitrous oxide emissions from soils: how well do we understand the processes and their controls? *Phil. Trans. R. Soc. B, 368*. doi:https://doi.org/10.1098/rstb.2013.0122

Byers, E., Krey, V., Kriegler, E., Riahi, K., Schaeffer, R., Kikstra, J., . . . van Vuuren, D. (2022). *AR6 Scenarios Database hosted by IIASA*.

Calvin, K., Bond-Lamberty, B., Jones, A., Shi, X., Vittorio, A. D., & Thornton, P. (2019). Characteristics of human-climate feedbacks differ at different radiative forcing levels. *Global and Planetary Change, 180*, 126-135.

Calvin, K., & Bond-Lamberty, B. I. (2018). Integrated human-earth system modeling—state of the science and future directions. *Environmental Reseach Letters, 13*, 063006.

Calvin, K., Patel, P., Clarke, L., Asrar, G., Bond-Lamberty, B., Cui, R. Y., . . . Wise, M. (2019). GCAM v5.1: representing the linkages between energy, water, land, climate, and economic systems. *Geoscientific Model Development, 12*, 677-698.

Camus, C., Infante, J., & Buschmann, A. H. (2019). Revisiting the economic profitability of giant kelp Macrocystis pyrifera (Ochrophyta) cultivation in Chile. *Aquaculture*. doi:10.1016/j.aquaculture.2018.12.030

Cantore, N., & Padilla, E. (2010). Equality and CO2 emissions distribution in climate change integrated assessment modelling. *Energy, 35*(10), 298-313.

Capron, M., Lucas, K., Stewart, J., Blaylock, R., Howden, S., Chambers, M., . . . Drach, A. (2020). AdjustaDepth TechnoEconomic Analysis for ARPA-E Phase 1 Contract DE-AR0000916. In.

Cayuela, M. L., Sánchez-Monedero, M. A., Roig, A., Hanley, K., Enders, A., & Lehmann, J. (2013). Biochar and denitrification in soils: when, how much and why does biochar reduce N 2 O emissions? *Scientific Reports, 3*, 1732. doi:https://doi.org/10.1038/srep01732

Chadwick, D., Sommer, S., Thorman, R., Fangueiro, D., Cardenas, L., Amon, B., & Misselbrook, T. (2011). Manure management: Implications for greenhouse gas emissions. *Animal Feed Science and Technology, 166*, 514-531. doi:https://doi.org/10.1016/j.anifeedsci.2011.04.036

Chay, F., Klitzke, J., Hausfather, Z., Martin, K., Freeman, J., & Cullenward, D. (2022). *Verification Confidence Levels for carbon dioxide removal.* Retrieved from https://carbonplan.org/research/cdr-verification-explainer

Cho, S. R., Verma, P. P., Das, S., Kim, G. W., Lim, J. Y., & Kim, P. J. (2022). A new approach to suppress methane emissions from rice cropping systems using ethephon. *Science of The Total Environment, 804*. doi:https://doi.org/10.1016/j.scitotenv.2021.150159

Clark, M. A., Domingo, N. G., Colgan, K., Thakrar, S., Tilman, D., Lynch, J., . . . Hill, J. D. (2020). Global food system emissions could preclude achieving the 1.5° and 2°C climate change targets. *Science, 370*, 705-708. doi:https://doi.org/10.1126/science.aba7357

Collins, W. D., Craig, A. P., Truesdale, J. E., Vittorio, A. V. D., Jones, A. D., Bond-Lamberty, B., . . . Hurtt, G. C. (2015). The integrated Earth system model version 1: formulation and functionality. *Geoscientific Model Development, 8*, 2203-2219.

Correa, T., Guitiérrez, G., Flores, R., Buschmann, A. H., Cornejo, P., & Bucarey, C. (2016). Production and economic assessment of giant kelp *Macrocystis pyrifera* cultivation for

abalone feed in the south of Chile. *Aquaculture Research, 47*, 698-707. doi:10.1111/are.12529

Costa, C., Wollenberg, E., Benitez, M., Newman, R., Gardner, N., & Bellone, F. (2022). Roadmap for achieving net-zero emissions in global food systems by 2050. *Scientific Reports, 12*. doi:https://doi.org/10.1038/s41598-022-18601-1

Creutzig, F., Agoston, P., Goldschmidt, J. C., Luderer, G., Nemet, G., & Pietzcker, R. C. (2017). The underestimated potential of solar energy to mitigate climate change. *Nature Energy, 2*(9), 17140.

Crippa, M., Solazzo, E., Guizzardi, D., Monforti-Ferrario, F., Tubiello, F. N., & Leip, A. (2021). Food systems are responsible for a third of global anthropogenic GHG emissions. *Nature Food, 2*, 198-209. doi:https://doi.org/10.1038/s43016-021-00225-9

Davis, S. J., Lewis, N. S., Shaner, M., Aggarwal, S., Arent, D., Azevedo, I. L., . . . Caldeira, K. (2018). Net-zero emissions energy systems. *Science*. doi:10.1126/science.aas9793

de Ramon N'Yeurt, A., Chynoweth, D. P., Capron, M. E., Stewart, J. R., & Hasan, M. A. (2012). Negative carbon via Ocean Afforestation. *Process Safety and Environmental Protection, 90*, 467-474.

DeAngelo, J., Azevedo, I., Bistline, J., Clarke, L., Luderer, G., Byers, E., & Davis, S. J. (2021). Energy systems in scenarios at net-zero CO2 emissions. *Nature Communications*(12). doi:https://doi.org/10.1038/s41467-021-26356-y

DeAngelo, J., Saenz, B., Arzeno-Soltero, I. B., Frieder, C., Long, M., Hamman, J., . . . Davis, S. J. (2023). Economic and biophysical limits to seaweed farming for climate change mitigation. *Nature Plants, 9*, 45-57. doi:https://doi.org/10.1038/s41477-022-01305-9

Deason, J., & Borgeson, M. (2019). Electrification of Buildings: Potential, Challenges, and Outlook. *Current Sustainable/Renewable Energy Reports, 6*, 131-139.

Dittmer, K. M., Darby, H. M., Goeschel, T. R., & Adair, E. C. (2020). Benefits and tradeoffs of reduced tillage and manure methods in a *Zea mays* silage system. *Journal of Environmental Quality, 49*(5), 1236-1250. doi:https://doi.org/10.1002/jeq2.20125

Dowling, J. A., Rinaldi, K. Z., Ruggles, T. H., Davis, S. J., Yuan, M., Tong, F., . . . Caldeira, K. (2020). Role of Long-Duration Energy Storage in Variable Renewable Electricity Systems. *Joule*. doi:10.1016/j.joule.2020.07.007

Dried Seaweed Price. (2022). Retrieved from https://www.alibaba.com/showroom/dried-seaweed-price.html

Droop, M. R. (1983). 25 Years of Algal Growth Kinetics: A Personal View. *Botanica Marina*. doi:10.1515/botm.1983.26.3.99

Duarte, C. M. (1992). Nutrient concentration of aquatic plants: Patterns across species. *Limnology and Oceanography*. doi:10.4319/lo.1992.37.4.0882

Duarte, C. M., Wu, J., Xiao, X., Bruhn, A., & Krause-Jensen, D. (2017). Can seaweed farming play a role in climate change mitigation and adaptation? *Frontiers in Marine Science*. doi:10.3389/fmars.2017.00100

Edwards, D. P., Lim, F., James, R. H., Pearce, C. R., Scholes, J., Freckleton, R. P., & Beerling, D. J. (2017). Climate change mitigation: potential benefits and pitfalls of enhanced rock weathering in tropical agriculture. *Biology Letters, 13*(4). doi:https://doi.org/10.1098/rsbl.2016.0715

EIA. (2021). Carbon Dioxide Emissions Coefficients. Retrieved from https://www.eia.gov/environment/emissions/co2_vol_mass.php

Fajardy, M., & Mac Dowell, N. (2017). Can BECCS deliver sustainable and resource efficient negative emissions? . *Energy & Environmental Science, 10*. doi:DOIhttps://doi.org/10.1039/C7EE00465F

Fajardy, M., Morris, J., Gurgel, A., Herzog, H., Mac Dowell, N., & Paltsev, S. (2021). The economics of bioenergy with carbon capture and storage (BECCS) deployment in a 1.5 °C or 2 °C world. *Global Environmental Change*. doi:10.1016/j.gloenvcha.2021.102262

Falcon, W., Naylor, R., & Shanker, N. (2022). Rethinking global food demand for 2050. *Population and Development Review, 48*(4), 921-957. doi:https://doi.org/10.1111/padr.12508

Fankhauser, S., Smith, S. M., Allen, M., Axelsson, K., Hale, T., Hepburn, C., . . . Wetzer, T. (2022). The meaning of net zero and how to get it right. *Nature Climate Change, 12*(1), 15-21. doi:10.1038/s41558-021-01245-w

FAO. (2013). *Dietary protein quality evaluation in human nutrition: Report of an FAO Expert Consultation.* Retrieved from https://www.sochob.cl/pdf/libros/Dietary%20protein%20quality%20evaluation%20in%20human%20nutrition.pdf

FAO. (2014). *Global Strategic Framework for Food Security & Nutrition (GSF), Third Version*. Retrieved from https://www.fao.org/fileadmin/templates/cfs/Docs1314/GSF/GSF_Version_3_EN.pdf

FAO. (2019). *The State of Food and Agriculture 2019: Moving forward on food loss and waste reduction.* Retrieved from Rome: https://www.fao.org/3/ca6030en/ca6030en.pdf

FAO. (2020a). *Fishery and Aquaculture Statistics. Global production by production source 1950-2018 (FishstatJ)*. Retrieved from www.fao.org/fishery/statistics/software/f:

FAO. (2020b). *The State of World Fisheries and Aquaculture 2020*. Retrieved from

FAO. (2022). *FAOSTAT Food Balances*. Retrieved from: https://www.fao.org/faostat/en/#data/FBS

FAO. (2023). *FAOSTAT Production, Crops and Livestock Products*. Retrieved from: https://www.fao.org/faostat/en/#data/QCL

Fay, M., Hallegatte, S., Vogt-Schilb, A., Rozenberg, J., & Narloch, U. (2015). Decarbonizing development: Three steps to a zero-carbon future. *Renewable Resources Journal*. doi:10.1596/978-1-4648-0479-3

Fisher-Vanden, K., & Weyant, J. (2020). The Evolution of Integrated Assessment: Developing the Next Generation of Use-Inspired Integrated Assessment Tools. *Annual Review of Resource Economics, 12*, 471-487.

Fofrich, R. A., Tong, D., Calvin, K. V., de Boer, H. S., Emmerling, J., Fricko, O., . . . Davis, S. J. (2020). Early retirement of power plants in climate mitigation scenarios. *Environmental Research Letters*. doi:10.1088/1748-9326/ab96d3

Foley, J. A., Ramankutty, N., Brauman, K. A., Cassidy, E. S., Gerber, J. S., Johnston, M., . . . Zaks, D. (2011). Solutions for a cultivated planet. *Nature, 478*, 337-342. doi:https://doi.org/10.1038/nature10452

Freeman, S., & von Keitz, M. (2017). Macroalgae Research Inspiring Novel Energy Resources (MARINER). In: U.S. Department of Energy Advanced Research Projects Agency - Energy.

Frieder, C. A., Yan, C., Chamecki, M., Dauhajre, D., McWilliams, J. C., Infante, J., . . . Davis, K. A. (2022). A Macroalgal Cultivation Modeling System (MACMODS): Evaluating the Role of Physical-Biological Coupling on Nutrients and Farm Yield. *Frontiers in Marine Science, 9*. doi:10.3389/fmars.2022.752951

Froehlich, H. E., Afflerbach, J. C., Frazier, M., & Halpern, B. S. (2019). Blue Growth Potential to Mitigate Climate Change through Seaweed Offsetting. *Current Biology*. doi:10.1016/j.cub.2019.07.041

Fuhrman J, M. H., Doney SC, Shobe W and Clarens AF. . Front. Clim. 1:11. (2019). (2019). From Zero to Hero?: Why Integrated Assessment Modeling of Negative Emissions Technologies Is Hard and How We Can Do Better. *Frontiers in Climate, 1*, 11.

Fuss, S., Canadell, J. G., Peters, G. P., Tavoni, M., Andrew, R. M., Ciais, P., . . . Yamagata, Y. (2014). Betting on negative emissions. *Nature Climate Change, 4*(10), 850-853. doi:10.1038/nclimate2392

Gambhir, A., Butnar, I., Li, P., Smith, P., & Strachan, N. (2019). A Review of Criticisms of Integrated Assessment Models and Proposed Approaches to Address These, through the Lens of BECCS. *Energies, 12*(9), 1747.

Gambhir, A., Rogelj, J., Luderer, G., Few, S., & Napp, T. (2019). Energy system changes in 1.5 °C, well below 2 °C and 2 °C scenarios. *Energy Strategy Reviews*. doi:10.1016/j.esr.2018.12.006.

Gao, G., Beardall, J., Jin, P., Gao, L., Xie, S., & Gao, K. (2022). A review of existing and potential blue carbon contributions to climate change mitigation in the Anthropocene. *Journal of Applied Ecology, 59*(7). doi:doi.org/10.1111/1365-2664.14173

Gao, G., Gao, L., Fu, Q., Li, X., & Xu, J. (2022). Coculture of the Pacific white shrimp Litopenaeus vannamei and the macroalga Ulva linza enhances their growth rates and functional properties. *Journal of Cleaner Production*. doi:doi.org/10.1016/j.jclepro.2022.131407

Gao, G., L., G., Jiang, M., Jian, A., & He, L. (2021). The potential of seaweed cultivation to achieve carbon neutrality and mitigate deoxygenation and eutrophication. *Environmental Research Letters, 17*. doi:https://doi.org/10.1088/1748-9326/ac3fd9

Gasser, T., Ciais, P., & Lewis, S. L. (2022). How the Glasgow Declaration on Forests can help keep alive the 1.5 C target. *Proceedings of the National Academy of Sciences, 119*(23), e2200519119.

Gasser, T., Guivarch, C., Tachiiri, K., Jones, C. D., & Ciais, P. (2015). Negative emissions physically needed to keep global warming below 2 °C. *Nature Communications, 6*(1), 7958. doi:10.1038/ncomms8958

Gattuso, J.-P., Williamson, P., Duarte, C. M., & Magnan, A. K. (2021). The Potential for Ocean-Based Climate Action: Negative Emissions Technologies and Beyond. *Frontiers in Climate, 2*.

GEA. (2012). *Global Energy Assessment: Toward a Sustainable Future* (T. B. Johansson, A. Patwardhan, N. Nakicenovic, & L. Gomez-Echeverri Eds.). New York, NY: Cambridge University Press and the International Institute for Applied Systems Analysis.

Ghadiryanfar, M., Rosentrater, K. A., Keyhani, A., & Omid, M. (2016). A review of macroalgae production, with potential applications in biofuels and bioenergy. *Renewable and Sustainable Energy Reviews*. doi:10.1016/j.rser.2015.10.022

Glasson, C. R. K., Kinley, R. D., de Nys, R., King, N., Adams, S. L., Packer, M. A., . . . Magnuson, M. (2022). Benefits and risks of including the bromoform containing seaweed *Asparagopsis* in feed for the reduction of methane production from ruminants. *Algal Research, 64*. doi:https://doi.org/10.1016/j.algal.2022.102673

Global Fishing Watch. (2020). *Distance from Port*. Retrieved from: https://globalfishingwatch.org/data-download/datasets/public-distance-from-port-v1

Graham, R., Wortman, S., & Pittelkow, C. (2017). Comparison of Organic and Integrated Nutrient Management Strategies for Reducing Soil N2O Emissions. *Sustainability, 9*. doi:https://doi.org/10.3390/su9040510

Gray, N., McDonagh, S., O'Shea, R., Smyth, B., & Murphy, J. D. (2021). Decarbonising ships, planes and trucks: An analysis of suitable low-carbon fuels for the maritime, aviation and haulage sectors. *Advances in Applied Energy*. doi:10.1016/j.adapen.2021.100008

Griscom, B. W., Adams, J., Ellis, P. W., Houghton, R. A., Lomax, G., Miteva, D. A., . . . Fargione, J. (2017). Natural climate solutions. *Proceedings of the National Academy of Sciences, 114*(44), 11645. doi:10.1073/pnas.1710465114

Grubler, A., Wilson, C., Bento, N., Boza-Kiss, B., Krey, V., McCollum, D. L., . . . Valin, H. (2018). A low energy demand scenario for meeting the 1.5 °C target and sustainable development goals without negative emission technologies. *Nature Energy, 3*(6), 515-527. doi:10.1038/s41560-018-0172-6

Guertal, E. A. (2009). Slow-release Nitrogen Fertilizers in Vegetable Production: A Review. *HortTechnology, 19*(1). doi:https://doi.org/10.21273/HORTSCI.19.1.16

Guivarch, C., & Rogelj, J. (2017). *Carbon price variations in 2°C scenarios explored*. Retrieved from USA:

Hadley, S., Wild-Allen, K., Johnson, C., & Macleod, C. (2015). Modeling macroalgae growth and nutrient dynamics for integrated multi-trophic aquaculture. *Journal of Applied Phycology, 27*(2), 901-916. doi:10.1007/s10811-014-0370-y

Hanson, C., Flanagan, K., Robertson, K., Axmann, H., Bos-Brouwers, H., Broeze, J., . . . Westra, E. (2019). *Reducing Food Loss and Waste: Ten Interventions to Scale Impact.* Retrieved from https://files.wri.org/d8/s3fs-public/reducing-food-loss-and-waste-ten-interventions-scale-impact_1.pdf

Hanssen, S. V., Daioglou, V., Steinmann, Z. J. N., Doelman, J. C., Van Vuuren, D. P., & Huijbregts, M. A. J. (2020). The climate change mitigation potential of bioenergy with carbon capture and storage. *Nature Climate Change, 10*(11), 1023-1029. doi:10.1038/s41558-020-0885-y

Harrison, C. S., Long, M. C., Lovenduski, N. S., & Moore, J. K. (2018). Mesoscale Effects on Carbon Export: A Global Perspective. *Global Biogeochemical Cycles, 32*(4), 680-703. doi:https://doi.org/10.1002/2017GB005751

Heck, V., Gerten, D., Lucht, W., & Popp, A. (2018). Biomass-based negative emissions difficult to reconcile with planetary boundaries. *Nature Climate Change*. doi:10.1038/s41558-017-0064-y

Hegwood, M., Burgess, M. G., Costigliolo, E. M., Smith, P., Bajželj, B., Saunders, H., & Davis, S. J. (2023). Rebound effects could offset more than half of avoided food loss and waste. *Nature Food, 5*, 585-595. doi:https://doi.org/10.1038/s43016-023-00792-z

Hepburn, C., Adlen, E., Beddington, J., Carter, E. A., Fuss, S., Dowell, N. M., . . . Williams, C. K. (2019). The technological and economic prospects for CO2 utilization and removal. *Nature, 575*, 87-97. doi:10.1038/s41586-019-1681-6

Hoffert, M. I., Caldeira, K., Jain, A. K., Haites, E. F., Harvey, L. D. D., Potter, S. D., . . . Wuebbles, D. J. (1998). Energy implications of future stabilization of atmospheric CO2 content. *Nature, 395*, 881-884.

Honan, M., Feng, X., Tricarico, J. M., & Kebreab, E. (2022). Feed additives as a strategic approach to reduce enteric methane production in cattle: modes of action,

effectiveness and safety. *Animal Production Science, 62*, 1303-1317. doi:https://doi.org/10.1071/AN20295

Honegger, M., & Reiner, D. (2018). The political economy of negative emissions technologies: consequences for international policy design. *Climate Policy, 18*(3), 306-321.

Hong, C., Burney, J. A., Pongratz, J., Nabel, J. E. M. S., Mueller, N. D., Jackson, R. B., & Davis, S. J. (2021). Global and regional drivers of land-use emissions in 1961–2017. *Nature*. doi:10.1038/s41586-020-03138-y

Huppmann, D., Kriegler, E., Krey, V., Riahi, K., Rogelj, J., Rose, S. K., . . . Zhang, R. (2018). IAMC 1.5°C Scenario Explorer and Data hosted by IIASA (Publication no. 10.22022/SR15/08-2018.15429). from Integrated Assessment Modeling Consortium & International Institute for Applied Systems Analysis https://data.ene.iiasa.ac.at/iamc-sr15-explorer

Huppmann, D., Rogelj, J., Krey, V., Kriegler, E., & Riahi, K. (2018). A new scenario resource for integrated 1.5 °C research. *Nature Climate Change*. doi:10.1038/s41558-018-0317-4

Hwang, E. K., Yotsukura, N., Pang, S. J., Su, L., & Shan, T. F. (2019). Seaweed breeding programs and progress in eastern Asian countries. *Phycologia, 58*(5), 484-495. doi:10.1080/00318884.2019.1639436

IEA. (2019). World energy balances. *IEA World Energy Statistics and Balances 2018*. doi:10.1787/data-00510-en

IEA. (2020). Clean Energy Innovation: Accelerating technology progress for a sustainable future. *Energy Technology Perspectives 2020*.

IEA. (2021). Global Energy Review 2021. 1-36.

IPCC. (2014). *Mitigation of Climate Change. Contribution of Working Group III to the IPCC 5th Fifth Assessment Report of the Intergovernmental Panel on Climate Change*. New York, NY: Cambridge University Press.

Jackson, R. B., Abernathy, S., Canadell, J. G., Cargnello, M., Davis, S. J., Féron, S., . . . Zickfeld, K. (2021). Atmospheric methane removal: A research agenda. *Phil. Trans. R. Soc. A, 379*(2210). doi:https://doi.org/10.1098/rsta.2020.0454

Jackson, R. B., Solomon, E. I., Canadell, J. G., Cargnello, M., & Field, C. B. (2019). Methane removal and atmospheric restoration. *Nature Sustainability, 2*, 436-438.

Jaffe, A. M. (2021). The Electrification of Everything: What You Need to Know. *The Wall Street Journal*. Retrieved from https://www.wsj.com/articles/electrification-of-everything-11620843173

Janssen, P. H. (2010). Influence of hydrogen on rumen methane formation and fermentation balances through microbial growth kinetics and fermentation thermodynamics. *Animal Feed Science and Technology, 160*(1), 1-22. doi:https://doi.org/10.1016/j.anifeedsci.2010.07.002

Jaureguiberry, P., Titeaux, N., Wiemers, M., Bowler, D. E., Coscieme, L., Golden, A. S., . . . Purvis, A. (2022). The direct drivers of recent global anthropogenic biodiversity loss. *Science Advances, 8*. doi:https://doi.org/10.1126/sciadv.abm9982

Jaxa-Rozen, M., & Trutnevyte, E. (2021). Sources of uncertainty in long-term global scenarios of solar photovoltaic technology. *Nature Climate Change, 11*, 266-273.

Jenkins, J. D., Luke, M., & Thernstrom, S. (2018). Getting to Zero Carbon Emissions in the Electric Power Sector. *Joule, 2*(12), 2498-2510.

Jian, J., Du, X., Reiter, M. S., & Stewart, R. D. (2020). A meta-analysis of global cropland soil carbon changes due to cover cropping. *Soil Biology and Biogeochemistry, 143*. doi:https://doi.org/10.1016/j.soilbio.2020.107735

Johnson, T. (2011). *Saving Fuel on Your Recreational or Charter Boat*. Retrieved from Alaska Sea Grant Marine Advisory Program: https://nsgl.gso.uri.edu/aku/akug11009.pdf

Jägermeyr, J., Müller, C., Ruane, A. C., Elliott, J., Balkovic, J., Castillo, O., . . . Rosenzweig, C. (2021). Climate impacts on global agriculture emerge earlier in new generation of climate and crop models. *Nature Food, 2*, 873-885. doi:https://doi.org/10.1038/s43016-021-00400-y

Keith, D. W., Holmes, G., St. Angelo, D., & Heidel, K. (2018). A Process for Capturing CO2 from the Atmosphere. *Joule, 2*(8), 1573-1594. doi:https://doi.org/10.1016/j.joule.2018.05.006

Kim, D.-G., Giltrap, D., & Sapkota, T. B. (2023). Understanding response of yield-scaled $N2_O$ emissions to nitrogen input: Data synthesis and introducing new concepts of

background yield-scaled $N2_O$ emissions and $N2_O$ emission-yield curve. *Field Crops Research, 290*. doi:https://doi.org/10.1016/j.fcr.2022.108737

Krause-Jensen, D., & Duarte, C. M. (2016). Substantial role of macroalgae in marine carbon sequestration. *Nature Geoscience*. doi:10.1038/ngeo2790

Kummu, M., de Moel, H., Porkka, M., Siebert, S., Varis, O., & Ward, P. J. (2012). Lost food, wasted resources: Global food supply chain losses and their impacts on freshwater, cropland, and fertiliser use. *Science of The Total Environment, 438*, 477-489. doi:https://doi.org/10.1016/j.scitotenv.2012.08.092

Lawrence, J., Haasnoot, M., & Lempert, R. (2020). Climate change: making decisions in the face of deep uncertainty. *Nature*. doi:10.1038/d41586-020-01147-5

Lawrencia, D., Wong, S. K., Low, D. Y. S., Goh, B. H., Goh, J. K., Ruktanonchai, U. R., . . . Tang, S. Y. (2021). Controlled release fertilizers: A review on coating materials and mechanism of release. *Plants, 10*(2), 238.

Lazcano, C., Zhu-Barker, X., & Decock, C. (2021). Effects of organic fertilizers on the soil microorganisms responsible for N2O emissions: A review. *Microorganisms, 9*(5), 983.

Lehahn, Y., Ingle, K. N., & Golberg, A. (2016). Global potential of offshore and shallow waters macroalgal biorefineries to provide for food, chemicals and energy: feasibility and sustainability. *Algal Research, 17*, 150-160. doi:https://doi.org/10.1016/j.algal.2016.03.031

Lempert, R. J., Groves, D. G., Popper, S. W., & Bankes, S. C. (2006). A general, analytic method for generating robust strategies and narrative scenarios. *Management Science*. doi:10.1287/mnsc.1050.0472

Levis, J. W., & Barlaz, M. A. (2011). What is the most environmentally beneficial way to treat commercial food waste? *Environmental science & technology, 45*(17), 7438-7444.

Li, G.-h., Cheng, G.-g., Lu, W.-p., & Lu, D.-l. (2021). Differences of yield and nitrogen use efficiency under different applications of slow release fertilizer in spring maize. *Journal of Integrative Agriculture, 20*(2), 554-564.

Lindroos, T. J., Rydén, M., Langørgen, Ø., Pursiheimo, E., & Pikkarainen, T. (2019). Robust decision making analysis of BECCS (bio-CLC)in a district heating and cooling grid. *Sustainable Energy Technologies and Assessments*. doi:10.1016/j.seta.2019.05.005

Luderer, G., Madeddu, S., Merfort, L., Ueckerdt, F., Pehl, M., Pietzcker, R., . . . Strefler, J. (2022). Impact of declining renewable energy costs on electrification in low-emission scenarios. *Nature Energy, 7*, 32-42. doi:https://doi.org/10.1038/s41560-021-00937-z

Luderer, G., Vrontisi, Z., Bertram, C., Edelenbosch, O. Y., Pietzcker, R. C., Rogelj, J., . . . Kriegler, E. (2018). Residual fossil CO2 emissions in 1.5–2 °C pathways. *Nature Climate Change, 8*, 626-633.

Macknick, J. (2014). Energy and CO2 emission data uncertainties. *Carbon Management, 2*(2), 189-205.

MacLaren, C., Mead, A., van Balen, D., Claessens, L., Etana, A., de Haan, J., . . . Labuschagne, J. (2022). Long-term evidence for ecological intensification as a pathway to sustainable agriculture. *Nature Sustainability, 5*(9), 770-779.

Mallareddy, M., Thirumalaikumar, R., Balasubramanian, P., Naseeruddin, R., Nithya, N., Mariadoss, A., . . . Vijayakumar, S. (2023). Maximizing Water Use Efficiency in Rice Farming: A Comprehensive Review of Innovative Irrigation Management Technologies. *Water, 15*, 1802. doi:https://doi.org/10.3390/w15101802

Marcillo, G., & Miguez, F. (2017). Corn yield response to winter cover crops: An updated meta-analysis. *Journal of Soil and Water Conservation, 72*(3), 226-239.

Marcucci, A., Kypreos, S., & Panos, E. (2017). The road to achieving the long-term Paris targets: energy transition and the role of direct air capture. *Climatic Change, 144*(2), 181-193. doi:10.1007/s10584-017-2051-8

Mathers, C., Heitman, J., Huseth, A., Locke, A., Osmond, D., & Woodley, A. (2023). No-till imparts yield stability and greater cumulative yield under variable weather conditions in the southeastern USA piedmont. *Field Crops Research, 292*, 108811.

Matthews, H. D., & Caldeira, K. (2008). Stabilizing climate requires near-zero emissions. *Geophysical Research Letters, 35*, L04705. doi:10.1029/2007GL032388

Matthews, H. D., Gillett, N. P., Stott, P. A., & Zickfeld, K. (2009). The proportionality of global warming to cumulative carbon emissions. *Nature*. doi:10.1038/nature08047

McCauley, J. I., Labeeuw, L., Jaramillo-Madrid, A. C., Nguyen, L. N., Nghiem, L. D., Chaves, A. V., & Ralph, P. J. (2020). Management of Enteric Methanogenesis in ruminants by Algal-Derived Feed Additives. *Current Pollution Reports, 6*, 188-205. doi:https://doi.org/10.1007/s40726-020-00151-7

McCollum, D. L., Zhou, W., Bertram, C., Boer, H.-S. d., Bosetti, V., Busch, S., . . . Riahi, K. (2018). Energy investment needs for fulfilling the Paris Agreement and achieving the Sustainable Development Goals. *Nature Energy, 3*, 589-599.

McQueen, N., Gomes, K. V., McCormick, C., Blumanthal, K., Pisciotta, M., & Wilcox, J. (2021). A review of direct air capture (DAC): scaling up commercial technologies and innovating for the future. *Progress in Energy, 3*(3), 032001.

Ming, T., Li, W., Yuan, Q., Davies, P., De Richter, R., Peng, C., . . . Zhou, N. (2022). Perspectives on removal of atmospheric methane. *Advances in Applied Energy, 5*, 100085.

Mingle, J. (2020). To Cut Carbon Emissions, a Movement Grows to 'Electrify Everything'. *Yale 360*. Retrieved from https://e360.yale.edu/features/to-cut-carbon-emissions-a-movement-grows-to-electrify-everything

Mueller, N. D., Gerber, J. S., Johnston, M., Ray, D. K., Ramankutty, N., & Foley, J. A. (2012). Closing yield gaps through nutrient and water management. *Nature, 490*(7419), 254-257.

Muratori, M., Calvin, K., Wise, M., Kyle, P., & Edmonds, J. (2016). Global economic consequences of deploying bioenergy with carbon capture and storage (BECCS). *Environmental Reseach Letters, 11*, 095004.

NASEM. (2021). *A Research Strategy for Ocean-based Carbon Dioxide Removal and Sequestration.* . Retrieved from https://doi.org/10.17226/26278:

Needell, Z., McNerney, J., Chang, M., & Trancik, J. (2016). Potential for widespread electrification of personal vehicle travel in the United States. *Nature Energy, 1*, 16112.

Nunes, M. R., van Es, H. M., Schindelbeck, R., Ristow, A. J., & Ryan, M. (2018). No-till and cropping system diversification improve soil health and crop yield. *Geoderma, 328*, 30-43.

Oldfield, E. E., Bradford, M. A., & Wood, S. A. (2019). Global meta-analysis of the relationship between soil organic matter and crop yields. *Soil, 5*(1), 15-32.

Ortiz, A. M. D., Outhwaite, C. L., Dalin, C., & Newbold, T. (2021). A review of the interactions between biodiversity, agriculture, climate change, and international trade: research and policy priorities. *One Earth, 4*(1), 88-101.

Owen, J. J., & Silver, W. L. (2015). Greenhouse gas emissions from dairy manure management: a review of field-based studies. *Global change biology, 21*(2), 550-565.

Patra, A., Park, T., Kim, M., & Yu, Z. (2017). Rumen methanogens and mitigation of methane emission by anti-methanogenic compounds and substances. *Journal of animal science and biotechnology, 8*, 1-18.

Patra, A. K. (2012). Enteric methane mitigation technologies for ruminant livestock: a synthesis of current research and future directions. *Environmental Monitoring and Assessment, 184*, 1929-1952.

Peker, E. (2019). *The Wall Street Journal*.

Pendrill, F., Gardner, T. A., Meyfroidt, P., Persson, U. M., Adams, J., Azevedo, T., . . . De Sy, V. (2022). Disentangling the numbers behind agriculture-driven tropical deforestation. *Science, 377*(6611), eabm9267.

Phillips, S. M. (2012). Dietary protein requirements and adaptive advantages in athletes. *British Journal of Nutrition, 108*(S2), S158-S167.

Pingali, P. L. (2012). Green revolution: impacts, limits, and the path ahead. *Proceedings of the national academy of sciences, 109*(31), 12302-12308.

Pittelkow, C. M., Liang, X., Linquist, B. A., Van Groenigen, K. J., Lee, J., Lundy, M. E., . . . Van Kessel, C. (2015). Productivity limits and potentials of the principles of conservation agriculture. *Nature, 517*(7534), 365-368.

Poore, J., & Nemecek, T. (2018). Reducing food's environmental impacts through producers and consumers. *Science, 360*(6392), 987-992.

Powlson, D. S., Stirling, C. M., Jat, M. L., Gerard, B. G., Palm, C. A., Sanchez, P. A., & Cassman, K. G. (2014). Limited potential of no-till agriculture for climate change mitigation. *Nature climate change, 4*(8), 678-683.

Pozo, C., Galán-Martín, Á., Reiner, D. M., Mac Dowell, N., & Guillén-Gosálbez, G. (2020). Equity in allocating carbon dioxide removal quotas. *Nature Climate Change*. doi:10.1038/s41558-020-0802-4

Quested, T., O'Connor, C., & Forbes, H. (2021). UNEP Food Waste Index Report 2021. *United Nations Environment Programme (UNEP), 70*.

Ray, D. K., Mueller, N. D., West, P. C., & Foley, J. A. (2013). Yield trends are insufficient to double global crop production by 2050. *PloS one, 8*(6), e66428.

Reid, W. V., Ali, M. K., & Field, C. B. (2020). The future of bioenergy. *Global Change Biology, 26*(1), 274-286. doi:https://doi.org/10.1111/gcb.14883

Reisinger, A., Clark, H., Cowie, A. L., Emmet-Booth, J., Gonzalez Fischer, C., Herrero, M., . . . Leahy, S. (2021). How necessary and feasible are reductions of methane emissions from livestock to support stringent temperature goals? *Philosophical Transactions of the Royal Society A, 379*(2210), 20200452.

Riahi, K., van Vuuren, D. P., Kriegler, E., Edmonds, J., O'Neill, B. C., Fujimori, S., . . . Tavoni, M. (2017). The Shared Socioeconomic Pathways and their energy, land use, and greenhouse gas emissions implications: An overview. *Global Environmental Change*. doi:10.1016/j.gloenvcha.2016.05.009

Richardson, O. (2020). weighted_distance_transform. Retrieved from https://github.com/0mar/weighted-distance-transform

Rizzo, G., Monzon, J. P., Tenorio, F. A., Howard, R., Cassman, K. G., & Grassini, P. (2022). Climate and agronomy, not genetics, underpin recent maize yield gains in favorable environments. *Proceedings of the National Academy of Sciences, 119*(4), e2113629119.

Roberts, D. (2017). The key to tackling climate change: electrify everything. *Vox*. Retrieved from https://www.vox.com/2016/9/19/12938086/electrify-everything

Roesijadi, G., Jones, S. B., Snowden-Swan, L. J., & Zhu, Y. (2010). *Macroalgae as a Biomass Feedstock: A Preliminary Analysis*. Retrieved from https://www.pnnl.gov/publications/macroalgae-biomass-feedstock-preliminary-analysis

Rogelj, J., Geden, O., Cowie, A., & Reisinger, A. (2021). Net-zero emissions targets are vague: three ways to fix. *Nature, 591*, 365-368.

Rogelj, J., Popp, A., Calvin, K. V., Luderer, G., Emmerling, J., Gernaat, D., . . . Tavoni, M. (2018). Scenarios towards limiting global mean temperature increase below 1.5 °C. *Nature Climate Change, 8*, 325-332. doi:10.1038/s41558-018-0091-3

Rogelj, J., Schaeffer, M., Meinshausen, M., Knutti, R., Alcamo, J., Riahi, K., & Hare, W. (2015). Zero emission targets as long-term global goals for climate protection. *Environmental Research Letters, 10*, 105007.

Rogelj, J., Shindell, D., Jiang, K., Fifita, S., Forster, P., Ginzburg, V., . . . Vilariño, M. V. (2018). Mitigation pathways compatible with 1.5°C in the context of sustainable development. In *Special Report on the impacts of global warming of 1.5 °C*. Geneva: Intergovernmental Panel on Climate Change.

Roque, B. M., Brooke, C. G., Ladau, J., Polley, T., Marsh, L. J., Najafi, N., . . . Salwen, J. K. (2019). Effect of the macroalgae Asparagopsis taxiformis on methane production and rumen microbiome assemblage. *Animal Microbiome, 1*, 1-14.

Roque, B. M., Salwen, J. K., Kinley, R., & Kebreab, E. (2019). Inclusion of Asparagopsis armata in lactating dairy cows' diet reduces enteric methane emission by over 50 percent. *Journal of Cleaner Production, 234*, 132-138. doi:https://doi.org/10.1016/j.jclepro.2019.06.193

Rosa, L., & Gabrielli, P. (2023). Achieving net-zero emissions in agriculture: a review. *Environmental Research Letters, 18*(6), 063002.

Ross, K., & Damassa, T. (2015). *Assessing the Post-2020 Clean Energy Landscape*. Retrieved from Washington, D.C.:

Rozenberg, J., Davis, S. J., Narloch, U., & Hallegatte, S. (2015). Climate constraints on the carbon intensity of economic growth. *Environmental Research Letters*. doi:10.1088/1748-9326/10/9/095006

Rubio, N. R., Xiang, N., & Kaplan, D. L. (2020). Plant-based and cell-based approaches to meat production. *Nature Communications, 11*(1), 6276.

Sachs, J. D., Schmidt-Traub, G., & Williams, J. (2016). Pathways to zero emissions. *Nature Geoscience, 9*, 799-801.

Samir, K. C., & Lutz, W. (2016). The human core of the Shared Socioeconomic Pathways: population scenarios by age, sex and level of education for all countries to 2100. *Global Environmental Change, 42*, 181-192. doi:10.1016/j.gloenvcha.2014.06.004

Sanderson, B. M., O'Neill, B. C., & Tebaldi, C. (2016). What would it take to achieve the Paris temperature targets? *Geophysical Research Letters, 43*(13). doi:10.1002/2016GL069563

Schils, R., Olesen, J. E., Kersebaum, K.-C., Rijk, B., Oberforster, M., Kalyada, V., . . . Manolova, V. (2018). Cereal yield gaps across Europe. *European Journal of Agronomy, 101*, 109-120.

Schomberg, H., Fisher, D., Reeves, D., Endale, D., Raper, R., Jayaratne, K., . . . Jenkins, M. (2014). Grazing winter rye cover crop in a cotton no-till system: Yield and economics. *Agronomy Journal, 106*(3), 1041-1050.

Searchinger, T., Waite, R., Hanson, C., Ranganathan, J., Dumas, P., Matthews, E., & Klirs, C. (2019). Creating a sustainable food future: A menu of solutions to feed nearly 10 billion people by 2050. Final report. In: WRI.

Siegel, D. A., DeVries, T., Doney, S., & Bell, T. (2021). Assessing the sequestration time scales of some ocean-based carbon dioxide reduction strategies. *Environmental Research Letters*. doi:10.1088/1748-9326/ac0be0

Slavin, J., & Carlson, J. (2014). Carbohydrates. *Advances in Nutrition, 5*(6), 760-761. doi:https://doi.org/10.3945/an.114.006163

Smith, M. E., Vico, G., Costa, A., Bowles, T., Gaudin, A. C., Hallin, S., . . . Blecharczyk, A. (2023). Increasing crop rotational diversity can enhance cereal yields. *Communications Earth & Environment, 4*(1), 89.

Smith, P., Davis, S. J., Creutzig, F., Fuss, S., Minx, J., Gabrielle, B., . . . Yongsung, C. (2016). Biophysical and economic limits to negative CO2 emissions. *Nature Climate Change, 6*. doi:10.1038/nclimate2870

Soleymani, M., & Rosentrater, K. A. (2017). Techno-economic analysis of biofuel production from macroalgae (Seaweed). *Bioengineering*. doi:10.3390/bioengineering4040092

Soofi, A. F., Manshadi, S. D., & Saucedo, A. (2022). Farm electrification: A road-map to decarbonize the agriculture sector. *The Electricity Journal, 35*(2), 107076.

Stehfest, E., van Zeist, W.-J., Valin, H., Havlik, P., Popp, A., Kyle, P., . . . Bodirsky, B. L. (2019). Key determinants of global land-use projections. *Nature communications, 10*(1), 2166.

Sugiyama, M. (2012). Climate change mitigation and electrification. *Energy Policy, 44*, 464-468.

Surana, K., Edwards, M. R., Kennedy, K. M., Borrero, M. A., Clarke, L., Fedorchak, R., . . . Williams, E. D. (2023). The role of corporate investment in start-ups for climate-tech innovation. *Joule, 7*(4), 611-618.

Temple, J. (2021). What it will take to achieve affordable carbon removal.

Tilman, D. (1998). The greening of the green revolution. *Nature, 396*(6708), 211-212.

Tilman, D., Balzer, C., Hill, J., & Befort, B. L. (2011). Global food demand and the sustainable intensification of agriculture. *Proceedings of the national academy of sciences, 108*(50), 20260-20264.

Tong, D., Zhang, Q., Zheng, Y., Caldeira, K., Shearer, C., Hong, C., . . . Davis, S. J. (2019). Committed emissions from existing energy infrastructure jeopardize 1.5 °C climate target. *Nature, 572*, 373-377. doi:10.1038/s41586-019-1364-3

Torok, V. A., Luyckx, K., & Lapidge, S. (2021). Human food waste to animal feed: opportunities and challenges. *Animal Production Science, 62*(12), 1129-1139.

Turner, P. A., Field, C. B., Lobell, D. B., Sanchez, D. L., & Mach, K. J. (2018). Unprecedented rates of land-use transformation in modelled climate change mitigation pathways. *Nature Sustainability, 1*, 240-245. doi:https://doi.org/10.1038/s41893-018-0063-7

U.S.DOE. (2022). Average Retail Fuel Prices in the United States. Retrieved from https://afdc.energy.gov/data/10326

UNCCD. (2022). *The Global Land Outlook*. Retrieved from https://www.unccd.int/resources/global-land-outlook/global-land-outlook-2nd-edition

UNFCCC. (2015). *Adoption of the Paris Agreement*. Retrieved from http://unfccc.int/resource/docs/2015/cop21/eng/l09r01.pdf

Ungerfeld, E. M. (2020). Metabolic hydrogen flows in rumen fermentation: principles and possibilities of interventions. *Frontiers in Microbiology, 11*, 589.

USDA. (2020). Seaweed, dried. Retrieved from https://fdc.nal.usda.gov/fdc-app.html#/food-details/1103574/nutrients

USDA. (2022). *National Weekly Feedstuff Wholesale Prices*. Retrieved from https://www.ams.usda.gov/mnreports/ms_gr852.txt

USDA, & USDHHS. (2020). *Dietary Guidelines for Americans, 2020-2025*. Retrieved from https://www.dietaryguidelines.gov/sites/default/files/2021-03/Dietary_Guidelines_for_Americans-2020-2025.pdf

van den Burg, S. W. K., van Duijn, A. P., Bartelings, H., van Krimpen, M. M., & Poelman, M. (2016). The economic feasibility of seaweed production in the North Sea. *Aquaculture Economics and Management*. doi:10.1080/13657305.2016.1177859

van Soest, H. L., den Elzen, M. G. J., & van Vuuren, D. P. (2021). Net-zero emission targets for major emitting countries consistent with the Paris Agreement. *Nature Communications, 12*, 2140.

Van Zeist, W.-J., Stehfest, E., Doelman, J. C., Valin, H., Calvin, K., Fujimori, S., . . . Kyle, P. (2020). Are scenario projections overly optimistic about future yield progress? *Global Environmental Change, 64*, 102120.

Vardon, D. R., Sherbacow, B. J., Guan, K., Heyne, J. S., & Abdullah, Z. (2022). Realizing "net-zero-carbon" sustainable aviation fuel. *Joule, 6*(1), 16-21. doi:https://doi.org/10.1016/j.joule.2021.12.013

Vendig, I., Guzman, A., De La Cerda, G., Esquivel, K., Mayer, A. C., Ponisio, L., & Bowles, T. M. (2023). Quantifying direct yield benefits of soil carbon increases from cover cropping. *Nature Sustainability*, 1-10.

Vermeulen, S. J., Challinor, A. J., Thornton, P. K., Campbell, B. M., Eriyagama, N., Vervoort, J. M., . . . Smith, D. R. (2013). Addressing uncertainty in adaptation planning for agriculture. *Proceedings of the National Academy of Sciences of the United States of America*. doi:10.1073/pnas.1219441110

Wenger, S., D'Alessandro, D., & Wright, C. (2022). Maximizing Global Cooling Potential in Carbon Dioxide Removal (CDR) Procurements: A Proposal for Tonne-Year Pricing. *Frontiers in Climate, 4*, 927408.

Wesołowska, M., Rymarczyk, J., Góra, R., Baranowski, P., Sławiński, C., Klimczyk, M., . . . Schimmelpfennig, L. (2021). New slow-release fertilizers-economic, legal and practical aspects: a Review. *International Agrophysics, 35*(1), 11-24.

White, T. (2000). Diet and the distribution of environmental impact. *Ecological economics, 34*(1), 145-153.

Wilcox, J., Kolosz, B., & Freeman, J. *CDR Primer* (J. Wilcox, B. Kolosz, & J. Freeman Eds.).

Wilks, M., & Phillips, C. J. (2017). Attitudes to in vitro meat: A survey of potential consumers in the United States. *PloS one, 12*(2), e0171904.

Wolfe, R. R., Baum, J. I., Starck, C., & Moughan, P. J. (2018). Factors contributing to the selection of dietary protein food sources. *Clinical Nutrition, 37*(1), 130-138.

Woodard, D. L., Davis, S. J., & Randerson, J. T. (2018). Economic carbon cycle feedbacks may offset additional warming from natural feedbacks. *Proceedings of the National Academy of Sciences, 116*(3), 759-764.

World Development Indicators. (2019). Washington, DC: World Bank.

Wu, J., Keller, D. P., & Oschlies, A. (2022). Carbon Dioxide Removal via Macroalgae Open-ocean Mariculture and Sinking: An Earth System Modeling Study. *Earth System Dynamics Discussions*. doi:https://doi.org/10.5194/esd-2021-104

Yim, S. C. S., Nakhata, T., Bartel, W. A., & Huang, E. T. (2005). Coupled nonlinear barge motions, Part I: Deterministic models development, identification and calibration. *Journal of Offshore Mechanics and Arctic Engineering, 127*(1). doi:10.1115/1.1854700

Yu, J., Zhang, S., Yang, W., Xin, Y., & Gao, H. (2020). Design and application of buoy single point mooring system with electro-optical-mechanical (EOM) cable. *Journal of Marine Science and Engineering, 8*(9). doi:10.3390/JMSE8090672

Zhang, R., & Fujimori, S. (2020). The role of transport electrification in global climate change mitigation scenarios. *Environmental Reseach Letters, 15*, 034019.

Zhou, P., & Wang, M. (2016). Carbon dioxide emissions allocation: A review. *Ecological Economics, 125*, 47-59.

Appendix A: Supplementary Information for Chapter 1

Supplementary Table A.1 | List of 177 scenarios evaluated in this study that reach global net-zero CO_2 emissions and included all output variables required for our analysis. Scenarios are listed first, followed by the model that ran the scenario (format: scenario, model).

1	ADVANCE_2020_1.5C-2100, AIM/CGE 2.0
2	ADVANCE_2020_1.5C-2100, IMAGE 3.0.1
3	ADVANCE_2020_1.5C-2100, MESSAGE-GLOBIOM 1.0
4	ADVANCE_2020_1.5C-2100, POLES ADVANCE
5	ADVANCE_2020_1.5C-2100, REMIND 1.7
6	ADVANCE_2020_1.5C-2100, WITCH-GLOBIOM 4.2
7	ADVANCE_2020_Med2C, MESSAGE-GLOBIOM 1.0
8	ADVANCE_2020_Med2C, POLES ADVANCE
9	ADVANCE_2020_Med2C, REMIND 1.7
10	ADVANCE_2020_Med2C, WITCH-GLOBIOM 4.2
11	ADVANCE_2020_WB2C, AIM/CGE 2.0
12	ADVANCE_2020_WB2C, IMAGE 3.0.1
13	ADVANCE_2020_WB2C, MESSAGE-GLOBIOM 1.0
14	ADVANCE_2020_WB2C, POLES ADVANCE
15	ADVANCE_2020_WB2C, REMIND 1.7
16	ADVANCE_2020_WB2C, WITCH-GLOBIOM 4.2
17	ADVANCE_2030_1.5C-2100, POLES ADVANCE
18	ADVANCE_2030_1.5C-2100, REMIND 1.7
19	ADVANCE_2030_Med2C, IMAGE 3.0.1
20	ADVANCE_2030_Med2C, MESSAGE-GLOBIOM 1.0
21	ADVANCE_2030_Med2C, POLES ADVANCE
22	ADVANCE_2030_Med2C, REMIND 1.7
23	ADVANCE_2030_Med2C, WITCH-GLOBIOM 4.2
24	ADVANCE_2030_Price1.5C, AIM/CGE 2.0
25	ADVANCE_2030_Price1.5C, MESSAGE-GLOBIOM 1.0
26	ADVANCE_2030_Price1.5C, POLES ADVANCE
27	ADVANCE_2030_Price1.5C, REMIND 1.7

28	ADVANCE_2030_Price1.5C, WITCH-GLOBIOM 4.2
29	ADVANCE_2030_WB2C, AIM/CGE 2.0
30	ADVANCE_2030_WB2C, IMAGE 3.0.1
31	ADVANCE_2030_WB2C, MESSAGE-GLOBIOM 1.0
32	ADVANCE_2030_WB2C, POLES ADVANCE
33	ADVANCE_2030_WB2C, REMIND 1.7
34	ADVANCE_2030_WB2C, WITCH-GLOBIOM 4.2
35	CD-LINKS_NPi2020_1000, IMAGE 3.0.1
36	CD-LINKS_NPi2020_1000, MESSAGEix-GLOBIOM 1.0
37	CD-LINKS_NPi2020_1000, POLES CD-LINKS
38	CD-LINKS_NPi2020_1000, REMIND-MAgPIE 1.7-3.0
39	CD-LINKS_NPi2020_1000, WITCH-GLOBIOM 4.4
40	CD-LINKS_NPi2020_1600, IMAGE 3.0.1
41	CD-LINKS_NPi2020_1600, MESSAGEix-GLOBIOM 1.0
42	CD-LINKS_NPi2020_1600, POLES CD-LINKS
43	CD-LINKS_NPi2020_1600, REMIND-MAgPIE 1.7-3.0
44	CD-LINKS_NPi2020_1600, WITCH-GLOBIOM 4.4
45	CD-LINKS_NPi2020_400, AIM/CGE 2.1
46	CD-LINKS_NPi2020_400, IMAGE 3.0.1
47	CD-LINKS_NPi2020_400, MESSAGEix-GLOBIOM 1.0
48	CD-LINKS_NPi2020_400, POLES CD-LINKS
49	CD-LINKS_NPi2020_400, REMIND-MAgPIE 1.7-3.0
50	CD-LINKS_NPi2020_400, WITCH-GLOBIOM 4.4
51	CEMICS-1.5-CDR12, REMIND 1.7
52	CEMICS-1.5-CDR20, REMIND 1.7
53	CEMICS-1.5-CDR8, REMIND 1.7
54	CEMICS-2.0-CDR12, REMIND 1.7
55	CEMICS-2.0-CDR20, REMIND 1.7
56	CEMICS-2.0-CDR8, REMIND 1.7
57	EMF33_1.5C_cost100, MESSAGE-GLOBIOM 1.0
58	EMF33_1.5C_cost100, POLES EMF33
59	EMF33_1.5C_cost100, REMIND-MAgPIE 1.7-3.0

60	EMF33_1.5C_full, MESSAGE-GLOBIOM 1.0
61	EMF33_1.5C_full, POLES EMF33
62	EMF33_1.5C_full, REMIND-MAgPIE 1.7-3.0
63	EMF33_1.5C_limbio, POLES EMF33
64	EMF33_1.5C_nofuel, POLES EMF33
65	EMF33_1.5C_nofuel, REMIND-MAgPIE 1.7-3.0
66	EMF33_Med2C_cost100, MESSAGE-GLOBIOM 1.0
67	EMF33_Med2C_cost100, POLES EMF33
68	EMF33_Med2C_cost100, REMIND-MAgPIE 1.7-3.0
69	EMF33_Med2C_full, MESSAGE-GLOBIOM 1.0
70	EMF33_Med2C_full, POLES EMF33
71	EMF33_Med2C_full, REMIND-MAgPIE 1.7-3.0
72	EMF33_Med2C_limbio, MESSAGE-GLOBIOM 1.0
73	EMF33_Med2C_nofuel, MESSAGE-GLOBIOM 1.0
74	EMF33_Med2C_nofuel, POLES EMF33
75	EMF33_Med2C_nofuel, REMIND-MAgPIE 1.7-3.0
76	EMF33_WB2C_cost100, AIM/CGE 2.1
77	EMF33_WB2C_cost100, IMAGE 3.0.2
78	EMF33_WB2C_cost100, MESSAGE-GLOBIOM 1.0
79	EMF33_WB2C_cost100, POLES EMF33
80	EMF33_WB2C_cost100, REMIND-MAgPIE 1.7-3.0
81	EMF33_WB2C_full, IMAGE 3.0.2
82	EMF33_WB2C_full, MESSAGE-GLOBIOM 1.0
83	EMF33_WB2C_full, POLES EMF33
84	EMF33_WB2C_full, REMIND-MAgPIE 1.7-3.0
85	EMF33_WB2C_limbio, MESSAGE-GLOBIOM 1.0
86	EMF33_WB2C_limbio, POLES EMF33
87	EMF33_WB2C_limbio, REMIND-MAgPIE 1.7-3.0
88	EMF33_WB2C_nobeccs, POLES EMF33
89	EMF33_WB2C_nobeccs, REMIND-MAgPIE 1.7-3.0
90	EMF33_WB2C_nofuel, IMAGE 3.0.2
91	EMF33_WB2C_nofuel, MESSAGE-GLOBIOM 1.0

92	EMF33_WB2C_nofuel, POLES EMF33
93	EMF33_WB2C_nofuel, REMIND-MAgPIE 1.7-3.0
94	EMF33_WB2C_none, REMIND-MAgPIE 1.7-3.0
95	EMF33_tax_hi_full, AIM/CGE 2.1
96	EMF33_tax_hi_full, IMAGE 3.0.2
97	EMF33_tax_hi_full, MESSAGE-GLOBIOM 1.0
98	EMF33_tax_hi_full, POLES EMF33
99	EMF33_tax_hi_full, REMIND-MAgPIE 1.7-3.0
100	IMA15-AGInt, IMAGE 3.0.1
101	IMA15-Def, IMAGE 3.0.1
102	IMA15-Eff, IMAGE 3.0.1
103	IMA15-LiStCh, IMAGE 3.0.1
104	IMA15-LoNCO2, IMAGE 3.0.1
105	IMA15-Pop, IMAGE 3.0.1
106	IMA15-RenElec, IMAGE 3.0.1
107	PEP_1p5C_full_NDC, REMIND-MAgPIE 1.7-3.0
108	PEP_1p5C_full_eff, REMIND-MAgPIE 1.7-3.0
109	PEP_1p5C_full_goodpractice, REMIND-MAgPIE 1.7-3.0
110	PEP_1p5C_full_netzero, REMIND-MAgPIE 1.7-3.0
111	PEP_1p5C_red_eff, REMIND-MAgPIE 1.7-3.0
112	PEP_2C_full_NDC, REMIND-MAgPIE 1.7-3.0
113	PEP_2C_full_eff, REMIND-MAgPIE 1.7-3.0
114	PEP_2C_full_goodpractice, REMIND-MAgPIE 1.7-3.0
115	PEP_2C_full_netzero, REMIND-MAgPIE 1.7-3.0
116	PEP_2C_red_NDC, REMIND-MAgPIE 1.7-3.0
117	PEP_2C_red_eff, REMIND-MAgPIE 1.7-3.0
118	PEP_2C_red_goodpractice, REMIND-MAgPIE 1.7-3.0
119	PEP_2C_red_netzero, REMIND-MAgPIE 1.7-3.0
120	SMP_1p5C_Def, REMIND-MAgPIE 1.7-3.0
121	SMP_1p5C_Sust, REMIND-MAgPIE 1.7-3.0
122	SMP_1p5C_early, REMIND-MAgPIE 1.7-3.0
123	SMP_1p5C_lifesty, REMIND-MAgPIE 1.7-3.0

124	SMP_1p5C_regul, REMIND-MAgPIE 1.7-3.0
125	SMP_2C_Def, REMIND-MAgPIE 1.7-3.0
126	SMP_2C_Sust, REMIND-MAgPIE 1.7-3.0
127	SMP_2C_early, REMIND-MAgPIE 1.7-3.0
128	SMP_2C_lifesty, REMIND-MAgPIE 1.7-3.0
129	SMP_2C_regul, REMIND-MAgPIE 1.7-3.0
130	SSP1-19, AIM/CGE 2.0
131	SSP1-19, GCAM 4.2
132	SSP1-19, IMAGE 3.0.1
133	SSP1-19, MESSAGE-GLOBIOM 1.0
134	SSP1-19, REMIND-MAgPIE 1.5
135	SSP1-19, WITCH-GLOBIOM 3.1
136	SSP1-26, GCAM 4.2
137	SSP1-26, IMAGE 3.0.1
138	SSP1-26, MESSAGE-GLOBIOM 1.0
139	SSP1-26, REMIND-MAgPIE 1.5
140	SSP1-26, WITCH-GLOBIOM 3.1
141	SSP1-34, GCAM 4.2
142	SSP1-34, IMAGE 3.0.1
143	SSP1-34, MESSAGE-GLOBIOM 1.0
144	SSP1-34, REMIND-MAgPIE 1.5
145	SSP1-34, WITCH-GLOBIOM 3.1
146	SSP2-19, AIM/CGE 2.0
147	SSP2-19, GCAM 4.2
148	SSP2-19, MESSAGE-GLOBIOM 1.0
149	SSP2-19, REMIND-MAgPIE 1.5
150	SSP2-26, AIM/CGE 2.0
151	SSP2-26, GCAM 4.2
152	SSP2-26, IMAGE 3.0.1
153	SSP2-26, MESSAGE-GLOBIOM 1.0
154	SSP2-26, REMIND-MAgPIE 1.5
155	SSP2-26, WITCH-GLOBIOM 3.1

156	SSP2-34, GCAM 4.2
157	SSP2-34, MESSAGE-GLOBIOM 1.0
158	SSP2-34, REMIND-MAgPIE 1.5
159	SSP3-34, AIM/CGE 2.0
160	SSP3-34, MESSAGE-GLOBIOM 1.0
161	SSP4-19, WITCH-GLOBIOM 3.1
162	SSP4-26, AIM/CGE 2.0
163	SSP4-26, GCAM 4.2
164	SSP4-26, IMAGE 3.0.1
165	SSP4-26, WITCH-GLOBIOM 3.1
166	SSP4-34, GCAM 4.2
167	SSP5-19, GCAM 4.2
168	SSP5-19, REMIND-MAgPIE 1.5
169	SSP5-26, AIM/CGE 2.0
170	SSP5-26, GCAM 4.2
171	SSP5-26, REMIND-MAgPIE 1.5
172	SSP5-34, GCAM 4.2
173	SSP5-34, REMIND-MAgPIE 1.5
174	TERL_15D_LowCarbonTransportPolicy, AIM/CGE 2.1
175	TERL_15D_NoTransportPolicy, AIM/CGE 2.1
176	TERL_2D_LowCarbonTransportPolicy, AIM/CGE 2.1
177	TERL_2D_NoTransportPolicy, AIM/CGE 2.1

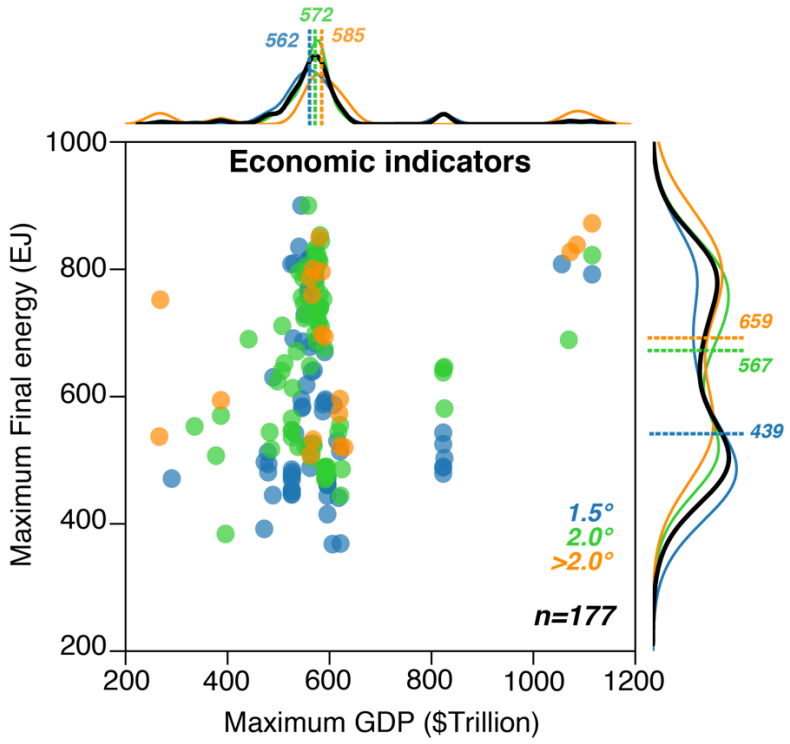

Supplementary Figure A.1 | Economic indicators for net-zero scenarios. Maximum final energy is plotted against maximum GDP ultimately reached in net-zero scenarios. Points represent individual scenarios, with color corresponding to warming level (blue = <1.5˚C, green = 2.0˚C, orange = >2.0˚C) and probability density distributions shown along each axis for each warming level (colors corresponding to warming levels). Median lines for each warming group are shown as dashed lines along distributions.

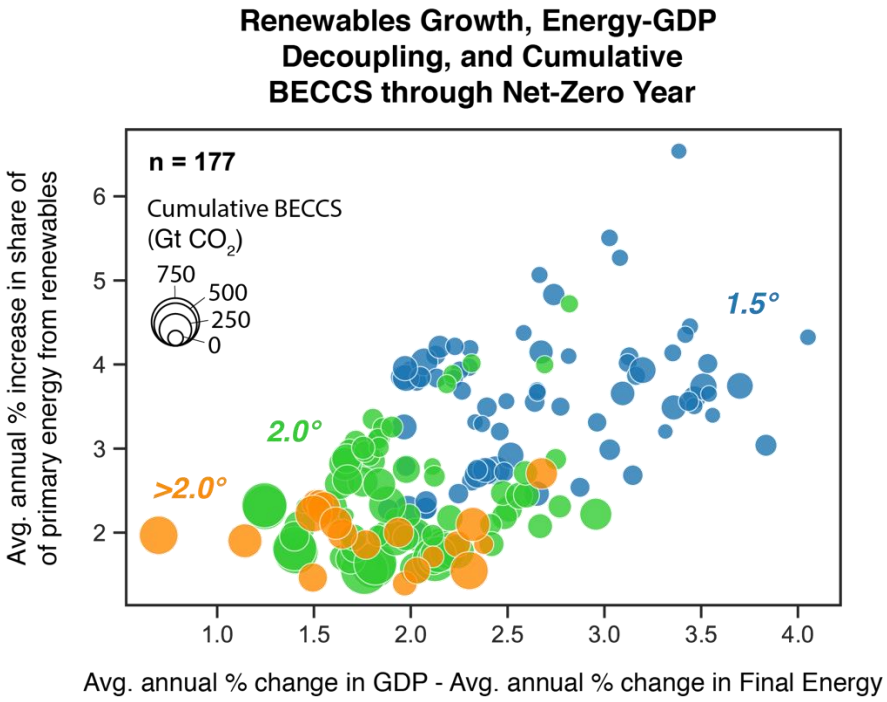

Supplementary Figure A.2 | Rate of energy system transformation by warming group up to net-zero year. Rate of energy system transformation is represented by the difference between average annual % change in GDP and final energy (x-axis) and the average annual % change in renewable energy share of primary energy (y-axis) through each scenario's net-zero year. Colors of points indicate warming level (blue = <1.5˚C, green = 2.0˚C, orange = >2.0˚C), and size of points corresponds to the cumulative carbon sequestered through bioenergy with carbon capture and storage (BECCS) through the net-zero year.

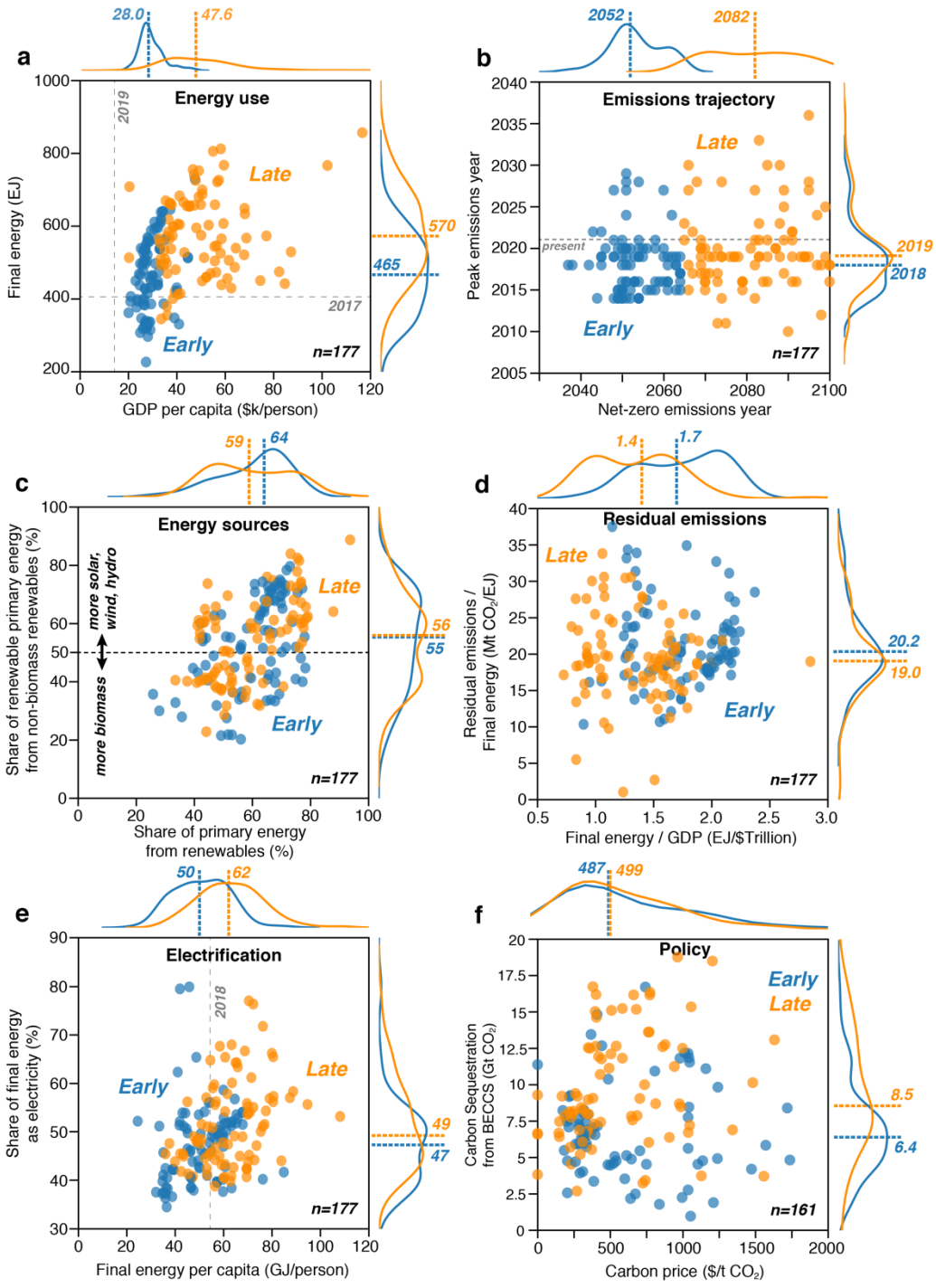

Supplementary Figure A.3 | Early vs. Late net-zero scenarios. Global scenarios that reach net-zero emissions before or at the median net-zero year 2064 ("Early") vs. after the median net-zero year ("Late") show differences in energy use (**a**), emissions trajectory (**b**), energy sources (**c**), residual emissions (**d**), electrification (**e**), and policy (**f**). Points represent individual scenarios, with frequency of scenarios shown along each axis for Early and Late scenario groups. Colored dashed lines and values indicate medians for Early vs. Late scenario groups. Gray dashed lines indicate reference values for the year shown in gray.

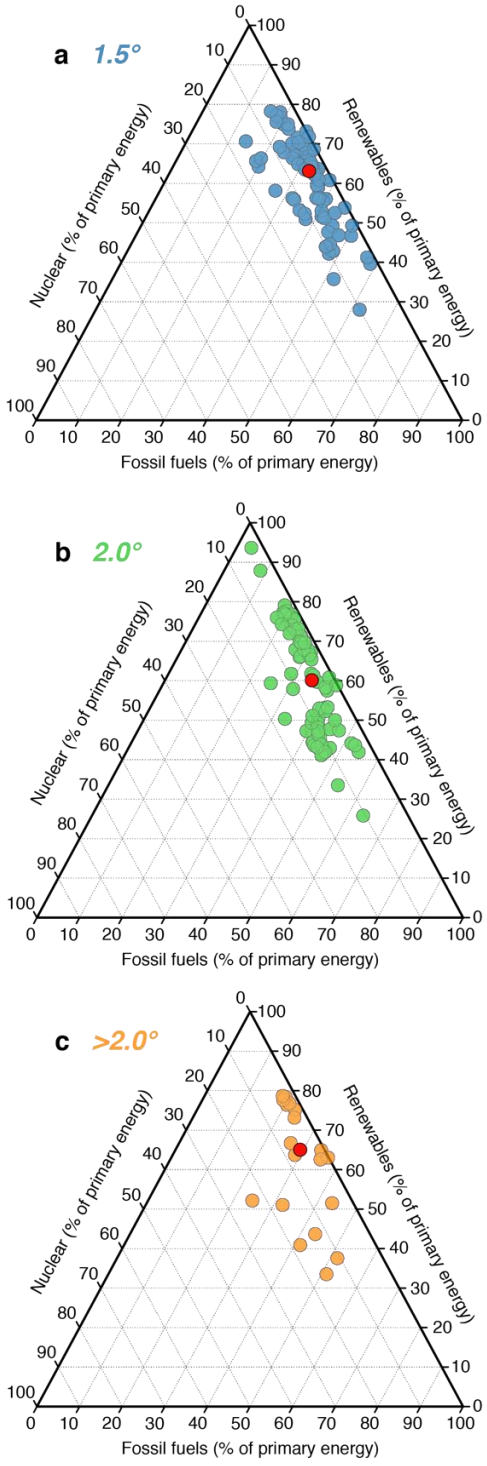

Supplementary Figure A.4 | Primary Energy Sources in Global Net-Zero Emissions Scenarios. Ternary diagrams show the percentage of primary energy from renewables (right axis), fossil fuels (bottom axis), and nuclear (left axis) for <1.5˚C (**a**), 2.0˚C (**b**), and >2.0˚C (**c**) scenarios. The three axis values for each individual point sum to 100%. Red points indicate the geometric median for each respective warming group.

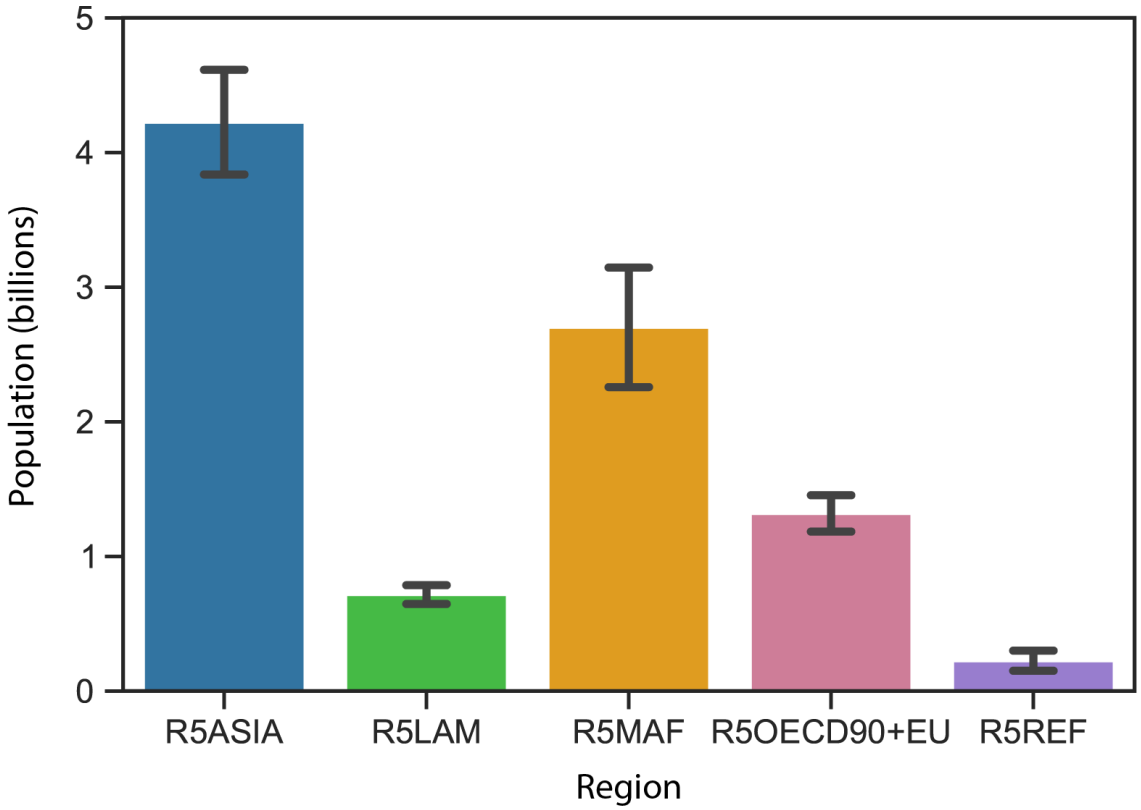

Supplementary Figure A.5 | Regional populations in net-zero year. Population in scenario net-zero years for R5ASIA (Asia), R5LAM (Latin America), R5MAF (Middle East+Africa), R5OECD90+EU (OECD and EU countries), and R5REF (Eastern Europe+Russia). Error bars indicate 1 standard deviation.

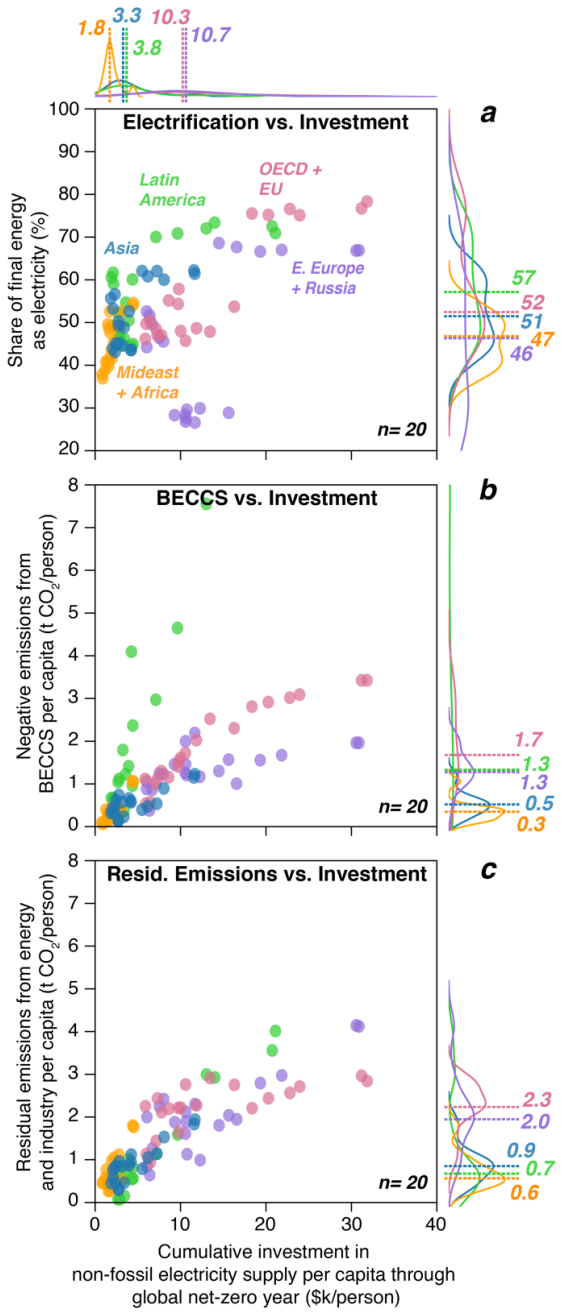

Supplementary Figure A.6 | Regional investment vs. electrification, negative emissions from BECCS, and residual energy+industry emissions. Scenarios that reach net-zero emissions globally and have regional outputs for investment in non-fossil electricity supply (n=20 scenarios with all regions, for a total of 100 data points) show regional differences in share of final energy as electricity (**a**), per capita negative emissions from BECCS (**b**), and per capita residual emissions from energy and industry (**c**). Points represent individual scenarios, with frequency of scenarios shown along each axis for each region (Asia = blue, Latin America = green, Middle East+Africa = orange, OECD+EU countries = pink, and Eastern Europe+Russia = purple). Colored dashed lines and values indicate medians for each region.

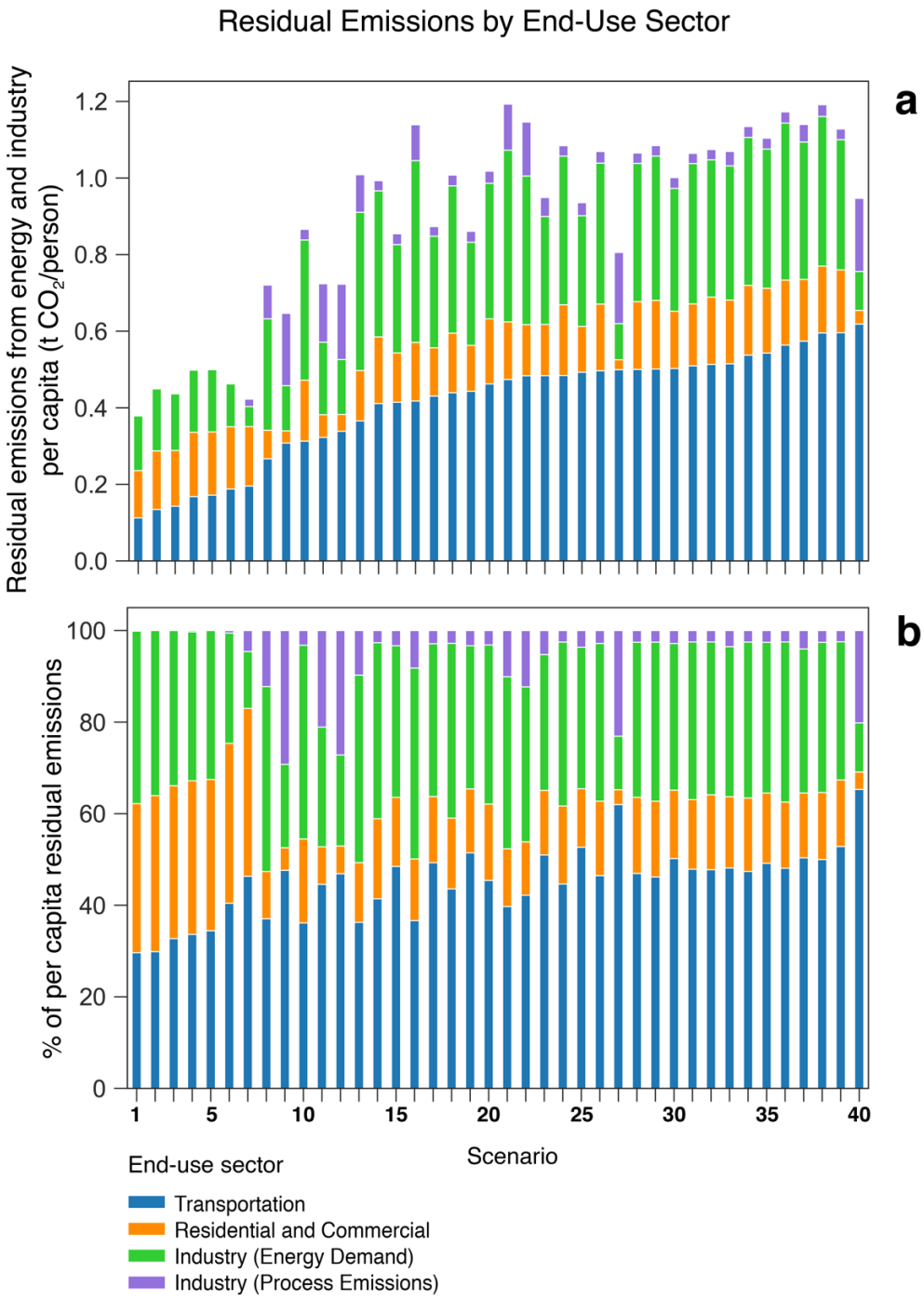

Supplementary Figure A.7 | Residual emissions by end-use sector in global net-zero year. Each bar represents an individual scenario output, numbered 1-40. Please see Table S2 for corresponding list of scenarios and numbers for this figure. Panel (**a**) shows total per capita residual emissions from four end-use sectors as the height of each bar, and the amount from each end-use sector is represented by color: transportation = blue, residential and commercial = orange, industry (energy demand) = green, and industry (process emissions) = purple. Panel (**b**) shows each end-use sector as a percentage of the total residual emissions from the four sectors.

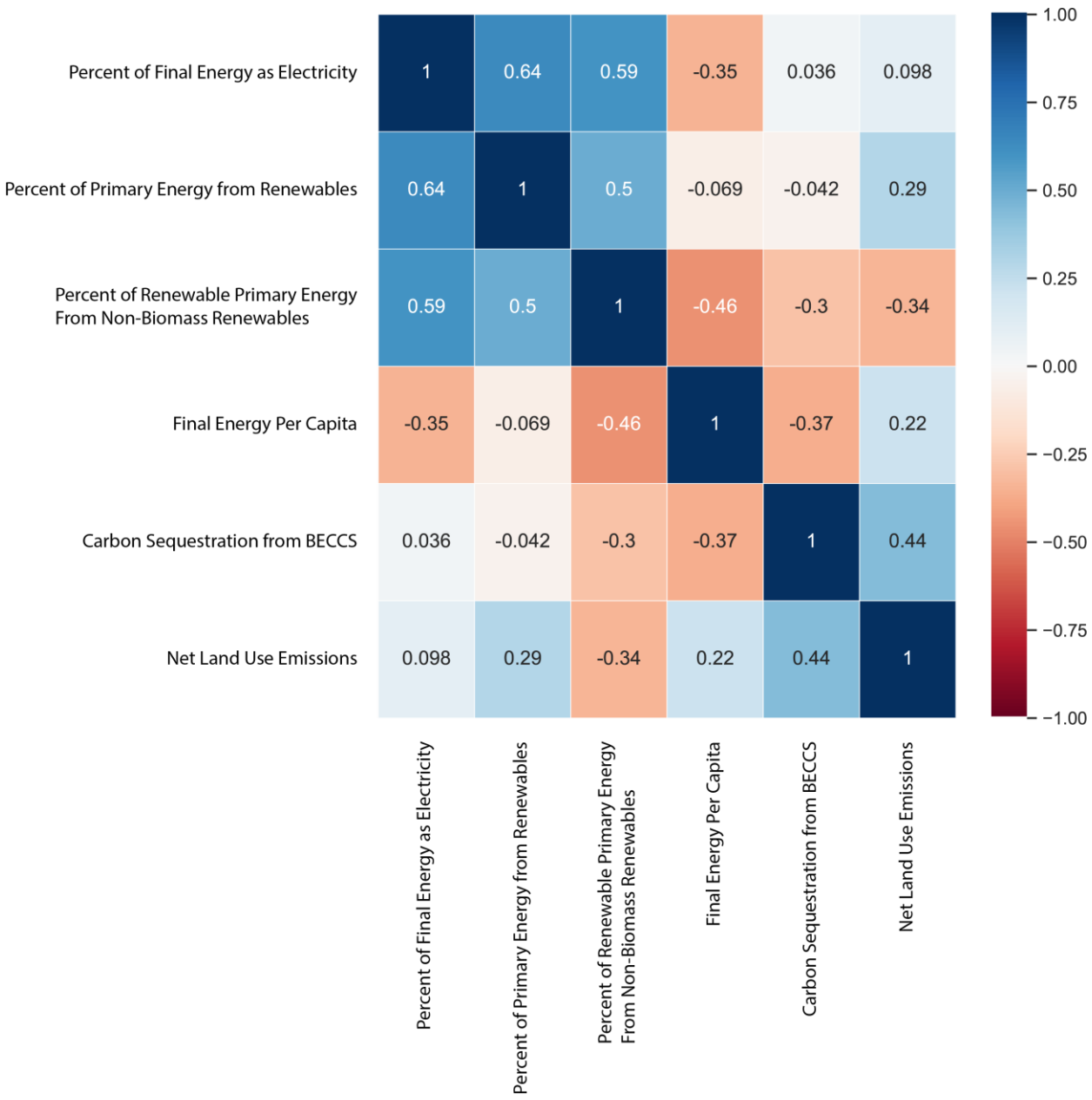

Supplementary Figure A.8 | Pairwise Correlation Matrix for Figure 4 Parameters. Pairwise correlation coefficients for Figure 4 columns are shown in a matrix, with positive correlation coefficients shaded blue and negative correlation coefficients shaded red. Darker shades indicate stronger positive or negative correlations.

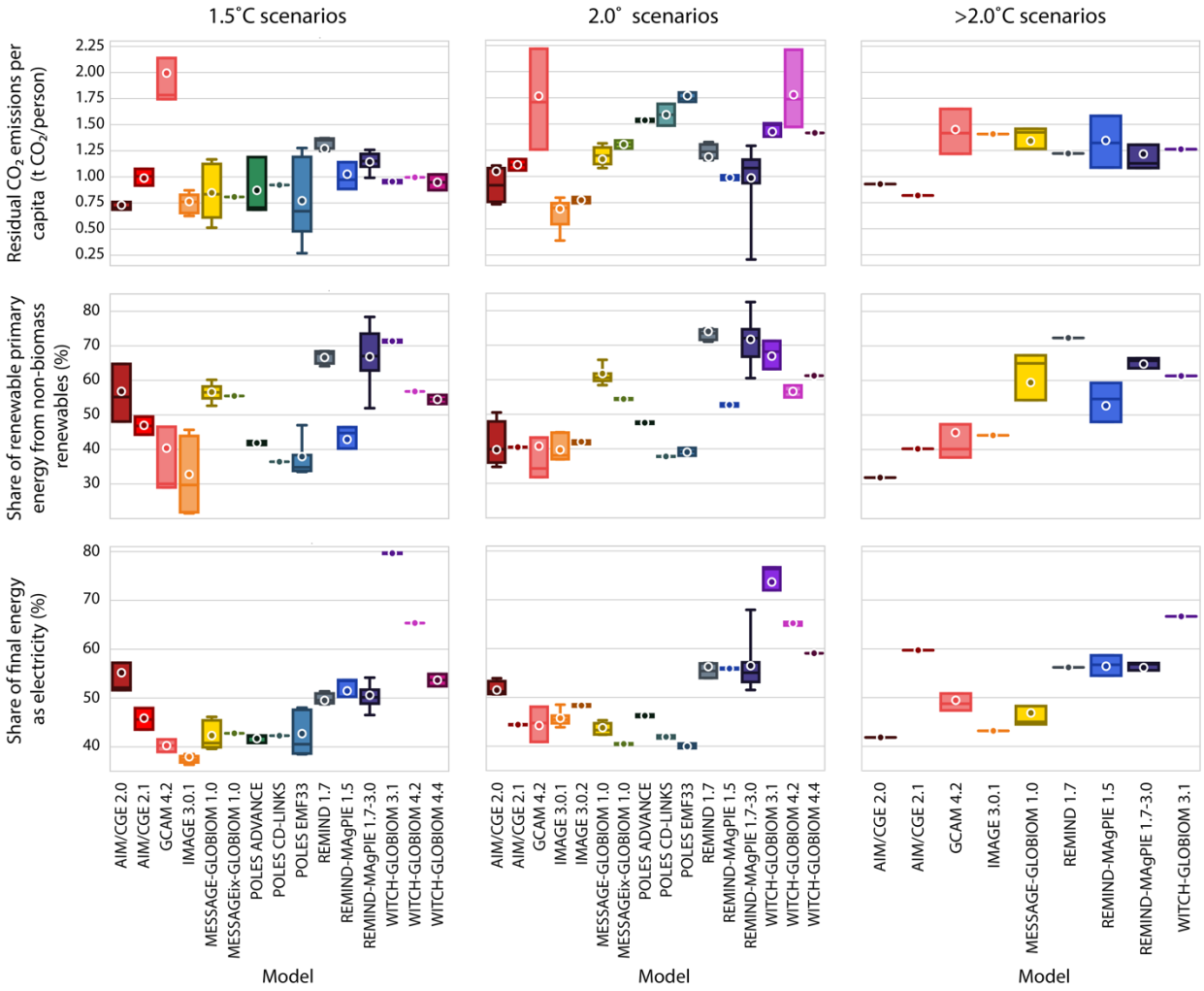

Supplementary Figure A.9 | Model comparison for parameters in global net-zero year. Residual CO_2 emissions per capita (top row), the share of renewable primary energy from non-biomass sources (middle row), and the share of final energy as electricity (bottom row) are shown for 1.5˚C (left column), 2.0˚C (middle column), and >2.0˚C (right column) scenarios, broken out by model. In each case, the boxes show the range from 25th to 75th percentiles, and the whiskers indicate the 5th and 95th percentiles where applicable (some models did not have enough scenario points to show 5th and 95th percentiles, since any points outside the box range were outliers). Lines and circles within the boxes denote the median and mean values, respectively. 15 models ran 1.5˚ scenarios, 16 models ran 2.0˚C scenarios, and 9 models ran >2.0˚C scenarios that reach net-zero emissions. For ease of comparison, box colors are consistent for each model throughout the figure (each model is always the same color across plots).

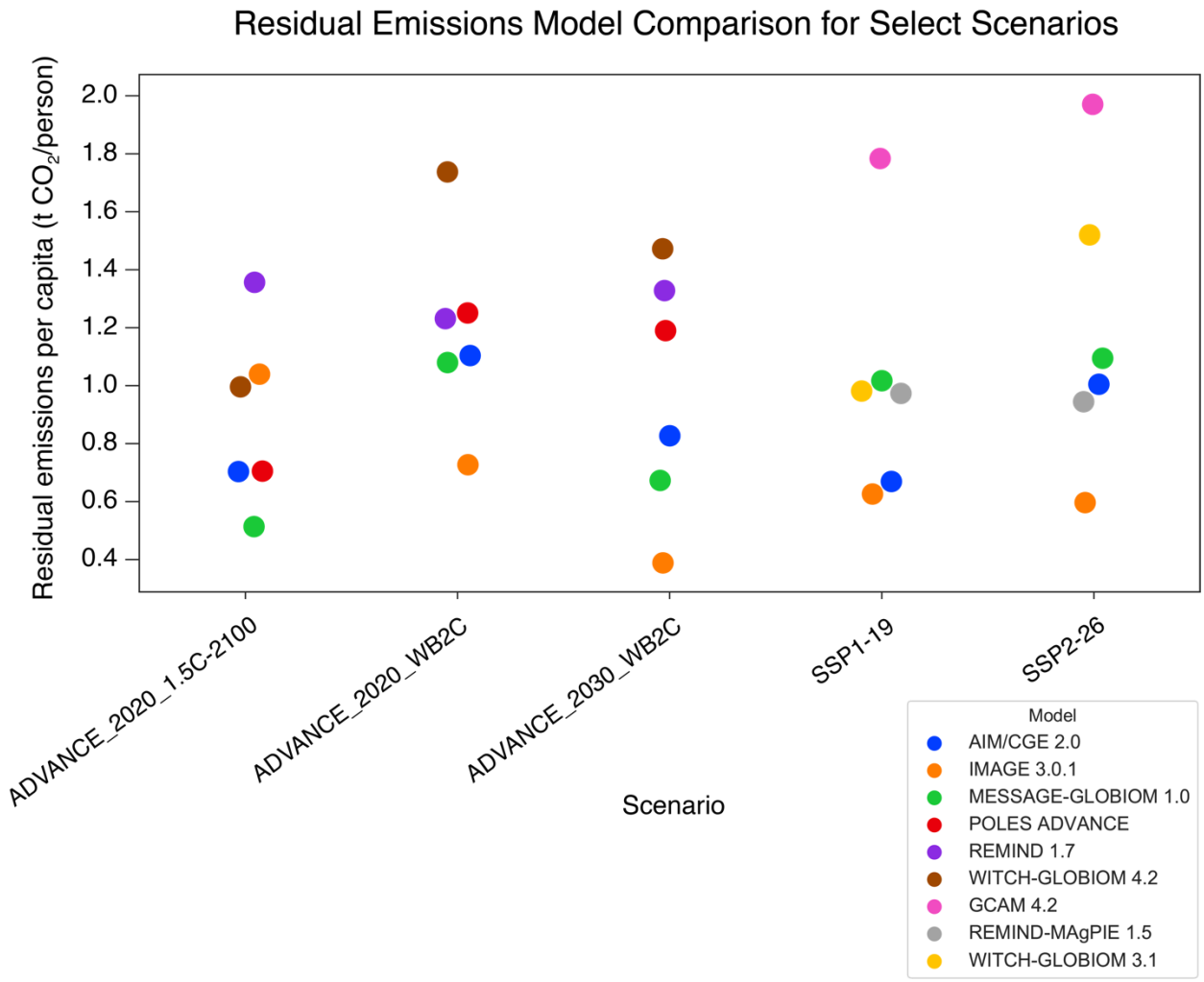

Supplementary Figure A.10 | Residual emissions model/scenario comparison in global net-zero year. Per capita residual emissions from energy+industry are shown for five scenarios, each of which was run by 6 models. Models AIM/CGE 2.0 (blue), IMAGE 3.0.1 (orange), and MESSAGE-GLOBIOM 1.0 (green) ran all five scenarios; Models POLES ADVANCE (red), REMIND 1.7 (purple), and WITCH-GLOBIOM 4.2 (brown) ran scenarios ADVANCE_2020_1.5C-2100, ADVANCE_2020_WB2C, and ADVANCE_2030_WB2C; Models GCAM 4.2 (pink), REMIND-MAgPIE 1.5 (gray), and WITCH-GLOBIOM 3.1 (yellow) ran scenarios SSP1-19 and SSP2-26. Of the models that ran all five scenarios, IMAGE 3.0.1 has the lowest residual emissions value for four of the five scenarios, AIM/CGE 2.0 is the bottom half of model values for all five scenarios, and MESSAGE-GLOBIOM 1.0 is in the bottom half of model values for four of the five scenarios. Of the models that only ran the ADVANCE scenarios, WITCH-GLOBIOM 4.2 is the highest in two of the three ADVANCE scenarios and is in the top half of model values for ADVANCE_2020_1.5C-2100, while POLES ADVANCE and REMIND 1.7 are in the top half of model values for two of the three ADVANCE scenarios, and REMIND 1.7 is the highest for ADVANCE_2020_1.5C-2100. Of the models that only ran the SSP scenarios, GCAM 4.2 is by far the highest for both SSP1-19 and SSP2-26, while REMIND-MAgPIE 1.5 in the bottom half of models for both and WITCH-GLOBIOM 3.1 is in the top half of models for both.

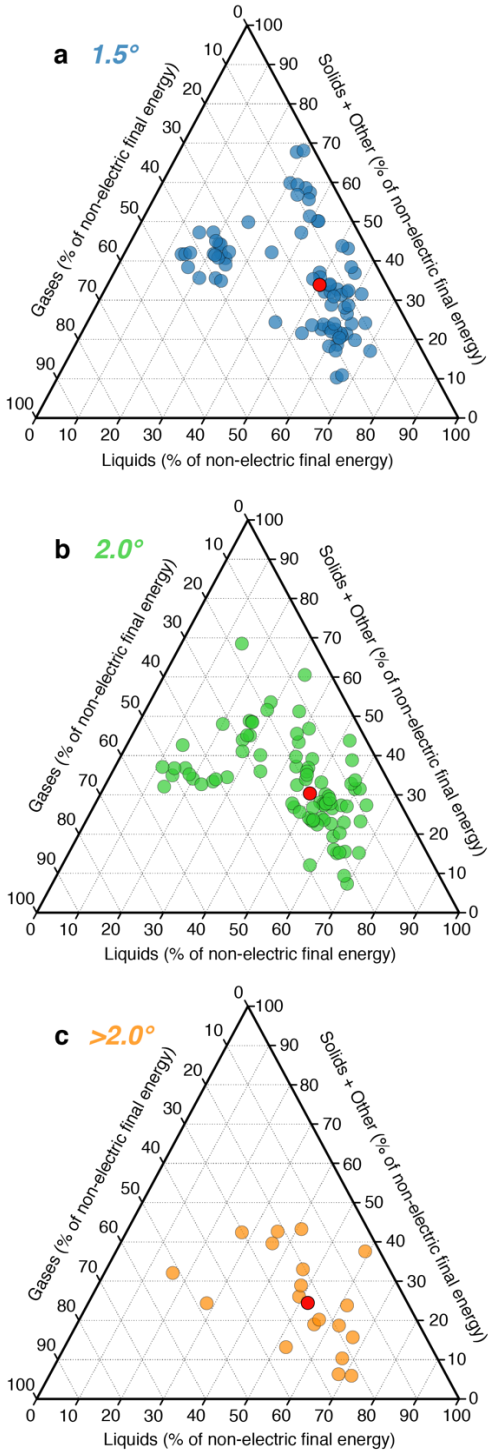

Supplementary Figure A.11 | Fuel Types for Non-Electric Final Energy in Global Net-Zero Emissions Scenarios. Ternary diagrams show the percentage of non-electric final energy from gases (left axis), liquids (bottom axis), and solids + other (right axis) for <1.5˚C (**a**), 2.0˚C (**b**), and >2.0˚C (**c**) scenarios. The three axis values for each individual point sum to 100%. Red points indicate the geometric median for each respective warming group.

Supplementary Table A.2 | List of 40 scenarios evaluated by end-use sector residual emissions in Supplementary Figure A.7. Only these 40 scenarios out of the original 177 had all required output variables for end-use sector analysis. Scenarios are listed first, followed by the model that ran the scenario (format: scenario, model).

1	IMA15-RenElec, IMAGE 3.0.1
2	IMA15-LiStCh, IMAGE 3.0.1
3	IMA15-LoNCO2, IMAGE 3.0.1
4	IMA15-Pop, IMAGE 3.0.1
5	IMA15-AGInt, IMAGE 3.0.1
6	IMA15-Def, IMAGE 3.0.1
7	IMA15-Eff, IMAGE 3.0.1
8	CEMICS-2.0-CDR8, REMIND 1.7
9	TERL_15D_LowCarbonTransportPolicy, AIM/CGE 2.1
10	SMP_2C_Sust, REMIND-MAgPIE 1.7-3.0
11	CEMICS-1.5-CDR8, REMIND 1.7
12	TERL_2D_LowCarbonTransportPolicy, AIM/CGE 2.1
13	CEMICS-2.0-CDR12, REMIND 1.7
14	SMP_2C_early, REMIND-MAgPIE 1.7-3.0
15	PEP_2C_red_netzero, REMIND-MAgPIE 1.7-3.0
16	CEMICS-2.0-CDR20, REMIND 1.7
17	PEP_2C_red_eff, REMIND-MAgPIE 1.7-3.0
18	SMP_2C_lifesty, REMIND-MAgPIE 1.7-3.0
19	PEP_2C_red_goodpractice, REMIND-MAgPIE 1.7-3.0
20	PEP_1p5C_full_netzero, REMIND-MAgPIE 1.7-3.0
21	CEMICS-1.5-CDR20, REMIND 1.7
22	CEMICS-1.5-CDR12, REMIND 1.7
23	PEP_1p5C_red_eff, REMIND-MAgPIE 1.7-3.0
24	PEP_2C_full_netzero, REMIND-MAgPIE 1.7-3.0
25	PEP_2C_red_NDC, REMIND-MAgPIE 1.7-3.0
26	PEP_1p5C_full_eff, REMIND-MAgPIE 1.7-3.0
27	TERL_15D_NoTransportPolicy, AIM/CGE 2.1
28	SMP_2C_Def, REMIND-MAgPIE 1.7-3.0

29	PEP_2C_full_goodpractice, REMIND-MAgPIE 1.7-3.0
30	SMP_1p5C_early, REMIND-MAgPIE 1.7-3.0
31	SMP_2C_regul, REMIND-MAgPIE 1.7-3.0
32	PEP_2C_full_eff, REMIND-MAgPIE 1.7-3.0
33	PEP_1p5C_full_goodpractice, REMIND-MAgPIE 1.7-3.0
34	PEP_2C_full_NDC, REMIND-MAgPIE 1.7-3.0
35	SMP_1p5C_Def, REMIND-MAgPIE 1.7-3.0
36	SMP_1p5C_lifesty, REMIND-MAgPIE 1.7-3.0
37	PEP_1p5C_full_NDC, REMIND-MAgPIE 1.7-3.0
38	SMP_1p5C_Sust, REMIND-MAgPIE 1.7-3.0
39	SMP_1p5C_regul, REMIND-MAgPIE 1.7-3.0
40	TERL_2D_NoTransportPolicy, AIM/CGE 2.1

Supplementary Table A.3 | List of 20 scenarios evaluated by investment in non-fossil electricity supply in Supplementary Figure A.6. Only these 20 scenarios (5 regions for each scenario, for a total of 100 data points in Supplementary Fig. 6) out of the original 175 regional scenarios had non-zero regional outputs for investment in non-fossil electricity supply in the global net-zero year. Scenarios are listed first, followed by the model that ran the scenario.

1	ADVANCE_2020_1.5C-2100, AIM/CGE 2.0
2	ADVANCE_2020_1.5C-2100, MESSAGE-GLOBIOM 1.0
3	ADVANCE_2020_1.5C-2100, WITCH-GLOBIOM 4.2
4	ADVANCE_2020_Med2C, MESSAGE-GLOBIOM 1.0
5	ADVANCE_2020_Med2C, WITCH-GLOBIOM 4.2
6	ADVANCE_2020_WB2C, AIM/CGE 2.0
7	ADVANCE_2020_WB2C, MESSAGE-GLOBIOM 1.0
8	ADVANCE_2020_WB2C, WITCH-GLOBIOM 4.2
9	ADVANCE_2030_Med2C, MESSAGE-GLOBIOM 1.0
10	ADVANCE_2030_Med2C, WITCH-GLOBIOM 4.2
11	ADVANCE_2030_Price1.5C, AIM/CGE 2.0
12	ADVANCE_2030_Price1.5C, MESSAGE-GLOBIOM 1.0
13	ADVANCE_2030_Price1.5C, WITCH-GLOBIOM 4.2
14	ADVANCE_2030_WB2C, AIM/CGE 2.0
15	ADVANCE_2030_WB2C, MESSAGE-GLOBIOM 1.0
16	ADVANCE_2030_WB2C, WITCH-GLOBIOM 4.2
17	TERL_15D_LowCarbonTransportPolicy, AIM/CGE 2.1
18	TERL_15D_NoTransportPolicy, AIM/CGE 2.1
19	TERL_2D_LowCarbonTransportPolicy, AIM/CGE 2.1
20	TERL_2D_NoTransportPolicy, AIM/CGE 2.1

Appendix B: Supplementary Information for Chapter 2

Supplementary Table B.1 | Technoeconomic model variables.

Variable	Unit	Model Range	Values reported in literature
Capital costs	$/km^2/year	10,000 – 1,000,000	929,676 [(van den Burg et al., 2016)] 550,000 – 950,000 [(Capron et al., 2020)] 375,910 [(Correa et al., 2016)] 210,580 [(Camus et al., 2019)]
Operating and maintenance costs	$/km^2/year	60,000 – 70,000	69,000 [(van den Burg et al., 2016)] 63,320 [(Camus et al., 2019)]
Seeded line cost (includes hatchery costs)	$/m	0.05 – 1.45	1.38 [(van den Burg et al., 2016)] 0.13 [(Camus et al., 2019)]
Labor costs (excludes harvest labor)	$/km^2/year	38,000 – 120,000	115,485 [(Camus et al., 2019)] 41,800 [(van den Burg et al., 2016)]
Harvest costs (includes harvest labor, excludes harvest transport)	$/km^2/harvest	120,000 – 400,000	381,265 [(Camus et al., 2019)] 138,000 [(van den Burg et al., 2016)]

Transport cost per ton of material (includes loading/unloading costs)	$/t/km	0.1 – 0.35	0.225 [(van den Burg et al., 2016)]
Transport emissions per ton of material	tCO_2/t/km	0 – 0.000045	0.00003 [(Aitken et al., 2014)]
Maintenance boat emissions	tCO_2/km	0 – 0.0035	0.0023653 (calculated using methods from [(Aitken et al., 2014; Johnson, 2011)])
Insurance costs	$/km^2/year	35,000 – 105,000	70,000 [(van den Burg et al., 2016)]
Aquaculture license costs	$/km^2/year	1,000 – 2,000	1,420 [(Camus et al., 2019)]
Atmospheric removal fraction	fraction (unitless)	0.4 – 1	0.4 – 0.75 [(Berger et al., 2022)] 0.5 (global average, from preliminary experiment by authors using [(Harrison et al., 2018)] informed by [(Bach et al., 2021)])
Seaweed yield	tDW/km^2/year	5th, 25th, median, 75th, and 95th percentile maps (randomly selected each simulation from normal distribution)	Results from G-MACMODS biophysical growth model Monte Carlo analysis [(Arzeno-Soltero et al., 2022)]

Seaweed market value for product end-use	$/tDW	400 – 800	Food: 500-800 (dried seaweed wholesale price from [("Dried Seaweed Price," 2022)]) Feed: 400-500 (values per ton dry animal feed and soybean meal from [(USDA, 2022; van den Burg et al., 2016)], assuming a direct replacement with dry seaweed) Fuel: 430 (dried seaweed price for bioethanol production, calculated based on bioethanol yield per ton seaweed (0.25) and average of 2021-2022 historical E85 fuel prices ($3.76/GGE) from [(U.S.DOE, 2022)], modeled range 400-500) Not product-specific: 400 (dried seaweed market price of $400/tDW from [(Buschmann et al., 2017)])
Conversion cost	$/tDW	20 – 80	48 (calculated with data from [(Roesijadi et al., 2010)] assuming plant meets full feedstock capacity)
Conversion emissions	tCO_2/tDW	0 – 0.01	0.0057 (calculated using data and methods from [(Roesijadi et al., 2010)])

Depth impact on capex	multiplier (unitless)	0 – 1	1 (estimation used in [(van den Burg et al., 2016)] that offshore depth can double capital costs)
Significant wave height impact on capex	multiplier (unitless)	0 – 1	Author assumption that high waviness impacts capital lifetime similarly to depth impact
GHG emissions avoided by replacement with seaweed product	tCO_2e/tDW	0.7 – 6.0	Food: 1-6 (considering global average emissions from GHGs per kcal for pulses, vegetables, fruits, oil crops, and cereals, from [(Hong et al., 2021)]) Feed: 1-3.1 (considering global average emissions from GHGs per kcal for oil crops and cereals, +- 50% uncertainty, from [(Hong et al., 2021)]) Fuel: 0.7-1 (assuming 3.2-3.5 tCO_2/t fossil fuel by fuel type from [(EIA, 2021)], 0.25t bioethanol/tDW from [(Roesijadi et al., 2010)], and energy density equivalence conversions by fuel type)

Supplementary Table B.2 | Constants in model.

Parameter	Unit	Model Range	Source
Total length of cultivation line per unit area	m/km^2	Tropical red: 5,000,000 Temperate red: 20,000,000 Tropical brown: 751,880 Temperate brown: 666,667	Calculated using species-specific line spacing from [(Arzeno-Soltero et al., 2022)]
Capital and other annualized equipment mass	$t/km^2/year$	Tropical red: 1,231.87 Temperate red: 4,927.50 Tropical brown: 185.24 Temperate brown: 164.25	Calculated using line spacing (above) and methods from extended methods in [(Aitken et al., 2014)]
Number of maintenance trips	$trips/km^2/year$	6	[(Aitken et al., 2014)]
Fraction of sunk carbon sequestered for 100 years	fraction (unitless)	0 – 1	[(Siegel et al., 2021)]
Depth beyond which capex increases via depth_mult	m	500	[(Yu, Zhang, Yang, Xin, & Gao, 2020)]
Significant wave height beyond which capex increases via wave_mult	m	3	[(Yim, Nakhata, Bartel, & Huang, 2005)]
Seaweed carbon fraction	tC/tDW	0.3	[(Arzeno-Soltero et al., 2022; Duarte, 1992)]
Seaweed caloric content	Kcal/tDW	2,980,000	[(USDA, 2020)]
Bioethanol yield from seaweed	t/tDW	0.25	[(Roesijadi et al., 2010)]

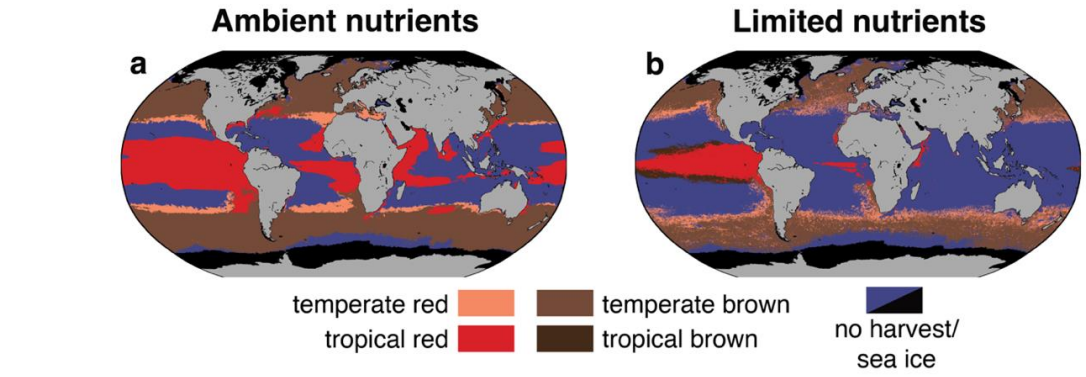

Supplementary Figure B.1 | Preferred seaweed type. The seaweed type that results in the most harvested biomass is shown for each ocean grid cell for the G-MACMODS standard run ambient nutrient scenario (**a**) and limited nutrient scenario (**b**). Modified from (Arzeno-Soltero et al., 2022).

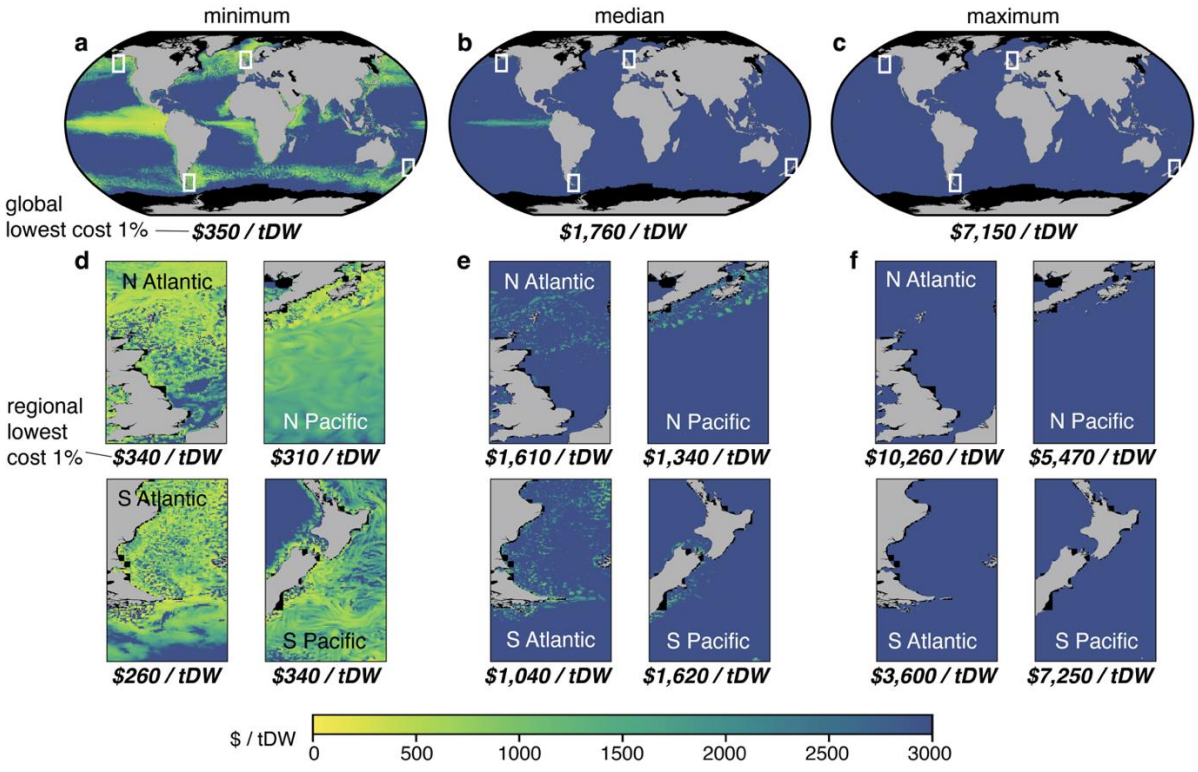

Supplementary Figure B.2 | Seaweed production and harvest cost using limited nutrient scenario. Estimated seaweed production costs vary considerably depending on assumed costs of farming capital, seeded lines, labor, and harvest (transport of harvested seaweed is not included). Across limited nutrient simulations, average farming cost in the 1% of global ocean areas with lowest cost ranges from $350/tDW (**a**) to $7,150/tDW (**c**), with a median of $1,760/tDW (**b**). Regional insets (**d-f**) reveal small-scale features in particularly low-cost areas.

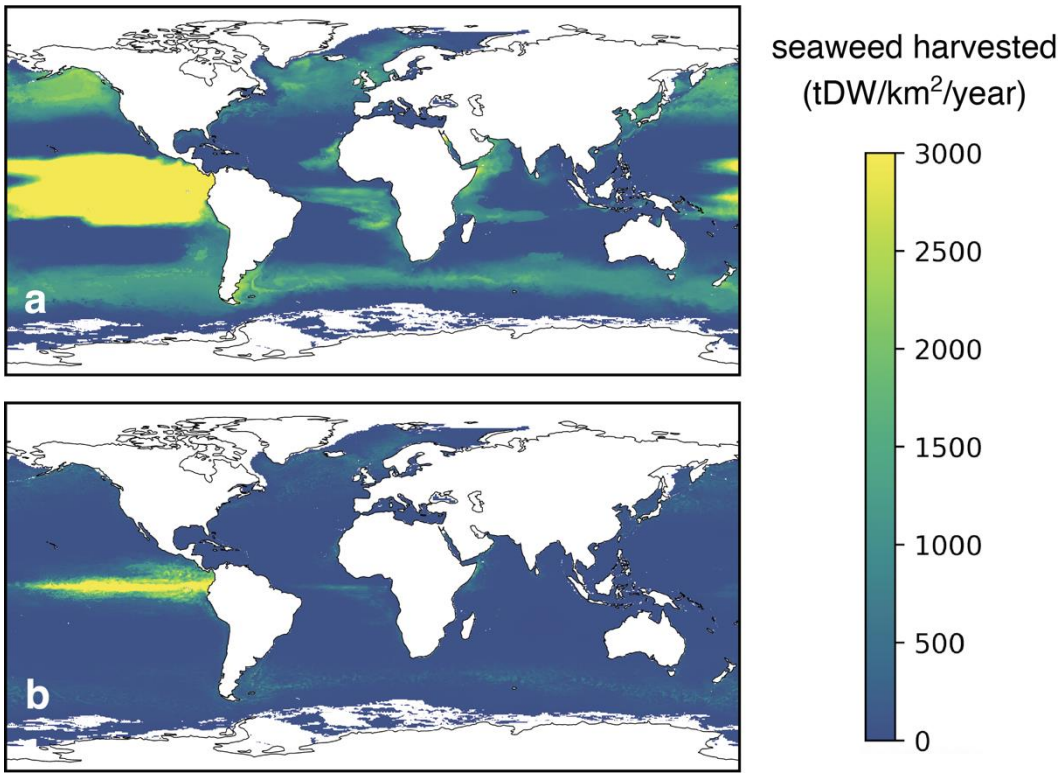

Supplementary Figure B.3 | Annual seaweed biomass harvested. Maps show amount of seaweed harvested annually (tDW/km^2/year) from median Monte Carlo results using ambient nutrients (**a**) and limited nutrients (**b**) in G-MACMODS [(Arzeno-Soltero et al., 2022)].

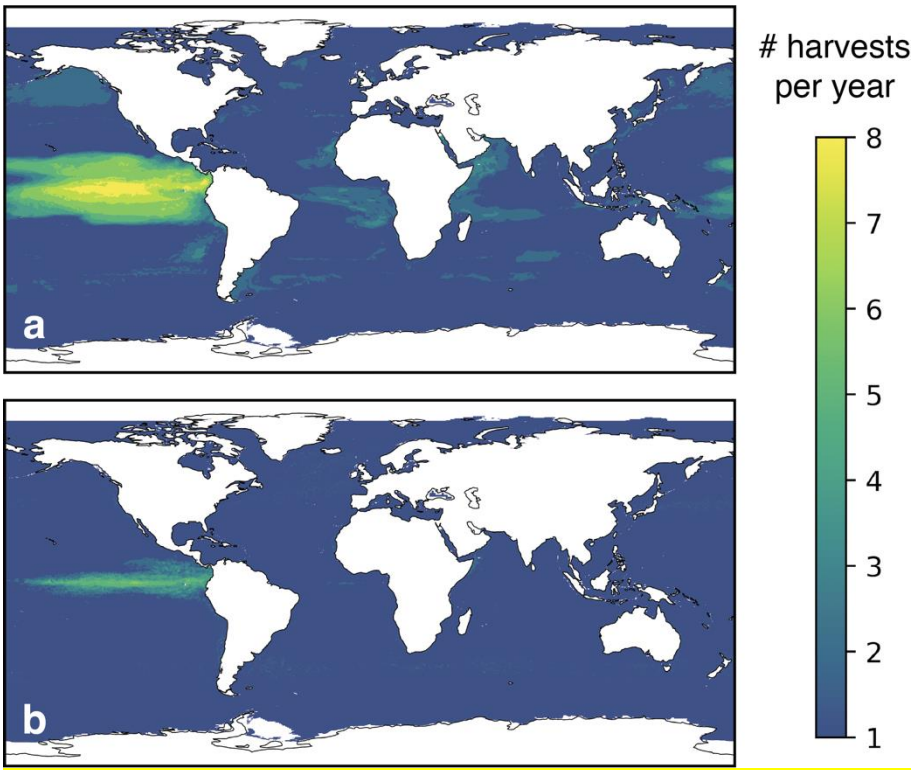

Supplementary Figure B.4 | Number of harvests required to reach maximum annual yield. Maps show number of harvests per year from median Monte Carlo results using ambient nutrients (**a**) and limited nutrients (**b**) in G-MACMODS [(Arzeno-Soltero et al., 2022)].

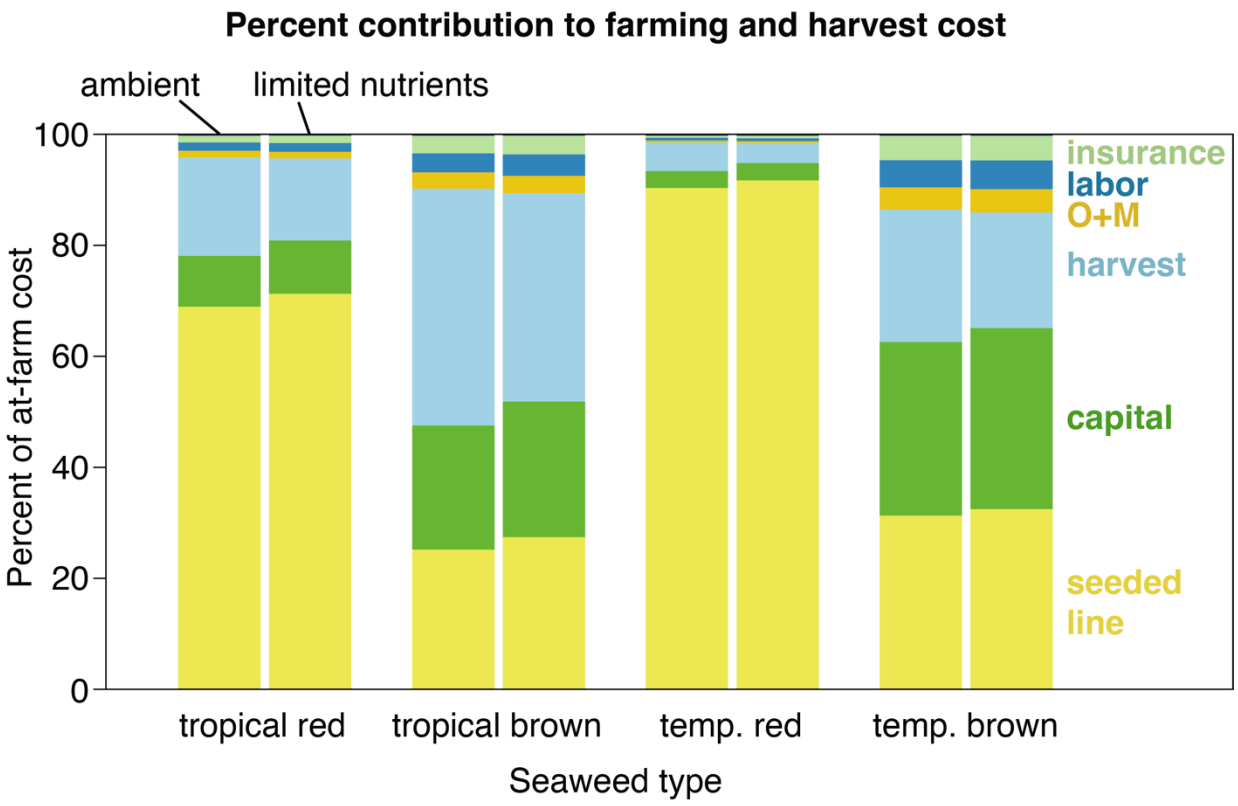

Supplementary Figure B.5 | Summary of total farming cost breakdown per km². Percent of total $/km² seaweed farming cost for four seaweed types in ambient nutrients (left bar for each type) and limited nutrients (right bar for each type) simulations. Note: does not include transportation costs.

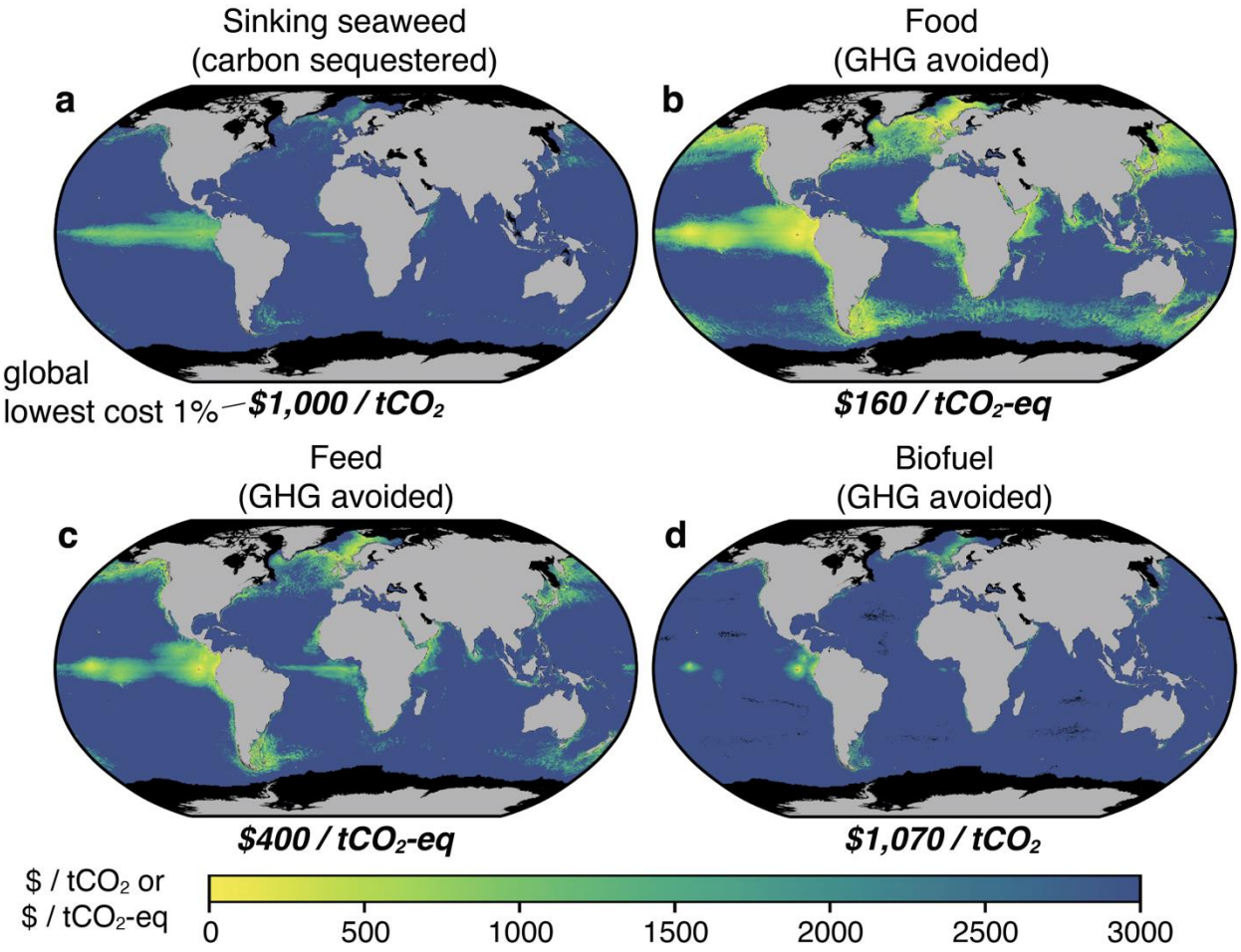

Supplementary Figure B.6 | Net cost of potential seaweed climate benefits for limited nutrient simulations. Costs of using farmed seaweed to sequester carbon or avoid GHG emissions vary in space according to estimated production costs as well as spatially-explicit differences in the costs and net emissions of transportation, sinking or conversion, and replacement of conventional market alternatives with seaweed products. Differentiation between seaweed product groups (**b-d**) is based on emissions avoided by seaweed products and market value for each product type. Maps show costs when propagating the most optimistic assumptions (5th percentile costs) from limited nutrient simulations. Average cost in the 1% of global ocean areas with lowest cost ranges from \$160/tCO_2-eq avoided when seaweed is used for food (**b**) to \$1,070/tCO_2 avoided when seaweed is used to produce biofuel (**d**).

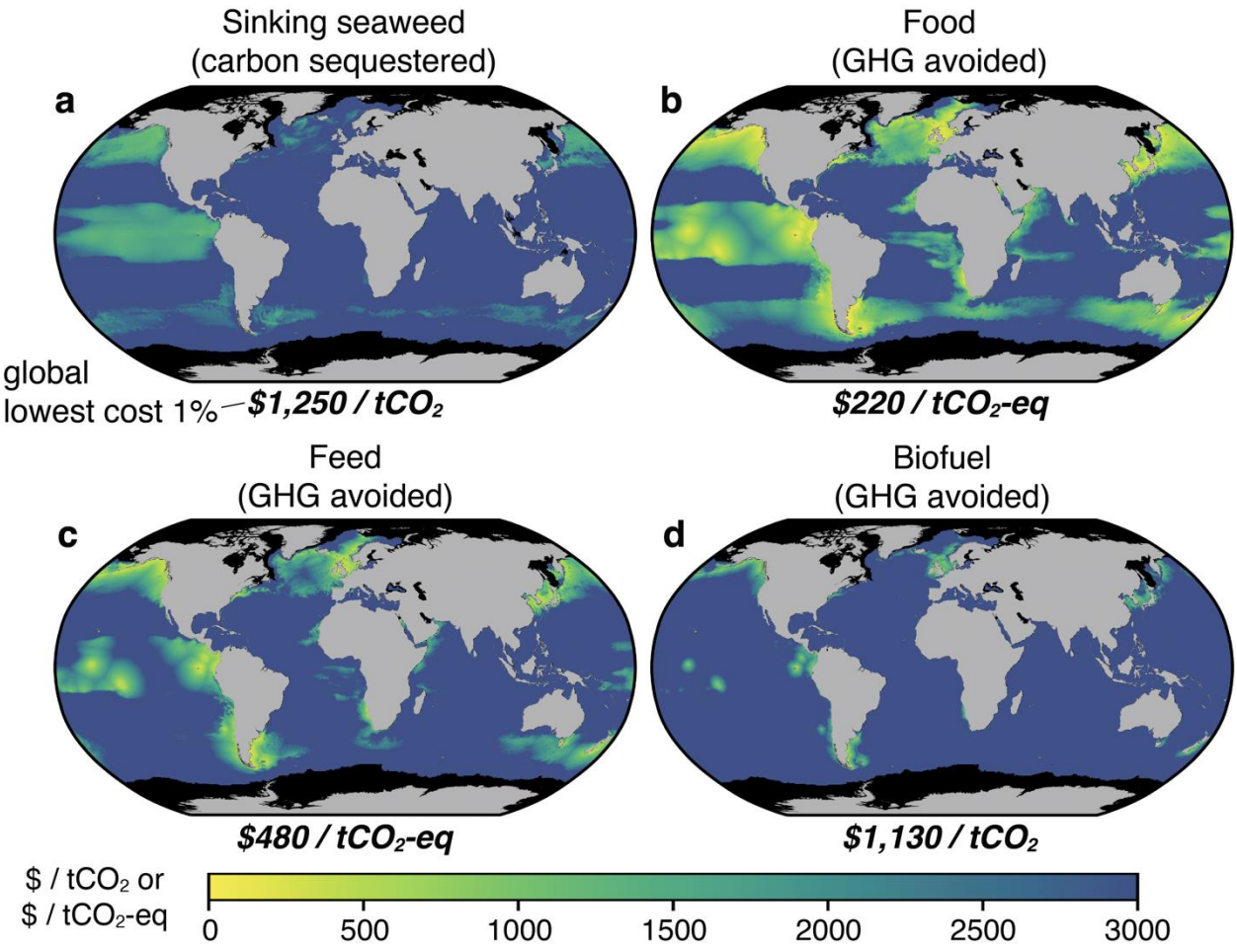

Supplementary Figure B.7 | Median net cost of potential seaweed climate benefits. Costs of using farmed seaweed to sequester carbon or avoid GHG emissions vary in space according to estimated production costs as well as spatially-explicit differences in the costs and net emissions of transportation, sinking or conversion, and replacement of conventional market alternatives with seaweed products. Differentiation between seaweed product groups (**b-d**) is based on emissions avoided by seaweed products and market value for each product type. Maps show median costs from ambient nutrient simulations. Average cost in the 1% of global ocean areas with lowest cost ranges from $220/tCO$_2$-eq avoided when seaweed is used for food (**b**) to $1,250/tCO$_2$ sequestered by sinking seaweed (**a**).

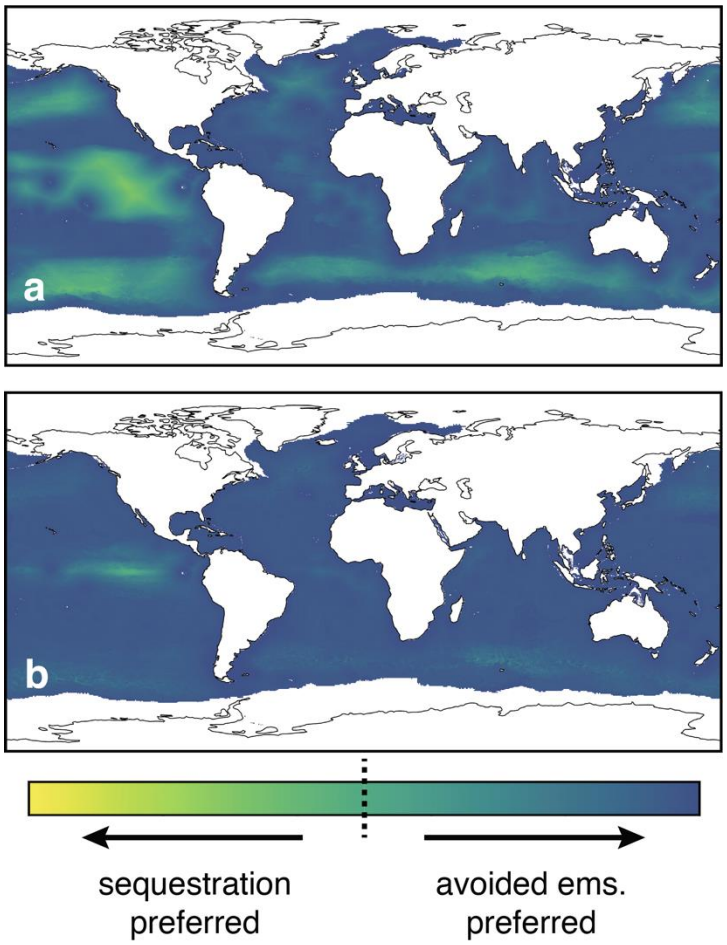

Supplementary Figure B.8 | Economic preference for sinking or products by location. Maps show the average across all ambient nutrient (**a**) and limited nutrient (**b**) simulations of whether carbon sequestration via sinking (yellow-green shades) or GHG emissions mitigation via products (green-blue shades) is cheaper. Sequestration via sinking is generally preferred in locations farthest from port.

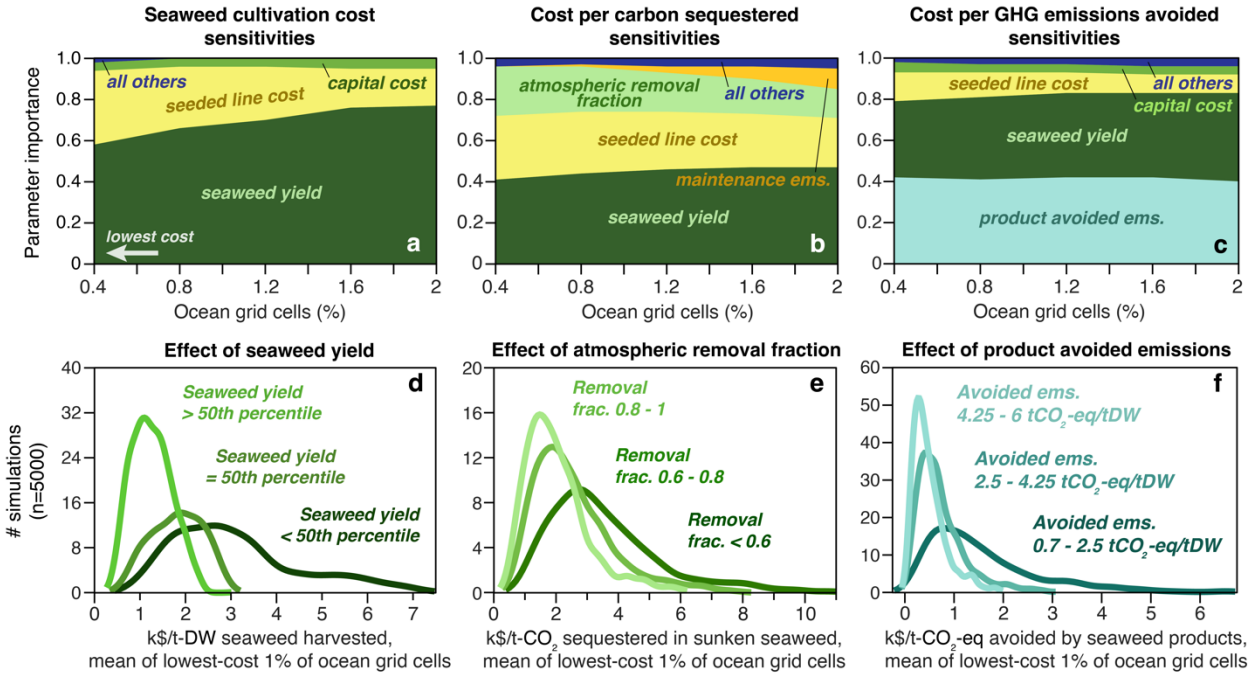

Supplementary Figure B.9 | Key cost sensitivities of seaweed production and climate benefits for limited nutrient simulations. Across our Monte Carlo simulations in the 2% of ocean grid cells where costs are lowest, estimated seaweed production cost is especially sensitive to the seaweed yield amount and seeded line cost (**a**), whereas costs of carbon sequestration (**b**) and GHG emissions avoided (**c**) are strongly influenced by the fraction of seaweed carbon that corresponds to an equivalent amount removed from the atmosphere and the assumed emissions avoided by seaweed products, respectively, in addition to seaweed yield and seeded line cost. Panels **d**-**f** show kernel density plots for the most important parameters in the cheapest 1% ocean areas, showing that the lowest production and climate benefit costs depend upon seaweed yield being at or above the median of potential seaweed yields (**d**), an assumed atmospheric removal fraction of >0.6-0.8 (**e**), and avoided emissions >2.5 tCO_2-eq/tDW (**f**).

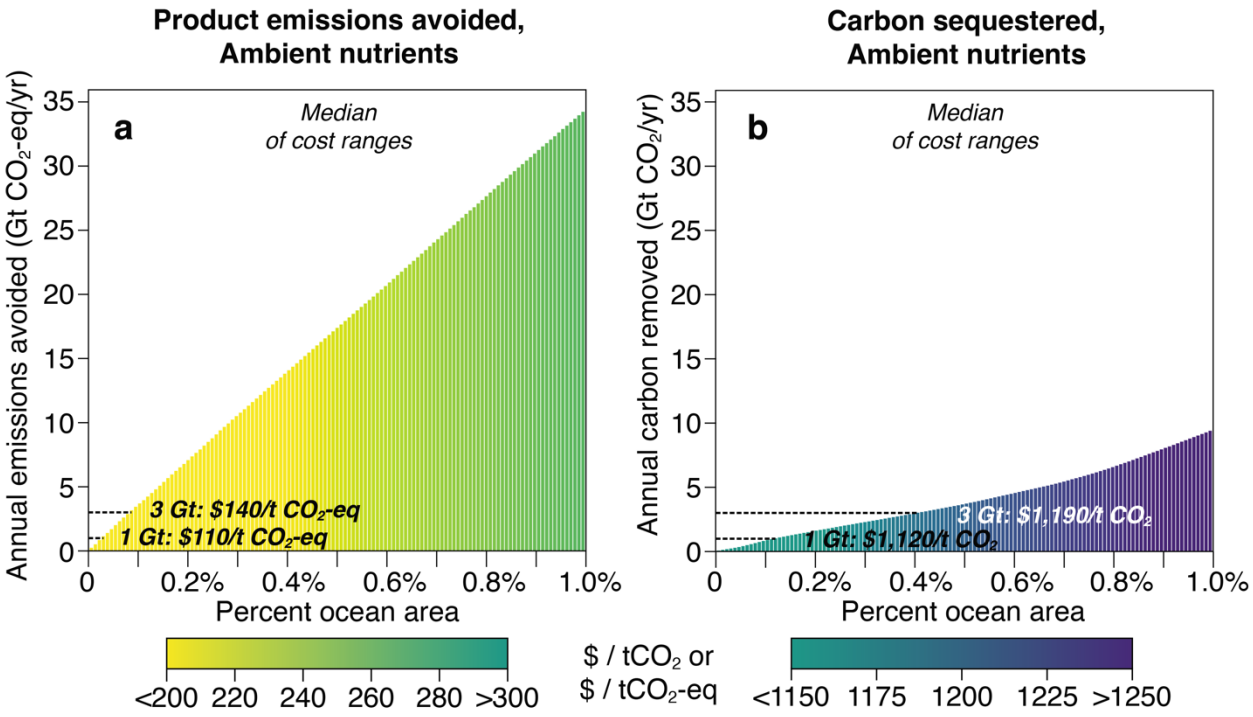

Supplementary Figure B.10 | Cumulative potential climate benefits of large-scale seaweed farming using median of cost simulations. Total GHG emissions avoided (**a**) or carbon sequestered (**b**) each year could reach gigaton-scales if seaweed were farmed over large areas of the ocean. Bars show the potential climate benefits as a function of the lowest-cost ocean area (0.1% of ocean area is roughly 360,000 km^2, nearly the area of Germany and 130 times the total area of current seaweed farms), and colors indicate the average cost per tCO_2-eq emissions avoided or tCO_2 sequestered using median net costs from ambient nutrient simulations.

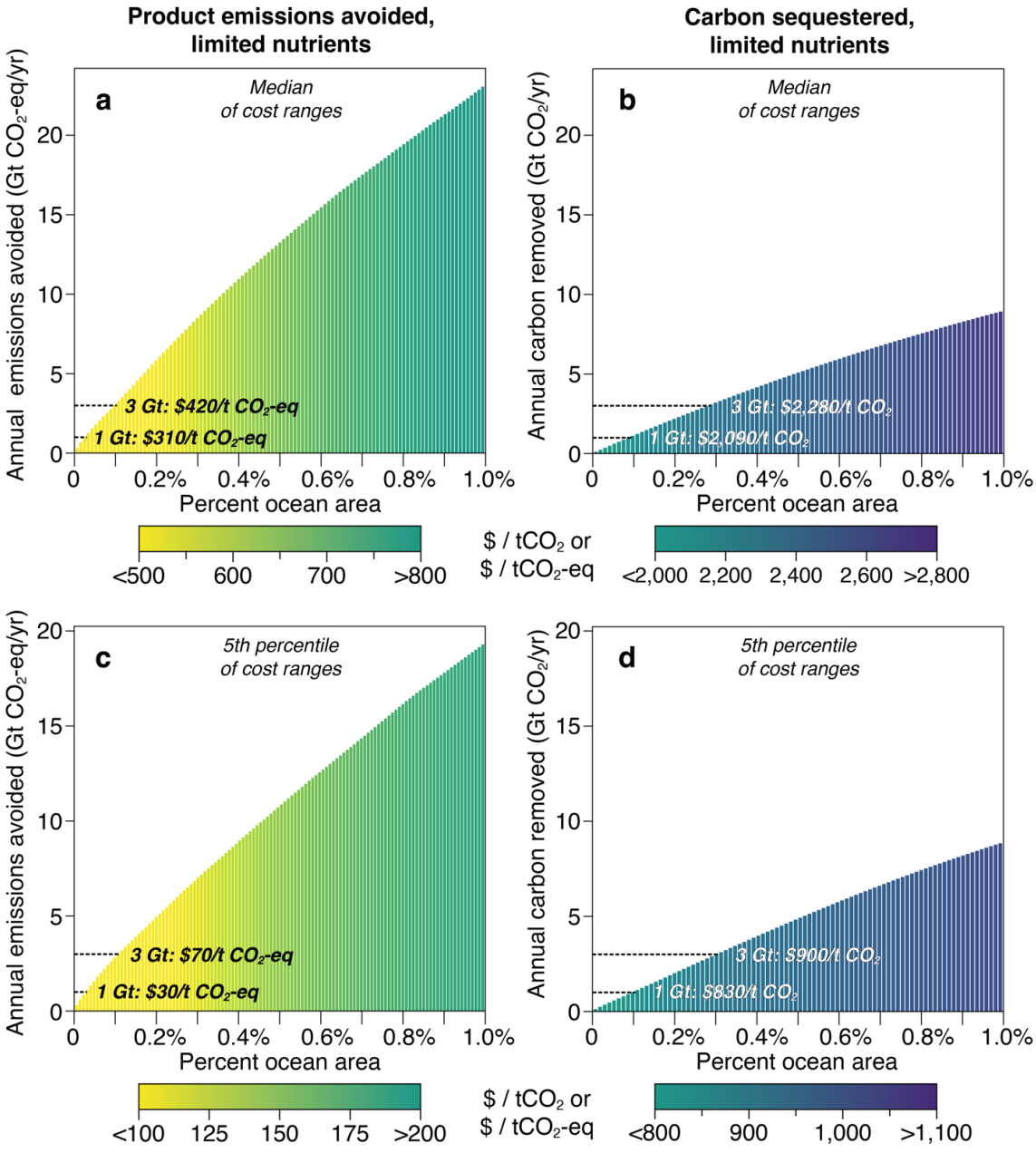

Supplementary Figure B.11 | Cumulative potential climate benefits of large-scale seaweed farming using limited nutrient simulations. Total GHG emissions avoided (**a, c**) or carbon sequestered (**b, d**) each year could reach gigaton-scales if seaweed were farmed over large areas of the ocean. Bars show the potential climate benefits as a function of the lowest-cost ocean area (0.1% of ocean area is roughly 360,000 km^2, nearly the area of Germany and 130 times the total area of current seaweed farms), and colors indicate the average cost (or profit) per tCO_2-eq emissions avoided or tCO_2 sequestered using median (**a, b**) and optimistically low (5th percentile; **c, d**) net costs from limited nutrient simulations.

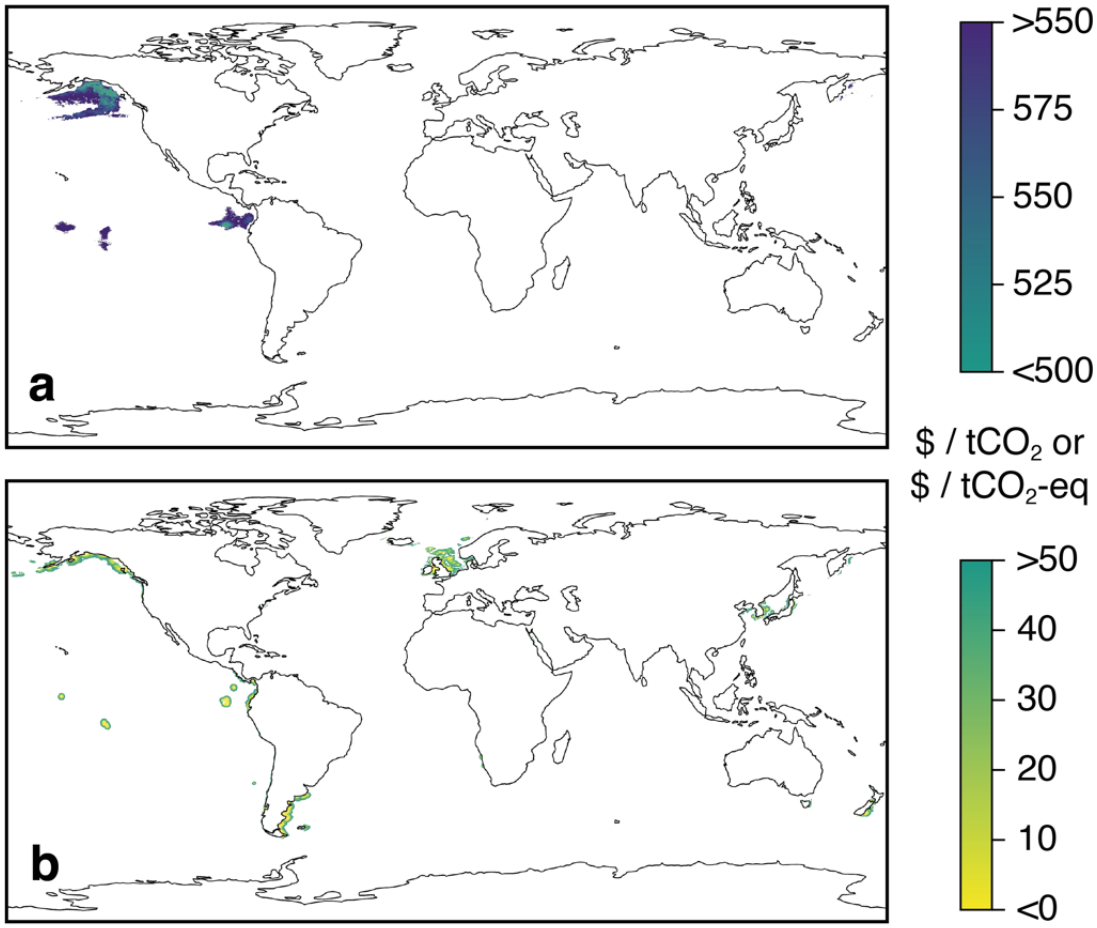

Supplementary Figure B.12 | Maps of lowest cost areas in Fig. 4. Maps show lowest-cost areas in the cheapest 1% of seaweed growth area for carbon sequestration (**a**) and GHG emissions avoided (**b**) in the 5th percentile of ambient nutrient simulations, with the color of shaded areas representing the net cost per ton of CO_2 or CO_2-eq.

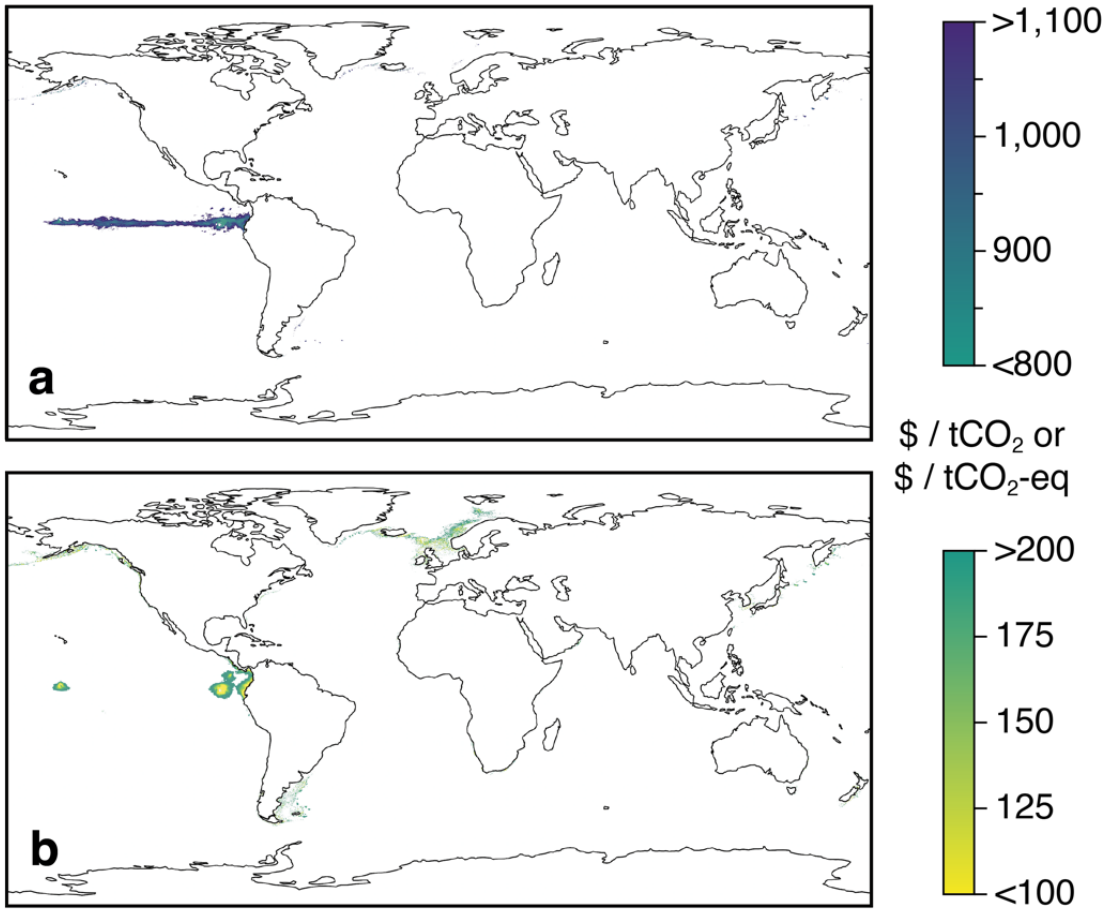

Supplementary Figure B.13 | Maps of lowest cost areas in Supplementary Fig. 11c,d. Maps show lowest-cost areas in the cheapest 1% of seaweed growth area for carbon sequestration (**a**) and GHG emissions avoided (**b**) in the 5th percentile of limited nutrient simulations, with the color of shaded areas representing the net cost per ton of CO_2 or CO_2-eq.

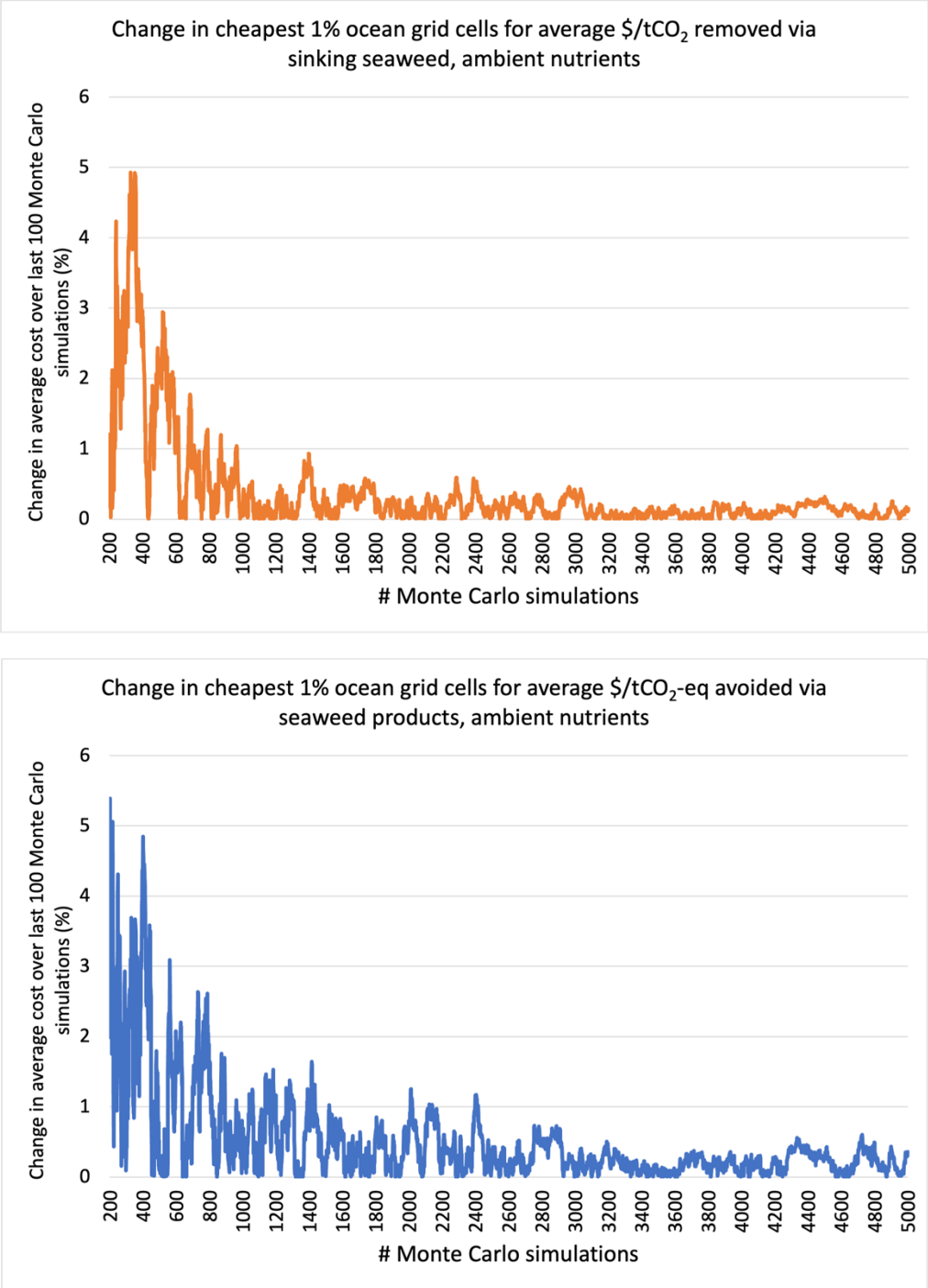

Supplementary Figure B.14 | Change in ambient nutrient scenario average costs of CDR (top) and avoided emissions (bottom) with successive Monte Carlo simulations. Monte Carlo simulation number (n) is shown on the x-axis, and the % change in the cheapest 1% ocean grid cells average cost over the previous 100 runs is shown on the y-axis.

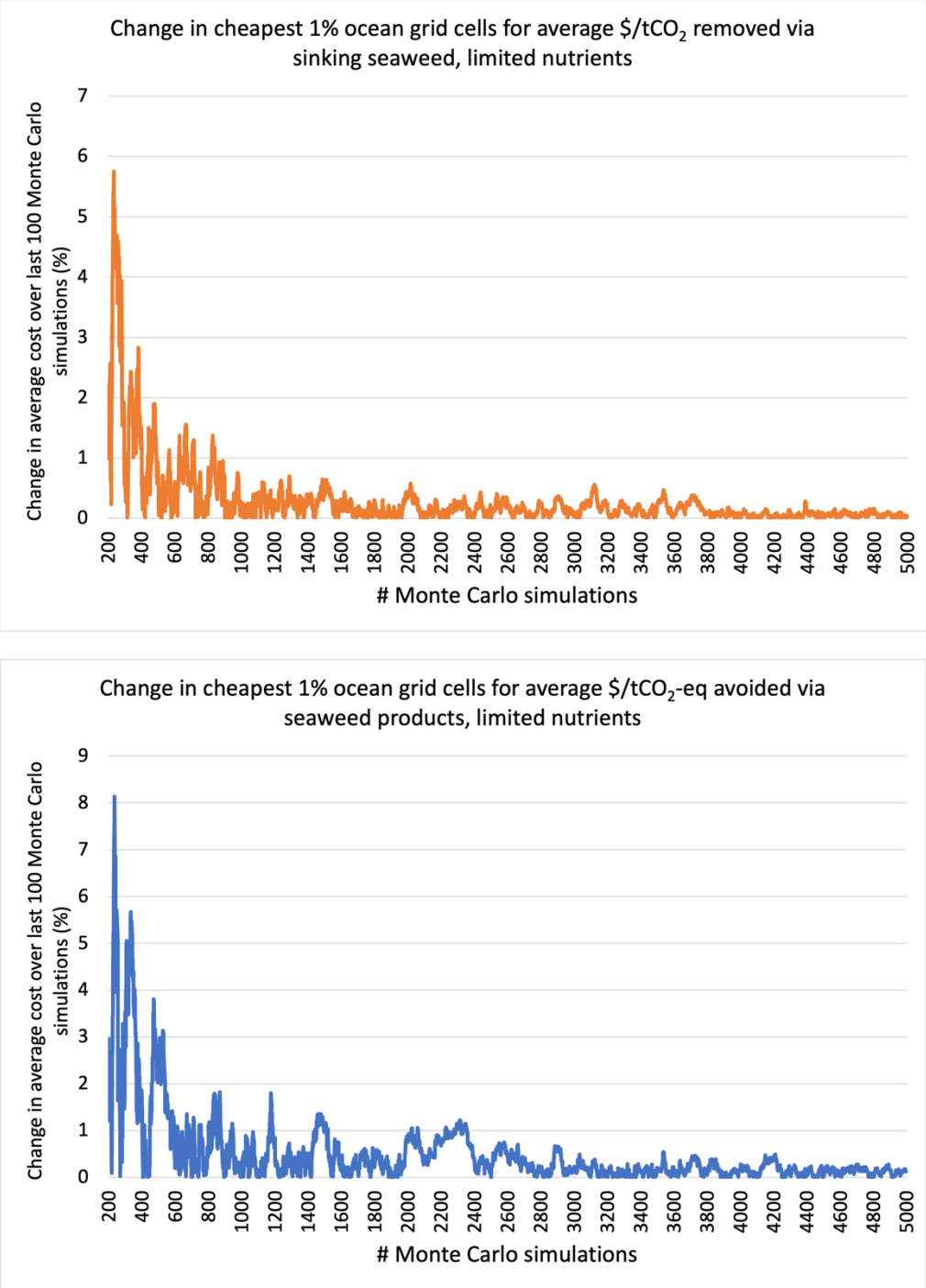

Supplementary Figure B.15 | Change in limited nutrient scenario average costs of CDR (top) and avoided emissions (bottom) with successive Monte Carlo simulations. Monte Carlo simulation number (n) is shown on the x-axis, and the % change in the cheapest 1% ocean grid cells average cost over the previous 100 runs is shown on the y-axis.

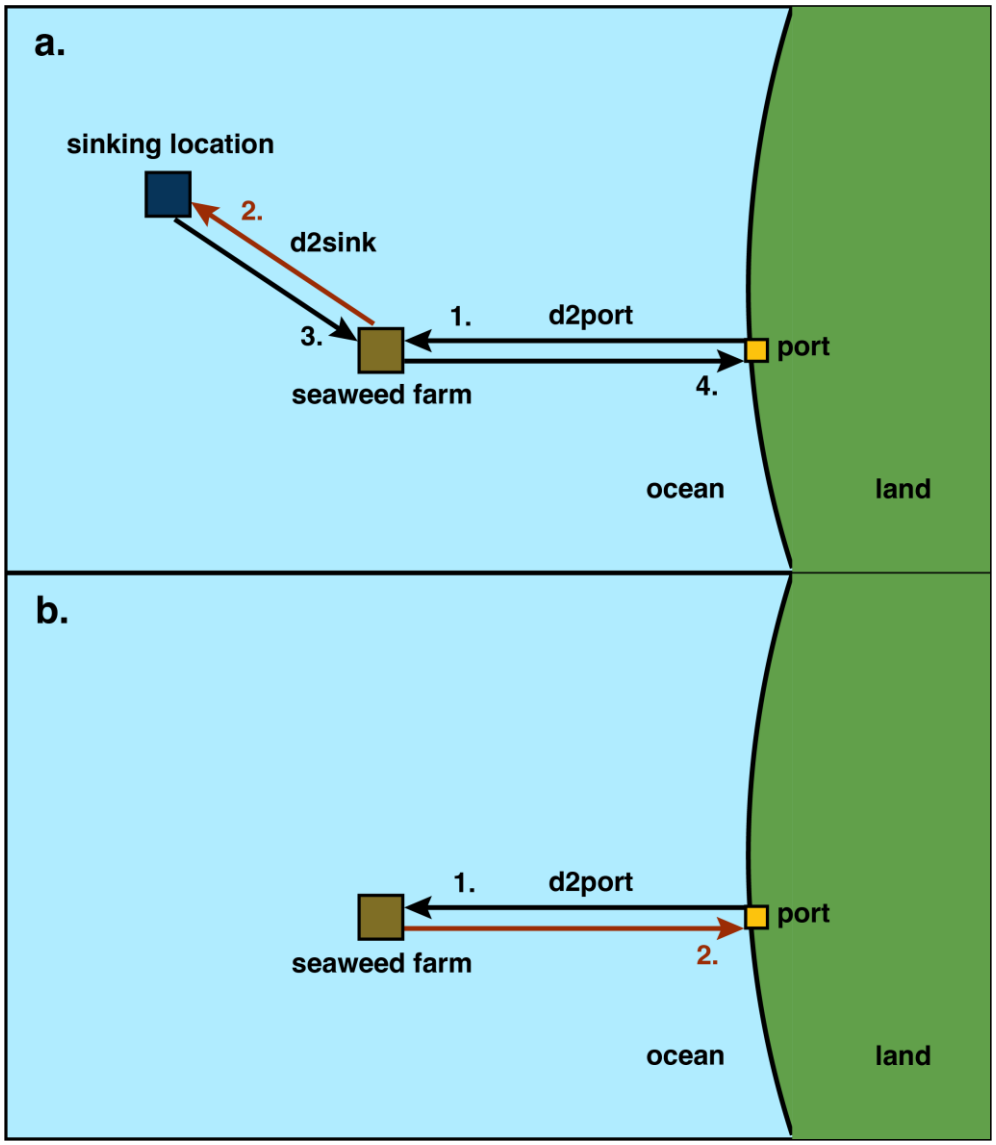

Supplementary Figure B.16 | Schematic of model transport framework for carbon sequestration via sinking (a) and avoided GHG emissions via products (b). Arrows indicate direction of transport, numbers next to arrows indicate order of transport steps, and red arrows indicate that harvested seaweed is being transported during that step.

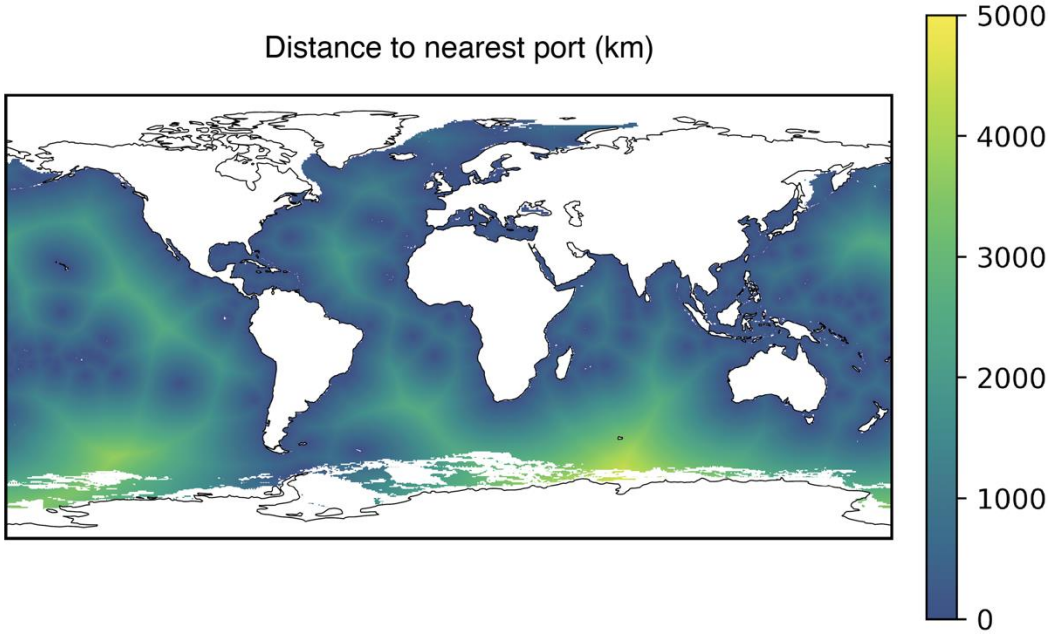

Supplementary Figure B.17 | Distance to port. Map shows the distance to the nearest port (km) from every ocean grid cell, interpolated from the Global Fishing Watch Distance from Port V1 dataset [(Global Fishing Watch, 2020)].

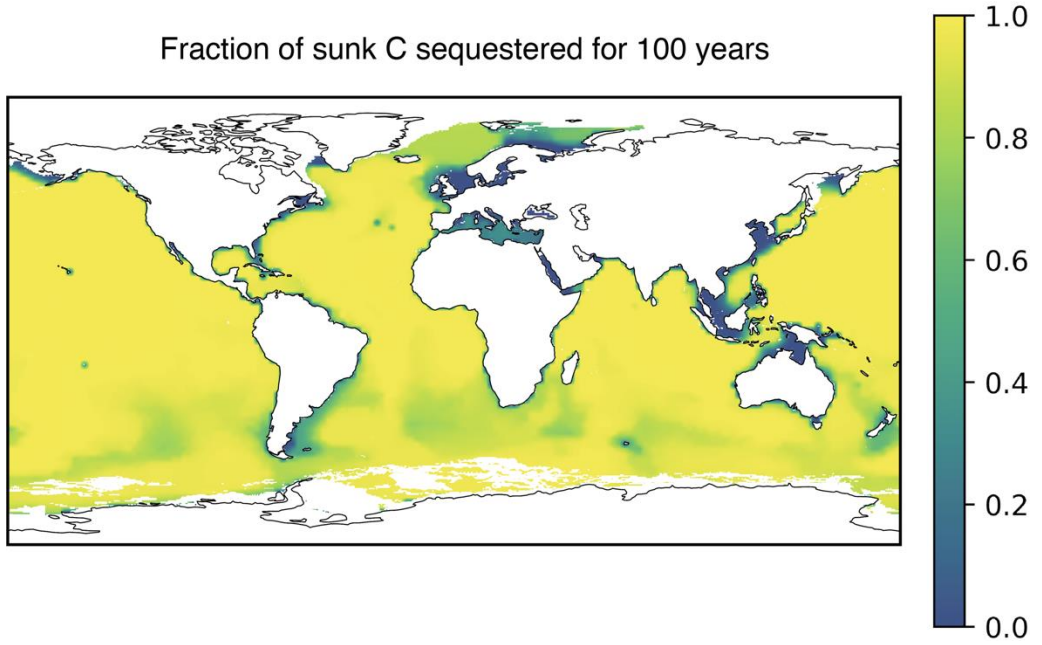

Supplementary Figure B.18 | Fraction of deposited carbon sequestered for 100 years. Data from Siegel et al. (2021)(Siegel et al., 2021) interpolated to 1/12-degree grid resolution.

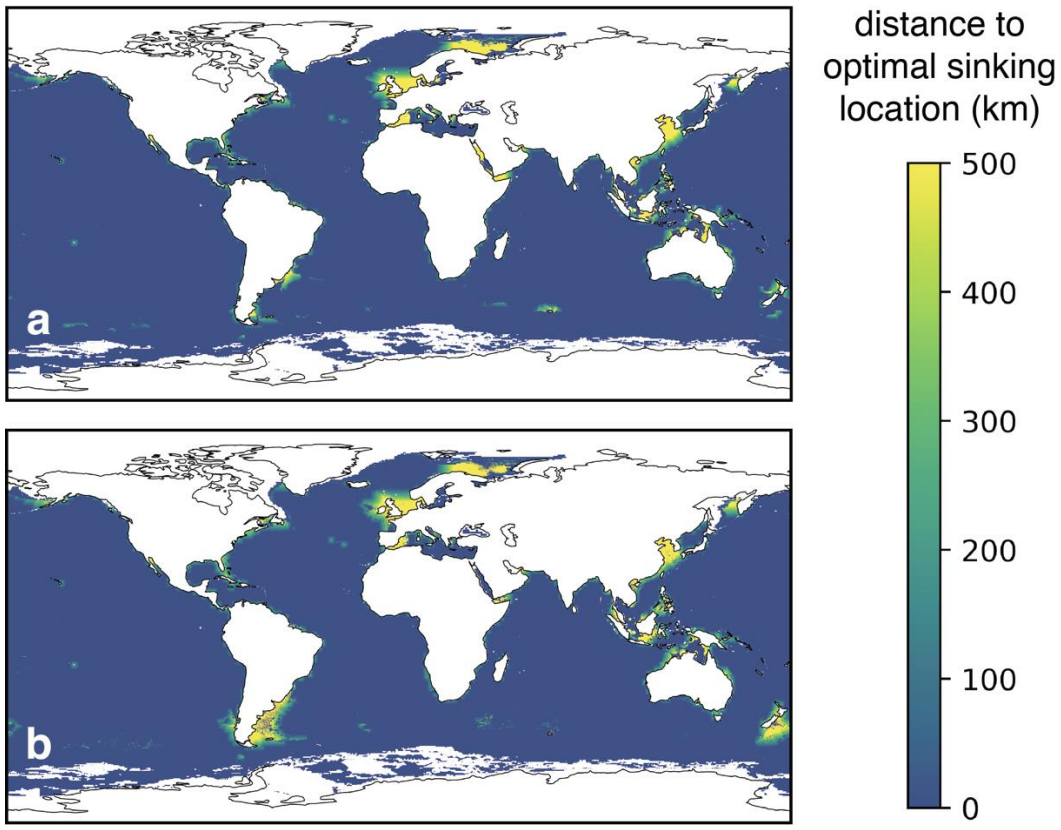

Supplementary Figure B.19 | Distance to economically-optimized sinking location. Maps show the shortest ocean distance from each seaweed growth pixel to the location at which the net CO_2 removed is maximized (incl. impacts of both increased sequestration fraction and transport emissions for different potential sinking locations) and the net cost is minimized for median ambient nutrient (**a**) and limited nutrient (**b**) scenarios. See *Methods* for detailed discussion of calculations.

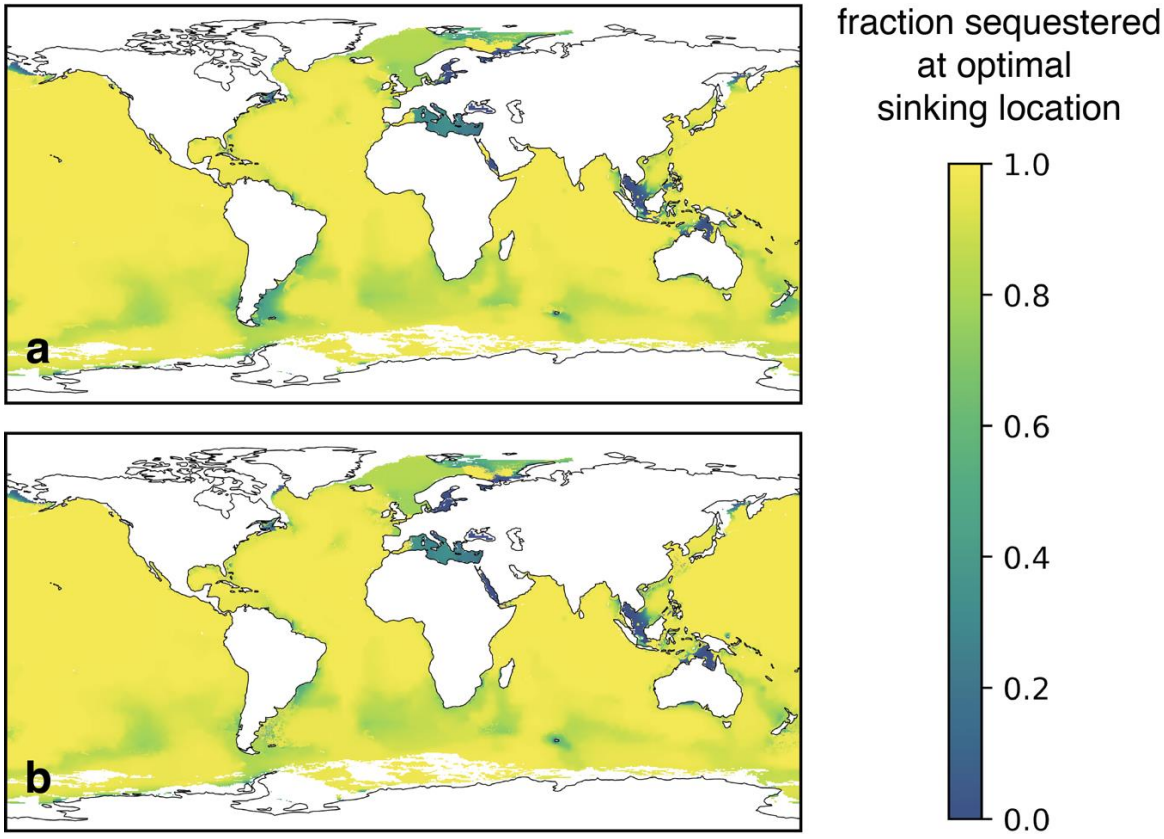

Supplementary Figure B.20 | Fraction of deposited carbon sequestered for 100 years with transport to optimal sinking location. After being transported to the optimal sinking location, the fraction sequestered for that location is applied to the grid cell where the seaweed was grown. The resulting adjusted fraction sequestered maps used in our economic calculations are shown for median ambient nutrient (**a**) and limited nutrient (**b**) scenarios.

Appendix C: Supplementary Information for Chapter 3

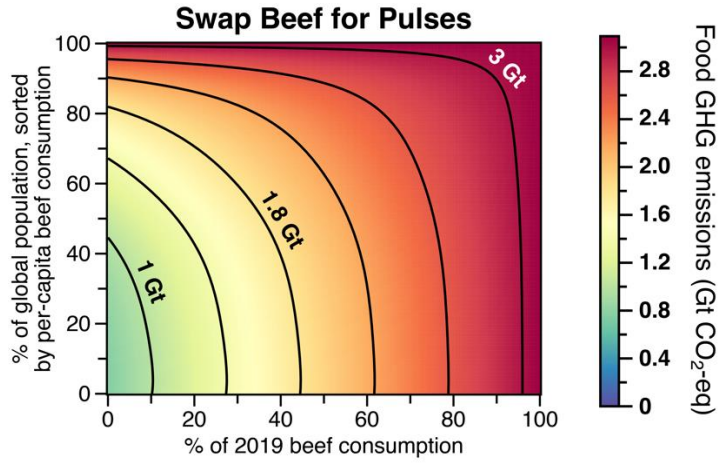

Supplementary Figure C.1 | Net emissions from dietary substitution of beef with mass-equivalent pulses. Contours show net emissions from beef consumption as a function of the percentage of the total population (sorted by per-capita beef consumption on the y-axis) that replaces some amount of beef consumption with mass-equivalent pulses (x-axis).